

# Chirality in Light–Matter Interaction

Andrew Lininger, Giovanna Palermo, Alexa Guglielmelli, Giuseppe Nicoletta, Madhav Goel, Michael Hinczewski,\* and Giuseppe Strangi\*

The scientific effort to control the interaction between light and matter has grown exponentially in the last 2 decades. This growth has been aided by the development of scientific and technological tools enabling the manipulation of light at deeply sub-wavelength scales, unlocking a large variety of novel phenomena spanning traditionally distant research areas. Here, the role of chirality in light–matter interactions is reviewed by providing a broad overview of its properties, materials, and applications. A perspective on future developments is highlighted, including the growing role of machine learning in designing advanced chiroptical materials to enhance and control light–matter interactions across several scales.

in biological nanostructures<sup>[5,6]</sup>—such as the gyroid molecular assemblies that produce the brilliant colors of butterfly wings<sup>[7]</sup>—and at larger scales in the structure of cells, tissues, and organs.

The modern history of chiral phenomena in optics, known as chiroptics, started in 1811 when François Arago observed colors in plane-polarized light transmitted through a quartz crystal.<sup>[8]</sup> A few years later, Jean-Baptiste Biot established that this optical response is caused by a rotation of the polarization plane of light and is present in solutions of some natural organic compounds. This observation was

subsequently understood by Louis Pasteur to originate from a molecular basis.<sup>[9]</sup> In 1824, Fresnel discovered circularly polarized light and the difference between refractive indices for materials illuminated with left (LCP) and right (RCP) circularly polarized light, studying the different interactions of RCP and LCP light in helicoidal arrangements of molecules.<sup>[10]</sup>

The first general definition of chirality, taken from the Greek word for “hand”, χεῖρ, was given by William Thompson (Lord Kelvin) in 1844 during a lecture at Johns Hopkins University: “I call any geometrical figure, or groups of points, chiral and say it has chirality, if its image in a plane mirror, ideally realized, cannot be brought to coincide with itself.”<sup>[11]</sup> Chirality has since become a central concept in our understanding of the light–matter interaction, whether described at the classical level, or in terms of quantum phenomena like excited states of matter (excitons) or hybrid states (polaritons) resulting from a strong coupling between light and matter.

Since the mid 20<sup>th</sup> century, the implications of chiroptics have been explored across a diverse spectrum of scientific disciplines, from global healthcare challenges to the search for extraterrestrial life to the development of novel quantum technologies. For example, biological molecules on Earth are often homochiral—most amino acids occur primarily as left-handed (L-) enantiomers while most sugars are right-handed (D-). While the origins of this homochirality are not completely understood, it offers a possible signature of life on other planets.<sup>[12]</sup> This concept was first explored in the Labeled Release experiment, which injected radioactive elements in the Martian soil during the Viking mission of 1976.<sup>[13]</sup> Optical detection of chirality plays an important role in probing DNA function and other key biological processes, including the molecular design of clinical drugs and the detection of clinical biomarkers—such as rare D-amino acids enantiomers associated with neurodegenerative diseases. Finally, in the realm of quantum information, there has been a recent revolution in terms of the transduction, manipulation, and storage of information controlled by coupling chiral states of light and matter.

## 1. Introduction

The interaction between matter and electromagnetic radiation traces back to the first instant after the Big Bang, but only during the last 2 centuries has humanity been able to rigorously describe this interaction, eventually controlling and manipulating it at the molecular scale. In that time, humanity has learned how to mold the flow of light by manipulating its phase, amplitude, polarization, and field distribution via material structures that enable specific functionalities. A key element of designing such systems is chirality, the asymmetry arising when a given object cannot be superimposed onto its mirror image. Chirality can manifest itself in terms of structural features, such as the handedness of a particular object, or in the behavior of particles under parity transformations. It can be found at every scale in nature, from the subatomic to the galactic, and is, notably, a crucial feature of all life on Earth. In particular, in biology, chirality occurs at the molecular level,<sup>[1–4]</sup>

A. Lininger, M. Goel, M. Hinczewski, G. Strangi  
Department of Physics  
Case Western Reserve University  
2076 Adelbert Rd, Cleveland, OH 44106, USA  
E-mail: mxh605@case.edu; gxs284@case.edu

G. Palermo, A. Guglielmelli, G. Nicoletta, G. Strangi  
Department of Physics  
NLHT-Lab  
University of Calabria and CNR-NANOTEC Istituto di Nanotecnologia  
Rende 87036, Italy

 The ORCID identification number(s) for the author(s) of this article can be found under <https://doi.org/10.1002/adma.202107325>.

© 2022 The Authors. Advanced Materials published by Wiley-VCH GmbH. This is an open access article under the terms of the Creative Commons Attribution-NonCommercial License, which permits use, distribution and reproduction in any medium, provided the original work is properly cited and is not used for commercial purposes.

DOI: 10.1002/adma.202107325

This review article provides an introduction to chirality in light–matter interactions, a broad overview of its many current applications, as well as a perspective on future developments—including the growing role of physics-assisted artificial intelligence in designing advanced chiroptical materials.

## 2. Theory of Chirality in the Light–Matter Interaction

### 2.1. Chiral and Superchiral Light

The interaction between light and matter at the macroscopic scale is described by classical electrodynamics, which is based upon Maxwell's equations.<sup>[16]</sup> In this framework, the achiral material response to an electromagnetic wave is described by the constitutive equations:

$$\begin{aligned} \mathbf{D} &= \epsilon_0 \bar{\epsilon} \mathbf{E} \\ \mathbf{B} &= \mu_0 \bar{\mu} \mathbf{H} \end{aligned} \quad (1)$$

where  $\mathbf{D}$  the electric displacement field,  $\mathbf{E}$  is the electric field,  $\mathbf{H}$  is the magnetic field, and  $\mathbf{B}$  is the inductive magnetic field,  $\epsilon_0$  is the vacuum permittivity,  $\mu_0$  is the vacuum permeability, and  $\bar{\epsilon}$  and  $\bar{\mu}$  are the material dependent relative permittivity and permeability, respectively. For isotropic materials, which have the same electromagnetic properties in every orientation, these two quantities reduce to scalars, resulting in the  $\mathbf{E}$  and  $\mathbf{D}$  fields (and the  $\mathbf{B}$  and  $\mathbf{H}$  fields) becoming parallel to one another. However, for anisotropic materials, or materials with different electromagnetic properties at different orientations,  $\bar{\epsilon}$  and  $\bar{\mu}$  take the form of second rank tensors. This means that the fields are no longer necessarily parallel. Anisotropic materials include some crystals and optical metamaterials—materials with engineered structural features much smaller than the wavelength of light ( $\lesssim \lambda/10$ )—among others.

By combining Maxwell's equations with the constitutive equations above, the wave equation can be obtained.<sup>[16]</sup> One important solution of this wave equation is represented by monochromatic plane waves, which are described by

$$\mathbf{E} = E_0 \mathbf{J} e^{i(kz - \omega t)} \quad (2)$$

where  $E_0$  is the wave amplitude,  $z$  is the propagation direction,  $\omega$  is the angular frequency,  $k$  is the wavenumber, and  $\mathbf{J}$  is the Jones vector.<sup>[17,18]</sup> The Jones vector is used to describe the state of polarization for a propagating light wave. Linearly polarized light (LPL) is described by a Jones vector with all real components

$$\mathbf{J}_{\text{LPL}}^\phi = \begin{pmatrix} \cos \phi \\ \sin \phi \\ 0 \end{pmatrix} \quad (3)$$

where  $\phi$  is the polarization angle, defined as the angle between the electric field vector and the propagation axis. LPL is confined to oscillate within a single plane, defined by the polarization angle and the axis of propagation. The Jones vector for circularly polarized light (CPL) contains an imaginary element and is given as<sup>[19]</sup>

$$\mathbf{J}_{\text{CPL}}^\pm = \frac{1}{\sqrt{2}} \begin{pmatrix} 1 \\ \pm i \\ 0 \end{pmatrix} \quad (4)$$

In case of the CPL, a single component of the electric field (the  $x$ -component) is either delayed (–) or advanced (+) by a phase factor  $\pi/2$  as compared to the  $y$ -component, as the wave propagates along the  $z$ -axis. Since only a single electric field component is manipulated, the electric field vector will rotate about the optical axis as the wave propagates. This can be contrasted with LPL, where the oscillation plane is fixed.<sup>[20]</sup> The rotation of propagating CPL has a definite handedness, making CPL waves geometrically chiral objects. The definition of the handedness in a chiral object is always arbitrary since the definition depends on the observer's perspective. We will adopt a common convention in classical optics, known as the detector's view: an observer in the detector plane views an oncoming CPL wave as rotating in the frontal plane. The handedness of the oncoming wave is defined by the direction of rotation for the electric field vector: right circularly polarized (RCP) light rotates clockwise, while left circularly polarized (LCP) light rotates counterclockwise. In this work, we use the notation “+” (RCP) and “–” (LCP) to label the handedness of a CPL wave (**Figure 1**).

An important class of materials is represented by bi-isotropic media, materials with the special optical property that the polarization state of incident light twists as it passes through the material. The constitutive relations are slightly modified for these materials<sup>[21,22]</sup>

$$\mathbf{D} = \epsilon \mathbf{E} + \xi \mathbf{H} \quad (5)$$

$$\mathbf{B} = \mu \mathbf{H} + \zeta \mathbf{E} \quad (6)$$

where  $\xi$  and  $\zeta$  are the magnetoelectric parameters (dimensionless), representing the coupling strength between the electric and magnetic fields.<sup>[23,24]</sup> These quantities are defined as

$$\xi = (\chi - i\kappa) \sqrt{\mu_0 \epsilon_0} \quad (7)$$

$$\zeta = (\chi + i\kappa) \sqrt{\mu_0 \epsilon_0} \quad (8)$$

where  $\chi$  is the Tellegen parameter and  $\kappa$  is the chirality parameter. The Tellegen parameter is used to describe the magnetoelectric effect, and materials with  $\chi \neq 0$  are termed non-reciprocal.<sup>[25,26]</sup> The chirality parameter is a quantifiable measurement of the degree of chiral handedness in the material, and changing the sign of  $\kappa$  is equivalent to taking a mirror image of the material. Chiral materials are characterized by  $\kappa \neq 0$  and  $\chi = 0$ , known as a Pasteur medium, or by  $\kappa \neq 0$  and  $\chi \neq 0$ , known as a bi-isotropic medium.<sup>[21]</sup>

The wave equation in the frequency domain takes on the following form when describing an electric field in a chiral material<sup>[27]</sup>

$$\nabla^2 \mathbf{E} + 2\omega\mu\xi(\nabla \times \mathbf{E}) + \omega^2\mu\epsilon\mathbf{E} = 0 \quad (9)$$

where the mode propagation constant satisfies the following equation

$$k^2 = \left( \frac{\omega^2\mu\epsilon - k^2}{2\omega\mu\xi} \right)^2 \quad (10)$$

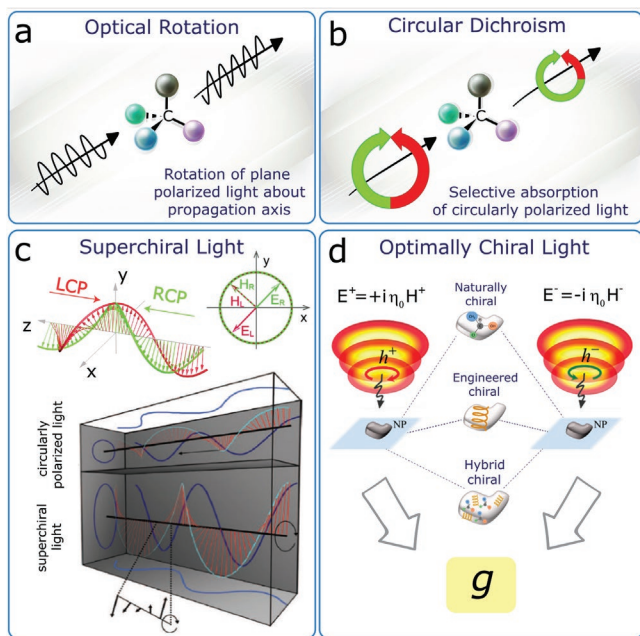


**Figure 1.** a,b) Schematics of the optical rotation (a) and circular dichroism (b) processes for light interacting with a chiroptically responsive molecule. c) (Top) Schematic of two counter-propagating circularly polarized light waves with opposite handedness; field vector projections onto the  $xy$ -plane: the electric field vectors produce destructive interference due to the phase difference between the two waves. (Bottom) A comparison between the electric field for circularly polarized and superchiral light: for CPL, the field vectors rotate about propagation axis at one revolution per wavelength; for superchiral light, the field vectors can completely revolve about the propagation axis in a distance shorter than the free-space wavelength. a–c) Top: Adapted with permission.<sup>[14]</sup> Copyright 2017, American Chemical Society. Bottom: Reproduced with permission.<sup>[14]</sup> Copyright 2011, American Association for the Advancement of Science. d) Structured light satisfying the optimally chiral condition (two electromagnetic fields with opposite helicity and equal time-averaged electric and magnetic energy) can be characterized by the dissymmetry factor ( $g$ ). Adapted with permission.<sup>[15]</sup> Copyright 2020, American Chemical Society.

This wave equation has two eigen solutions in the form of CPL waves

$$k_L = -\omega\mu\xi + \omega\sqrt{\mu\varepsilon + \mu^2\xi^2} \quad (11)$$

$$k_R = \omega\mu\xi + \omega\sqrt{\mu\varepsilon + \mu^2\xi^2} \quad (12)$$

This result demonstrates the double mode propagation in the medium, termed polarization birefringence by Engheta and Jaggard.<sup>[28]</sup> As a result of these mode propagation constants, an RCP wave propagates through a chiral medium with phase velocity  $v_+ = \omega/k_R$ , while an LCP wave propagates with  $v_- = \omega/k_L$ . The different phase velocities between the two circular polarization states implies that a linearly polarized light wave cannot transverse the chiral media without its polarization state being altered in the process. This results in a chiroptically responsive material, whereby for linearly polarized light the polarization plane is rotated about the propagation axis as the light wave propagates. This is referred to as the optical rotation or optical rotatory dispersion (ORD).<sup>[29–35]</sup> The optical rotation is quantified by a rotation in the polarization angle, which

depends on the thickness of chiral material through which the wave propagates and the wavelength of incident light

$$\gamma = \frac{\pi d(n_+ - n_-)}{\lambda_0} \quad (13)$$

where  $n_{\pm}$  is the refractive index of the chiral material (defined as  $n_{\pm} = \sqrt{\mu\varepsilon \pm \xi}$ ),  $\lambda_0$  is the vacuum wavelength, and  $d$  is the material thickness.<sup>[29]</sup> Similarly,  $\gamma$  can be quantified by comparing the difference between transmitted complex phases of incident light from each of the two circular polarization states:  $\gamma = [\arg(T_+) - \arg(T_-)]/2$ , where  $T_+$  and  $T_-$  are the complex transmission coefficients for RCP and LCP waves, respectively. It is interesting to note that chiral materials can exhibit a negative refractive index—occurring when  $\xi > \sqrt{\mu\varepsilon}$ —even while  $\varepsilon$  and  $\mu$  are both positive. This property makes chiral materials extremely promising for cutting edge optical applications involving negative index materials, such as lensing at resolutions below the diffraction limit.<sup>[36–38]</sup>

When  $k_L$  and  $k_R$  are complex, incident RCP and LCP waves experience differential attenuation when passing through the material, in addition to the differential phase velocity. This effect, whereby RCP and LCP waves are attenuated at different rates, is referred to as the circular dichroism (CD) (Figure 1).<sup>[29,39–42]</sup> The ellipticity can be used to represent the strength of the CD from the relative magnitude of the two transmitted polarization states. Ellipticity is calculated as

$$\eta = \frac{1}{2} \sin^{-1} \left( \frac{|T_+|^2 - |T_-|^2}{|T_+|^2 + |T_-|^2} \right) \quad (14)$$

The strength of the CD can also be related to the optical chirality  $C$ , defined in a general way by Tang and Cohen in 2010,<sup>[43]</sup> as representing the degree of helicity in a general (not only CPL) electromagnetic field.<sup>[44–49]</sup>  $C$  is given by

$$C = -\frac{\varepsilon_0\omega}{2} \text{Im}(\mathbf{E}^* \cdot \mathbf{B}) \quad (15)$$

It should be noted that for achiral structures a large CD response can be generated by anisotropy as well as the optical chirality. In practice, the two effects can be difficult to differentiate and are easy to mistakenly identify. Therefore in these systems, the chiral effect cannot be determined solely on the basis of the CD. The variation in the optical chirality,  $\Delta C$ , for RCP ( $C^+$ ) and LCP ( $C^-$ ) electromagnetic fields ( $\Delta C \equiv C^+ - C^-$ ) is directly proportional to the differential absorption rate for CPL interacting with a chiral material

$$\Delta a \equiv a^+ - a^- = -\frac{2}{\varepsilon_0} \text{Im}(\xi)\Delta C \quad (16)$$

where  $\text{Im}(\xi)$  is the imaginary part of the electric–magnetic mixed dipole polarizability.<sup>[50]</sup> Tang and Cohen demonstrated theoretically<sup>[43]</sup> and experimentally<sup>[14b]</sup> that a particular configuration of the incident CPL field can lead to enhancement in the optical chirality  $C$ , and similarly to an increase of the CD signal. In this scheme, two incident CPL fields with the same frequency and opposite handedness are superimposed with opposite propagation directions. These two fields will interfere with each other, generating a standing wave pattern. The

resultant spatial field pattern is termed superchiral light. The electric energy density of the superchiral field is given by

$$U_e(z) = \frac{\epsilon_0}{2} [E_1^2 + E_2^2 - 2E_1E_2 \cos(2kz)] \quad (17)$$

where  $k$  is the wave vector, and  $E_1$  and  $E_2$  are the electric field amplitudes for the LCP (propagating right to left) and RCP waves (propagating left to right), respectively. At the nodes of the superchiral field, the electric dipole-allowed transitions are effectively suppressed, and the local chirality is enhanced with respect to the optical chirality in the incident field. This local enhancement of the chiral fields results in a local enhancement of the chiroptical activity of the material near the field nodes.<sup>[14b,51]</sup> However, it should be noted that by scaling inversely with the electric field energy density, as opposed to the total electromagnetic field energy density, Tang and Cohen's formalism can lead to limitations at the nanoscale.<sup>[52]</sup>

An important quantity in nanoscale chiroptics is the dissymmetry factor, first introduced by Kuhn in 1930.<sup>[53]</sup> Considering the interaction between a chiral molecule and CPL, he showed theoretically that the chirality of a molecule is revealed in the difference between the extinction powers ( $P_{\text{ext}}$ ) for two CPL waves with opposite handedness, normalized to their arithmetic average

$$g_{\text{CPL}} = 2 \frac{P_{\text{ext}}^+ - P_{\text{ext}}^-}{P_{\text{ext}}^+ + P_{\text{ext}}^-} \quad (18)$$

Starting from this expression, Tang and Cohen<sup>[43]</sup> derived the dissymmetry factor for two mirror-image fields as a special case of Equation (18)

$$g = g_{\text{CPL}} \frac{cC}{2U_e\omega} \quad (19)$$

where  $c$  is the speed of light,  $C$  is the optical chirality,  $\omega$  is the angular frequency, and  $U_e$  is the energy density of the electric field, as defined in Equation (17). This is the quantity which, in Tang and Cohen's approach, is maximized near the electric field nodes. Based on this expression there are two ways of effectively maximizing the chiral dissymmetry: maximizing the optical chirality, or minimizing the electric field energy density. However, the second approach has limitations in practical application. By only considering the electric and not the total electromagnetic energy density, it is possible for the  $g$  factor to be only artificially increased. This analysis ignores the contribution due to the magnetic energy density, which is not always valid, especially at or near the node of the electric field energy due to the conservation of energy.<sup>[52,54]</sup> This may not correspond to a real advantage in terms of detection. In these situations,  $U_e$  should be replaced by the total electromagnetic field energy.

This optical chirality definition was recently further elaborated by Hanifeh et al., translating the concept of CD at the nanoscale into the dissymmetry factor, and making the concept suitable for any type of electromagnetic field including structured light.<sup>[15]</sup> This formalism allowed the authors to discriminate and investigate the chirality of dielectric nanoparticles. Interestingly, this analysis introduces an upper bound for the helicity density.<sup>[15]</sup> Electromagnetic fields at this upper bound are called optimally chiral, which indicates that the optical chirality is maximized for a given time average of the energy density.

The electric and magnetic field components of optimally chiral fields satisfy the condition<sup>[55]</sup>

$$\mathbf{E} = \pm i\eta_0\mathbf{H} \quad (20)$$

where  $\eta_0$  represents the intrinsic wave impedance of vacuum, and the sign determines the handedness. Additionally, the calculation of the dissymmetry factor for optimally chiral fields can be performed without explicitly knowing the helicity and energy densities of the field, as seen in the following expression

$$g = -4\eta_0^{-1} \frac{\Re(\alpha_{\text{em}})}{\Im(\alpha_{\text{ee}})} \quad (21)$$

where  $\Re(\alpha_{\text{em}})$  and  $\Im(\alpha_{\text{ee}})$  are the real part of the electromagnetic polarizability and the imaginary part of the electric polarizability of the nanoparticle, respectively.<sup>[15]</sup> These recent innovations, including superchiral and optimally chiral light, have the potential to present a wide array of new applications for chiroptical systems. Some examples of these recent designs are outlined in the following sections.

## 2.2. Chiral Properties of Structured Light

Traditionally, optical illumination in the light–matter interaction has focused on utilizing a limited set of common field modes, such as plane waves, spherical wavefronts, and Gaussian beam modes. However, this approach has recently been challenged by the growth of structured light approaches. Structured light is generally any light field in which the spatial inhomogeneity of a field parameter is important, or non-trivial. This category includes arbitrarily designed wavefronts that are not limited to traditional spatial distributions.<sup>[56]</sup> Structured light fields have begun to revolutionize the light–matter interaction by introducing the tailored spatial distribution of field properties such as the amplitude and phase, and abstract dynamic properties such as the momentum, energy, and angular momentum of the electromagnetic field. The principle of structured light has already led to new and exciting applications of optics such as optical vortices and superoscillatory optical fields.<sup>[57,58]</sup>

The angular momentum of light, a conserved quantity of the light field, can be used to quantify the amount of rotation contained in a light field. This quantity is defined as<sup>[16]</sup>

$$\mathbf{L} = \epsilon_0 \int \mathbf{r} \times (\mathbf{E} \times \mathbf{B}) dV \quad (22)$$

where  $\mathbf{L}$  is the angular momentum,  $\mathbf{r}$  is the spatial position, and the integral is over a volume of space. We can distinguish two distinct and independent angular momenta components associated with the light field:  $\mathbf{L}_o$ , the orbital angular momentum (OAM), and  $\mathbf{L}_s$ , the spin angular momentum (SAM). These quantities are decomposed from the total angular momentum as follows<sup>[59,60]</sup>

$$\mathbf{L} = \epsilon_0 \int \sum_i E_i (\mathbf{r} \times \nabla) A_i dV + \epsilon_0 \int \mathbf{E} \times \mathbf{A} dV = \mathbf{L}_o + \mathbf{L}_s \quad (23)$$

where  $\mathbf{A}$  is the vector potential.

OAM, which describes the spatial distribution of the field and is independent of the polarization state of light, is an angular momentum corresponding with the helical wavefront

of a beam as it travels in space. SAM describes the rotation of the light field between the distinct polarization states. This quantity is connected to the internal spin degree of freedom for the photon, a spin-1 gauge boson. Both OAM and SAM angular momenta can be characterized as either longitudinal (aligned with the mean momentum) or transverse (orthogonal to the mean momentum). Light characterized by a longitudinal SAM is circularly polarized and by convention the helicity parameter, or spin quantum number  $\sigma$ , assumes the values  $-1$  for LCP, and  $+1$  for RCP.<sup>[61–63]</sup> Although the concept of SAM is more general, the circularly polarized beams considered above can be explained in terms of expressing these polarization states. In many optical applications, only traditional circularly polarized light is utilized for simplicity, without OAM contributions. However, a range of studies have unlocked important effects by considering interesting structured light beams containing OAM and SAM. Some such studies are explained below.

A light field possessing OAM is characterized by the OAM quantum number  $l$ , also known as the “topological charge”, which can assume either integer or half-integer values.<sup>[62,64–66]</sup> There are several types of beams modes which possess OAM, such as Bessel beams,<sup>[67]</sup> Ince–Gaussian beams,<sup>[68]</sup> and Mathieu beams,<sup>[69]</sup> among others. One important type of beam possessing OAM is the Laguerre–Gaussian (LG) beam,<sup>[70]</sup> of which has an amplitude distribution in cylindrical coordinates  $(r, \phi, z)$  given as

$$LG_n^l(r, \phi, z) = l_n^{|l|} \frac{w_0}{w(z)} \sqrt{\frac{2n!}{\pi(n+|l|)!}} \left( \frac{\sqrt{2}r}{w(z)} \right)^{|l|} \left( \frac{2r^2}{w(z)^2} \right) \exp \left[ -\frac{r^2}{w(z)^2} - i \left( \frac{kr^2}{2R_z} + l\phi - \varphi(z) \right) \right] \quad (24)$$

where  $w(z)$  is the radius of the beam,  $w_0$  is the beam waist radius at  $z = 0$ ,  $k$  is the wavenumber in the embedded medium,  $R_z$  is the radius of curvature for the beam wavefront, and  $\varphi(z)$  is the Gouy phase.<sup>[63]</sup>  $l_n^{|l|}$  is the generalized Laguerre polynomial of order  $n$  and degree  $|l|$ , where the order  $n$  is the number of concentric radial modes (observed as concentric intensity rings around the central singularity), and  $l$  is the number of helices in the beam (relating to the azimuthal phase and the OAM).<sup>[63]</sup> The sign of  $l$  determines the handedness: for  $l > 0$ , the beam is right-handed; while for  $l < 0$ , the beam is left-handed (see **Figure 2**).<sup>[71]</sup> Note that when  $n = 0$  and  $l = 0$ , the LG beam is identical to the fundamental Gaussian beam.

Circularly polarized LG beams carry both SAM and OAM. When incident upon a chiral material, the interaction between light possessing SAM and the material results in a transfer of SAM from the light to internal electronic degrees of freedom. When the incident light possesses OAM, the interaction of light with the particles of the material can induce a torque, which can produce a rotation of the particle along the axis of the beam.<sup>[72]</sup> The OAM transfer phenomenon can be explained in terms of a multipole interaction between the electromagnetic modes in the material and the incident light field.<sup>[72–74]</sup> OAM momentum transfer was first observed by Beth in 1936, in regards to the torque exerted by CPL on a birefringent waveplate.<sup>[75]</sup> Since then, chiroptical mechanical forces have been utilized in a number of applications, especially following the development of optical tweezers.<sup>[76–78]</sup> In particular, the OAM in a helical LG

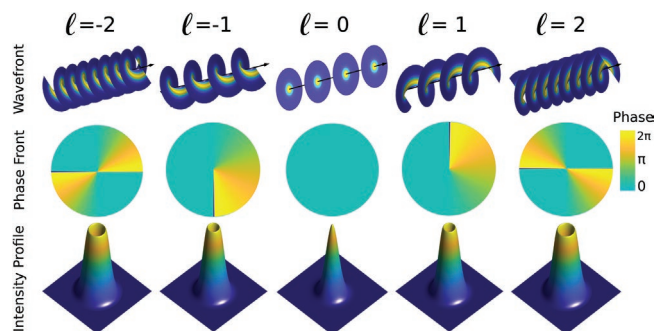


**Figure 2.** Intensity and phase profiles for the primary mode of a Laguerre–Gaussian beam ( $n = 0$ ) with  $l = (\pm 2, \pm 1, 0)$ . The first row shows the helical intensity wavefront for the different OAM modes, propagating along the optical axis. The second row shows the corresponding azimuthal phase profiles in the range  $(0, 2\pi)$ , and the third row shows the corresponding planar intensity profile.

beam mode can be utilized to induce mechanical rotation of a trapped particle,<sup>[79,80]</sup> and has been observed in polymerized cholesteric liquid crystal droplets.<sup>[81]</sup> In another example, OAM induced rotation was utilized to precisely rotate and control Ag nanowires based on their plasmonic response.<sup>[82]</sup> In general, the angular momentum transfer depends on comparing the handedness of the trapped particle and the incident light beam.<sup>[83]</sup> Harnessing the optomechanical force inherent in light containing OAM provides a convenient way to introduce torque into optomechanical systems, as opposed to other methods such as rotation of the polarization state in a non-helical beam.

Another application of optomechanical forces induced by chiral light–matter interactions is chiral sorting, or enantiomeric separation, with photoinduced force. Similar to the optical trapping case, it has been experimentally demonstrated that when illuminated by chiral light, chiral particles are subject to an optomechanical force which depends on the handedness.<sup>[84]</sup> This can be combined with a range of interesting forces which exist for chiral particles in the vicinity of a surface, when interacting with light angular momentum to create custom force profiles.<sup>[85–87]</sup> By utilizing these SAM/OAM based forces, passive chiral separation of enantiomers can be achieved. This is an important task in many areas of chemistry, in particular in pharmaceuticals. Furthermore, chiral photo-induced forces can be used as a tool to precisely study nanoscale chirality by investigating the presence and effect of micro- to nanoscale forces.<sup>[88,89]</sup> These studies clearly show how angular momentum can be a powerful tool to consider in the design of chiroptical systems. Furthermore, these principles can be readily integrated with a range of metamaterial systems, similar to those shown below, providing a convenient platform for tailoring forces through the constructive use of angular momentum with metamaterial design.

### 3. Chiral Photonic Metamaterials

Chirality is a fundamental property of a wide variety of natural systems, on length scales ranging over several orders of magnitude, from enantiomeric molecules to chiral asymmetries in organism-scale biological structures. The interaction between

chiral light and chiral matter is maximized for structures with geometric chiral properties on length scales comparable with the wavelength of light. Unfortunately, many molecules are geometrically chiral on much shorter length scales, leading to a relatively weak chiroptical response with visible light.<sup>[90–92]</sup> However, by employing modern nanoscale fabrication techniques, it has recently become possible to design and manufacture metamaterials with engineered geometric chirality.<sup>[93–95]</sup> Optical metamaterials are materials whose dimensions have been engineered at a scale much smaller (typically  $\lesssim \lambda/10$ ) than the wavelength of light ( $\lambda$ ). However, the sizes of the relevant dimensions are typically much larger than those encountered in molecular chirality. Therefore, these systems can be designed and optimized to produce a significantly enhanced chiroptical response—well beyond those typically observed in natural systems—by controlling the geometry and constituent materials with nanometer level precision.<sup>[6,96]</sup> This level of discrete control is difficult to achieve for natural chiral systems.<sup>[97]</sup>

Chiral metamaterials can be composed of either 3D or 2D structures—2D metamaterials are referred to as metasurfaces—and can exhibit either intrinsic or extrinsic geometric chirality.<sup>[98]</sup> Intrinsic geometric chiral metamaterials are those whose constitutive elements exhibit geometric chirality.<sup>[99,100]</sup> We consider intrinsic geometric chirality as existing on the order of the geometrical unit of the metamaterial which we define as the smallest continuous material unit which is intentionally designed. These materials can often be designed to produce optically intrinsic electromagnetic behavior, namely a chiroptical response at normal incidence. Tuning of the structure is important in this respect, since geometrically chiral materials do not necessarily support this intrinsic chiral response.

Opposed to intrinsic, extrinsic chiral metamaterials are composed of geometrical units that are themselves geometrically achiral or homogeneous.<sup>[101–103]</sup> Extrinsic chiroptical activity arises from the interaction of the metamaterial with the local environment. This can be typically be effected through symmetry breaking arising from another material or the interaction with light at non-normal incidence.<sup>[104,105]</sup> It should be noted that we are considering optical photonic metamaterials as distinct from their substrate. Therefore a geometrically achiral material structure with symmetry breaking as a result of the substrate would be properly extrinsically chiral in 3D, although this class of materials may be designed to support a typically intrinsic optical response. A limitation of extrinsic chiral metamaterials is that the magnitude of the extrinsic chiroptical response generally goes to zero at normal incidence and changes sign upon a reversal of the incidence angle. However, the magnitude of the chiroptical response typically increases for large oblique incident angles of the illuminating light, allowing geometrically achiral structures to create a strong chiral response.

The chiroptical response is strongly dependent upon a superposition of the electromagnetic fields induced in the material by the incident light. Specifically, both the induced electric ( $p$ ) and magnetic ( $m$ ) multipole momenta in the material are responsible for the observed chiroptical response.<sup>[28,104,106]</sup> To obtain this response, the  $p$  and  $m$  momenta must both have non-zero in-plane components, ( $p_{\parallel}, m_{\parallel} \neq 0$ ) which implies that the electric and magnetic multipoles are not orthogonal.<sup>[107,108]</sup> Orthogonal multipole momenta for an extrinsic chiral metasurface—with

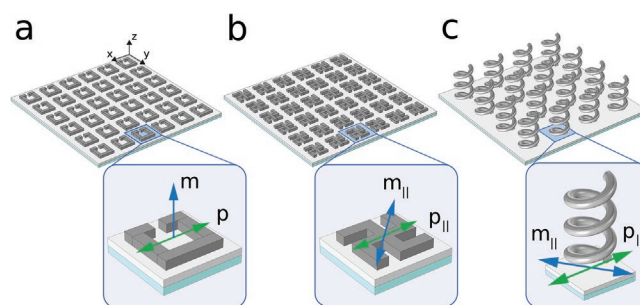


**Figure 3.** Chiroptical multipole response for various types of metasurface geometries, classified by the chiral geometry type. The insets show the structure overlaid with the relative orientation of electric ( $p$ , green) and magnetic ( $m$ , blue) multipole momenta for normal incidence illumination. a) A 2D extrinsic chiral metasurface: the electric and magnetic dipole moments are perpendicular. The illumination to produce chiroptical effects is off from the normal. b) A 2D structure which has been tuned to produce an intrinsic chiroptical response at normal incidence. In this case, the refractive index contrast between the substrate and superstrate enforces an overall 3D geometric chirality for the material. c) A 3D intrinsic chiral metamaterial. In (b) and (c) the electric and magnetic dipole moments both have in-plane components ( $p_{\parallel}$  and  $m_{\parallel}$ ). a–c) Adapted under the terms of the CC-BY Creative Commons Attribution 4.0 International license (<https://creativecommons.org/licenses/by/4.0>).<sup>[107]</sup> Copyright 2018, The Authors, published by Springer Nature.

an incident wavevector at non-normal incidence to the plane—are shown in **Figure 3a**. For structures with 3D intrinsic chirality, (Figure 3c) this condition is satisfied at normal incidence. Structures with only 2D intrinsic geometric chirality are not intrinsically chiral in 3D, for example the gammadion structure in Figure 3b without the substrate. However, structures which are not properly intrinsically chiral in 3D can be designed to support a typically intrinsic chiral response (namely chiroptical activity at normal incidence) by appropriate tuning of the multipole momenta as described above (Figure 3b).<sup>[28,106,107]</sup> In these cases, the refractive index contrast between the substrate and the superstrate can provide a symmetry breaking in the third dimension, enforcing an overall 3D geometric chirality. These principles explain the extraordinary enhancement of the chiroptical response observed in chiral metamaterials, and the observed chiroptical properties at normal incidence in intrinsic metamaterials.<sup>[109,110]</sup>

### 3.1. Description of Chiral Metasurfaces and Chiral Metamaterials

Advances in modern nanoscale fabrication techniques have led to the creation of many chiroptical system designs based on applying the principles reported in the previous sections. Some promising recent systems include: metal nanoparticles (NPs)<sup>[111,112]</sup> and nanorods (NRs),<sup>[113]</sup> semiconductor quantum dots (QDs),<sup>[114,115]</sup> 3D hybrid systems,<sup>[116]</sup> and dielectric and plasmonic metasurfaces.<sup>[107]</sup> Plasmonic chiral metamaterials will be discussed in detail in the following section. Chiral photonic systems have been utilized in a wide array of fields such as: biology, medicine, and chemistry. Beyond solely enhancing the molecular chiroptical response, chiroptically responsive metamaterials have been shown to increase

conductivity, film-forming properties, and biocompatibility in chiral composite materials.<sup>[117,118]</sup> Furthermore, chiroptically active metasurface designs have shown promise as a platform for advanced optical applications, including negative refraction, super-resolution imaging, and invisibility cloaking.<sup>[36,38,119]</sup> Some of the notable recent chiroptical platforms are:

1. **Nanoparticles:** NPs are small metallic particles with overall dimensions in the range of a micrometer to a few nanometers.<sup>[120]</sup> Because of their small size—on the order of the wavelength of light—NPs have several interesting physical properties, including an extremely high surface area/volume ratio compared to bulk particles.<sup>[121,122]</sup> NPs have enjoyed a diverse range of applications in recent years, due to their strong electromagnetic resonance in (or near) the visible range. The origin of this strong optical response is the presence of a plasmonic resonance—discussed in detail below—which can lead to strong signal enhancement in CD spectroscopy. For this reason, chiral NPs are widely used in the fabrication of chemical sensors and bio-sensors, and are an important tool for bioimaging and biodiagnosis.<sup>[123]</sup> In the context of metamaterials, chiral plasmonic structures based on NPs have been produced by several different techniques, including nanoscale lithography and molecular self-assembly.<sup>[111,112]</sup>

Since they can be functionalized with relative ease, NPs are amenable to so-called “bottom-up” fabrication approaches, such as molecular self-assembly. These processes rely on the natural affinity of molecules to aggregate into stable, well-defined structural elements. In this approach, NPs are often selectively functionalized to the molecular scaffolding, creating a de facto NP structure.<sup>[124]</sup> Several recent studies have utilized this molecular self-assembly technique to produce helical chiral NP structures supporting an enhanced chiroptical response.<sup>[125–128]</sup> The plasmonic and structural chiral properties of chiral NPs can be exploited for interesting sensing applications. For instance, Markovich et al. synthesized chiral plasmonic silver NPs and were able to experimentally demonstrate a temperature-dependent CD response.<sup>[129]</sup>

2. **Quantum dots:** QDs differ from the vast majority of other particles in that their optical and electrical properties are primarily due to quantum mechanical effects. These systems are composed of nanometer-scale semiconductor particles, sized to create a strong optical interaction.<sup>[130,131]</sup> The relevant optical processes in QD systems are based on photoluminescence. This process results in the emission of light with energy equal to the difference between the highest occupied molecular orbital (HOMO) and lowest unoccupied molecular orbital (LUMO) energy states.<sup>[132,133]</sup> In particular, chiral QDs have been explored for a diverse array of applications, including: photocatalysis,<sup>[134]</sup> sensors,<sup>[135]</sup> and fluorescent chiral nanoprobe.<sup>[136]</sup> The synthesis of chiral QDs from semiconducting materials is generally mediated by incorporating chiral enantiomers of penicillamine and cysteine as stabilizers. This process has been used to produce CdS, CdSe and CdTe QDs showing enhanced chiroptical activity.<sup>[137]</sup> Moloney et al.<sup>[114,115]</sup> demonstrated that the chiroptical properties of QD systems are directly related to the chiral stabilizers used

during the synthesis procedure. By exploiting this effect, the resulting chiroptical effects could be controlled by a modification of the synthesis procedure.

3. **Metamaterials:** Finally, we will consider lithographically fabricated metamaterials and metasurfaces composed of chiral photonic nanostructures, of the type seen in Figure 3. These systems can support an extremely large range of engineered optical responses, due to the relative freedom in designing the geometric structure. The ability of designed metamaterials to produce extreme optical responses has generally led to the increasing adoption of metamaterial systems in many fields such as photonics, nanotechnology, plasmonics, and bio-nanomaterials.<sup>[110,138,139]</sup> Chiral metamaterials are a class of metamaterials in which the nanoscale chiral geometry is designed specifically to generate an enhanced chiroptical response.<sup>[137,140]</sup> In particular, several metallic chiral metasurfaces supporting a plasmonic resonance have demonstrated extreme chiroptical behavior, as shown in the following sections. It has been demonstrated that chiral metamaterials provide a pathway to obtaining negative refractive index materials, leading to interesting optical properties such as left-handed refraction and perfect lensing.<sup>[36,38]</sup> In chiral materials, this can be achieved while both the permittivity  $\epsilon$  and permeability  $\mu$  of the constituent materials remain positive. In another interesting regime, Tretyakov et al.<sup>[141]</sup> developed a model for chiral materials in which both  $\epsilon$  and  $\mu$  are equal to zero (referred to as chiral nihility). This effect has been experimentally confirmed in the microwave, terahertz, and optical regimes.<sup>[142]</sup>

As an example, Zhu et al.<sup>[107]</sup> recently proposed a planar chiral nanostructure based on an dielectric/metallic gammadion-shaped chiral planar nanostructure. It should be noted that the gammadion form has been previously utilized by several researchers.<sup>[143–145]</sup> The system structure was created by electron beam lithography, followed by atomic layer deposition of titanium. The resulting structure was experimentally confirmed to possess a strong chiroptical response (CD near 90%), with an advantageous design in terms of size reduction, complexity, and manufacturing cost. Similarly, Palermo et al. recently utilized a 3D intrinsic chiral metasurface combined with hyperbolic metamaterials to design a high sensitivity biosensing platform.<sup>[146,147]</sup>

### 3.1.1. Fabrication Techniques

The production of chiral nanostructures can generally be classified into one of two distinct approaches: top-down or bottom-up fabrication.<sup>[151–155]</sup> The top-down approach classifies those techniques which start from a much larger volume and progressively remove material to produce the final design. This includes techniques such as: scanning probe lithography, soft lithography, e-beam lithography, focused-ion beam lithography, direct laser writing (DLW), and nanoimprint lithography.<sup>[156–161]</sup> An example of top-down fabrication is the creation of 3D nanohelices via DLW of a specific metamaterial pattern from a large body of photopolymerizable material, followed by electroplating with gold.<sup>[162]</sup> The bottom-up approach is based on

the growth or natural self-aggregation of molecular precursors into physical nanostructures. In contrast to top-down, where material was being removed, here material is being added to create the desired structure. Bottom-up lithography techniques include: chemical<sup>[163]</sup> and physical vapor deposition,<sup>[164]</sup> dip pen lithography,<sup>[165]</sup> molecular self-assembly,<sup>[166]</sup> and nucleation and growth.<sup>[167,168]</sup> This method is based on a delicate balance between various forces, which include static and/or transient electromagnetic, van der Waals, capillary, friction, and convective forces.<sup>[139]</sup> One obvious disadvantage of the top-down approaches is waste production- with concerns of possible environmental pollution- which occurs during the reduction of the macrostructure to the nanostructure. This problem does not occur in the bottom-up approach. However, with the bottom-up approach, it is generally more difficult to control the final geometry of the resultant nanostructures. This is due, in part, to the difficulty of obtaining a homogeneous distribution of the precursors necessary to create the nanostructures, and the limited range of potential designs based on natural physical processes in techniques such as molecular self-assembly.

In 1996, Robbie et al.,<sup>[169]</sup> reported the first optical activity from artificially constructed nanohelices, fabricated by glancing-angle deposition (GLAD). The resulting structures can

be seen in **Figure 4a**. To fabricate this structure, magnesium fluoride was evaporated onto the sample which was mounted on a tilted substrate. By rotating the substrate, the researchers were able to control the directional growth of the deposition and obtain nanohelices with lengths of 50–2000 nm. This structure was shown to produce a significant enhancement in the ORD spectra.

Another fabrication approach that is recently growing in importance is DLW. This technique utilizes a focused laser pulse with full 3D range of motion to selectively polymerize a photopolymerizable material. Using this technique, structures can be fabricated with full 3D properties in the range of micrometers to nanometers, with a resolution of less than 100 nm.<sup>[170,171]</sup> An example of 3D intrinsic chiral nanohelices fabricated with DLW is shown in **Figure 4b**. It can be seen that the fabricated structures possess excellent chiroptical properties. DLW has become widespread in various fields, including biomedical engineering,<sup>[172]</sup> regenerative medicine,<sup>[173]</sup> microfluidics,<sup>[174]</sup> and optics,<sup>[175]</sup> due to its high resolution, excellent design freedom, and the potential bio-compatibility of the polymerized material.

A different approach to nanoscale fabrication is “DNA origami”, which is the bottom-up self-assembly nanostructures

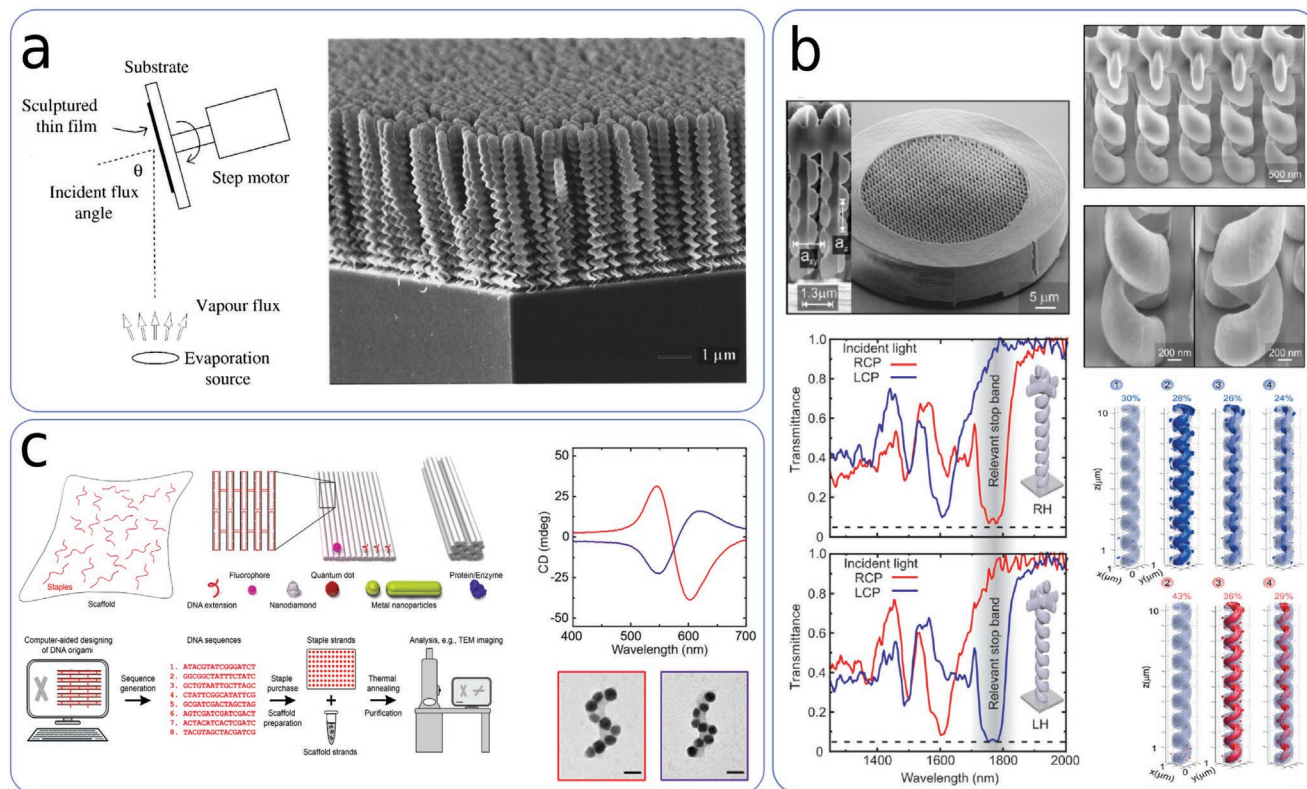


**Figure 4.** Examples of 3D chiral metamaterials created with advanced fabrication techniques. a)  $\text{MgF}_2$  sculptured nanohelices on a glass substrate deposited via glancing-angle deposition. In this technique the substrate is placed at an angle to induce directional growth, and rotated throughout the deposition process to create the helical structure. Reproduced with permission.<sup>[148]</sup> Copyright 1997, American Vacuum Society. b) Nanohelices fabricated via direct laser writing with SU-8 photoresist. By tuning the metamaterial geometry, a transmittance stop band was created with a chiral dependence. Reproduced with permission.<sup>[149]</sup> Copyright 2007, Wiley-VCH. c) Gold nanoparticle helices fabricated with DNA origami. Long DNA scaffolds are formed into complex shapes via thermal annealing and DNA “staples”. The staples are generally created via DNA sequencing technology. Au nanoparticles can then be functionalized to the structure at specific locations to create optically active materials, such as the two nanohelices shown. Reproduced with permission.<sup>[150]</sup> Copyright 2018, American Chemical Society.

via a nanoscale folding of DNA to create 2D and 3D configurations.<sup>[176–179]</sup> This technique is especially amenable to including plasmonic NPs, since they can be specifically attached to the DNA backbone at selected positions with a common functionalization process. This allows DNA origami to be used as a platform for engineering chiral plasmonic nanostructures. Typically single-stranded DNA—for example, from a M13 bacteriophage virus—is modified and utilized as a scaffold in the fabrication procedure.<sup>[176]</sup> Once the DNA (currently just precursors to the final structure) has been sufficiently modified and functionalized with NPs, the structure is assembled by mixing the precursors together and thermal annealing the DNA solution in a saline buffer solution to add the necessary energy for the assembly transition. The final structure is then typically separated from the solution by purifying the DNA with agarose gel electrophoresis.<sup>[150]</sup> In 2012, Kuzyk et al.,<sup>[180]</sup> used the DNA origami approach to create nanohelical NP structures, utilizing the procedure outlined above and specifically attaching NPs to targeted binding sites on a 24 strand linear DNA bundle. The resulting structures were shown to exhibit a significant CD and ORD response in the visible spectrum. The procedure and fabricated structures can be seen in Figure 4c.

An alternative bottom-up approach was recently proposed by Passaseo et al.,<sup>[181]</sup> This approach utilizes focused ion/electron beam induced deposition (FEBID/FEBED) to grow helical nanostructures on a substrate. In the FEBID method, an ion/electron beam decomposes a metal-organic target, and the material is then selectively placed to grow 3D nanostructures with full 3D design freedom, through manipulation of the beam parameters.<sup>[182,183]</sup> Nanohelical structures were experimentally demonstrated with this procedure, showing promise for future applications.

In terms of obtaining structural information about the fabricated nanostructure, electron microscopy has proven to be an important tool, including both scanning (SEM) and transmission electron microscopy (TEM). By utilizing electrons instead of photons as in a typical microscope, these tools have a much greater resolution capability than can typically be obtained by an optical microscope.<sup>[184–186]</sup> As an example, Ohsuna et al. utilized both SEM and TEM to investigate the mesoporous structure of a chiral material, confirming the existence of chiral channels.<sup>[187,188]</sup>

### 3.2. Chiral Plasmonics

In the nanofabricated structures shown above, the design target is generally to increase the chiroptical responsiveness, either increasing the electromagnetic fields near the structure for sensing applications or increasing the chiroptical activity of the structure itself. Although most geometrically chiral nanoscale systems exhibit some degree of enhancement, the chiroptical response can be increased by further increasing the coupling between the incident light and the chiral material.<sup>[189–191]</sup> In this light, plasmonic systems have been demonstrated to exhibit strong input and output coupling—showing a high level of responsiveness in terms of the input light and also producing a significant electromagnetic response—and have shown an ability to strongly concentrate electromagnetic energy. The

advent of modern nanofabrication techniques has led to the ability of fabricating specially engineered chiral plasmonic nanostructures, allowing researchers to harness the power of plasmonics for chiroptical applications.<sup>[96,192–194]</sup>

Plasmonics is an important branch of nanophotonics, encompassing a wide array of structures and applications spanning decades.<sup>[195]</sup> This field is based on an interaction between incident light and a lossy (metal) structure, whereby the oscillating incident light creates the resonant excitation oscillation in the surface charge density. This effect is essentially the electronic charge oscillating back and forth on the metal surface, in response to input energy from the incident light. This excitation is termed a surface plasmon polariton (SPP).<sup>[196,197]</sup> Only a broad overview of the effect is provided here; for more details, the reader is referred to several recent works with comprehensive introductions to the field of nanoscale plasmonics.<sup>[198–203]</sup> Since the SPP is confined to the interface between the metal and surrounding environment, the SPP mode effectively concentrates energy from the incident light field into a small (can be deeply sub-wavelength) volume, localized to the metal surface. This can produce a huge local enhancement in the electromagnetic field strength, as seen by the surrounding material.<sup>[204]</sup> Furthermore, the inclusion of multiple plasmonic nanostructures in sufficiently close vicinity can produce a strong coupling between individual plasmonic nanostructure modes, leading to the creation of a large-scale hybridized electromagnetic mode. This hybridization allows the system to produce a distinctly collective response over a large-scale nanostructured surface, which significantly alters the interaction between the SPP mode and any material in the vicinity. Excitation of a plasmon resonance also influences the magnitude of the radiated output signal. Plasmon resonance is associated with a large dipole response, which couples extremely well to the far-field radiation at resonance.<sup>[91]</sup> These properties of the plasmon–light interaction, both strong input and output electromagnetic coupling and a significant local enhancement of the field strength, make plasmonics an ideal tool for enhancing the inherently weak chiroptical response in natural chiral materials.

Chiral plasmonics refers to metallic nanoscale chiral structures which exhibit a notable effect on the chiroptical response by employing a plasmonic resonance as the main optical mode.<sup>[211,212]</sup> Many plasmonic nanostructures have been designed with the objective of modifying and enhancing the typical chiroptical response seen in natural chiral materials. Some of these designs include: nanoparticle assemblies<sup>[152,213–215]</sup> such as self-assembled gold nanorods,<sup>[216]</sup> tetrahedral nanoparticle structures,<sup>[217]</sup> and general nanocrystal assemblies.<sup>[218]</sup> Another approach to chiral plasmonics involves utilizing atomically thin 2D crystals, such as twisted van der Waals heterostructures<sup>[219]</sup> and monolayer MoSe<sub>2</sub>.<sup>[220]</sup> Similarly, many chiral plasmonic systems have been found which show an external chirality enhancement effect, including: metallic nanowires<sup>[221]</sup> and topological systems where the plasmonic mode arises from interaction between electrons and the Berry curvature.<sup>[222]</sup> Complex resonances can be utilized such as bound state in continuum modes,<sup>[223]</sup> dichroic coupling,<sup>[224]</sup> and the interaction with complex structured light.<sup>[74]</sup>

In particular, combining plasmonic nanoparticles with DNA has proven to be a powerful approach for chiral

plasmonics.<sup>[180,205,225–230]</sup> The DNA molecule has naturally helical geometry, which imparts a definite chirality to the structural morphology making DNA a natural intrinsic chiral material. More about the biological function of DNA chirality is discussed below. Beyond its intrinsic chirality, DNA has been shown to be a versatile and robust tool for the creation and manipulation of nanoscale structures with strong chiroptical responses by utilizing the DNA origami technique. Lan et al., have recently applied DNA origami to the design of 3D chiral nanostructures by employing a v-shaped “DNA adapter”.<sup>[205]</sup> A schematic of the design is shown in Figure 5a, along with an AFM image of the DNA nanostructure. This innovation allowed the researchers to create self-assembled, facily tunable stair-like and spiral-like chiral nanostructures with tuned handedness. Tuning of these structures is accomplished by varying a spacer length between the two arms of the DNA adapter (similar to a DNA ruler), a convenient method for adapting the nanoscale geometry and

tuning the optical response. The DNA origami technique was also employed by Kuzyk et al. to create reconfigurable plasmonic nanostructures based on the DNA origami approach.<sup>[231]</sup> These structures utilize DNA-regulated dynamic conformal changes to alter the 3D nanostructure geometry through the addition of specific DNA “fuel” strands. These strands can bind to specific points on the DNA bundles, altering the relative angle between two DNA bundles and manipulating the structure. A distinct and dynamically switchable CD spectral response was demonstrated in this system by modulating between distinct left and right-handed configurations.

Enhancement of the chiroptical response from chiral plasmonic nanostructures is a result of the nanoscale geometrical design and lithographic fabrication of the metallic structure and is an engineered property. Since the plasmonic response is localized to the near-field region, a structure with definite chiral structure will impart the corresponding handedness into

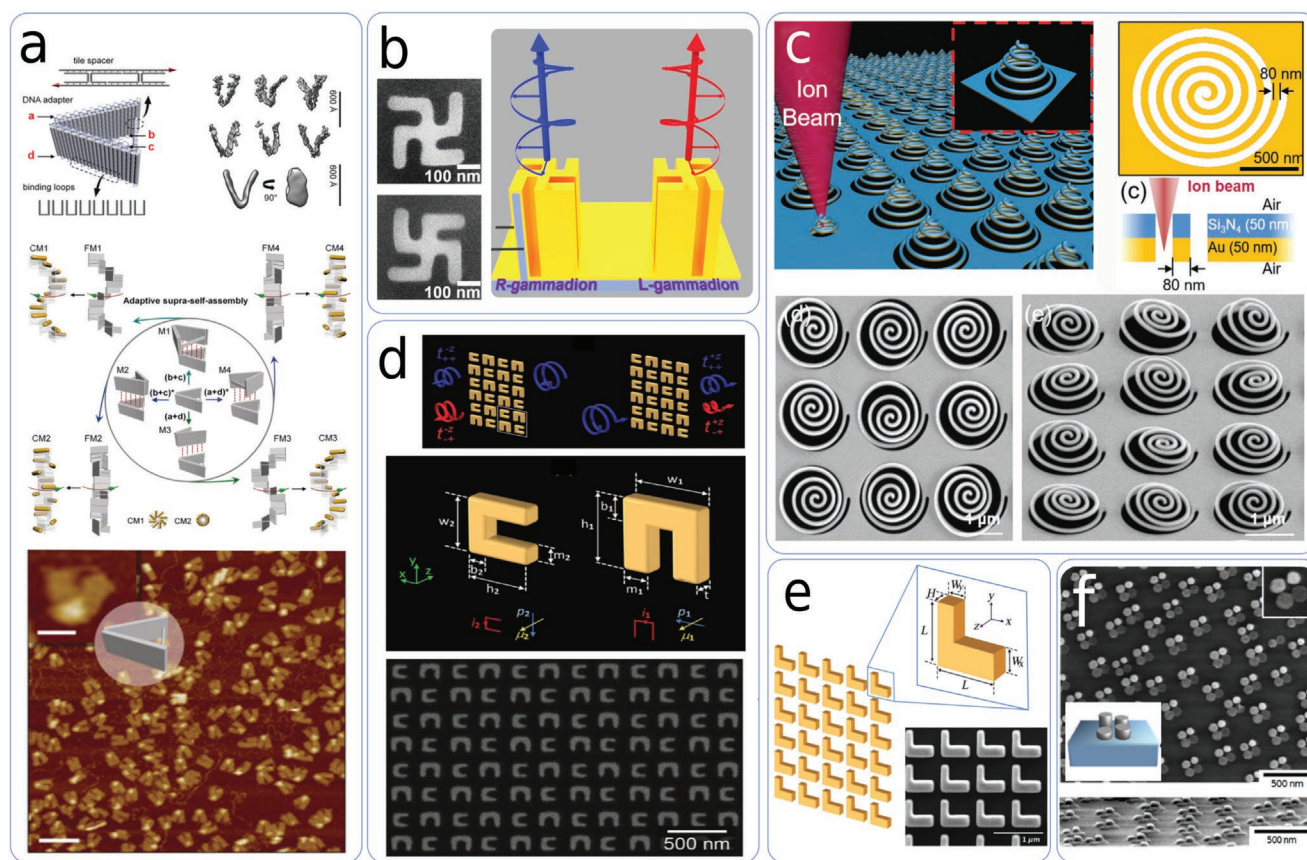


**Figure 5.** Examples of recent chiral plasmonic metasurface geometries. a) Chiral metasurface enabled by plasmonic nanoparticles combined with DNA origami. DNA surface adapters were developed to programmatically assemble 3D chiral structures via self-assembly. Reproduced with permission.<sup>[205]</sup> Copyright 2017, Wiley-VCH. b–f) Other examples include schematic and scanning electron microscopy (SEM) images of: b) a gammadion-shaped metal–GaN metamaterial which can support circularly polarized lasing in nanocavities; c) an Archimedes spiral metasurface produced via FIB milling on a Au/Si<sub>3</sub>N<sub>4</sub> layered structure, which produces a broadband chiroptical response in the mid-IR regime; d) a U-shaped metasurface composed of two different sized Au meta-atoms arranged in a periodic grid, supporting an asymmetric transmission response which is dependent upon the anisotropy; e) an L-shaped metasurface composed of Au nanoantennas with an asymmetric transmission response; and f) a metasurface composed of deposited metallic oligomers: the structure operates via a near field coupling between multiple metallic nanopillars, forming a quasi-3D metamaterial capable of producing a chiroptical response in the visible to near-IR range. b) Reproduced under the terms of the CC-BY Creative Commons Attribution 4.0 International license (<https://creativecommons.org/licenses/by/4.0>).<sup>[206]</sup> Copyright 2020, The Authors, published by Springer Nature. c) Reproduced with permission.<sup>[207]</sup> Copyright 2019, The Authors, published by Wiley-VCH. d) Reproduced with permission.<sup>[208]</sup> Copyright 2013, Wiley-VCH. e) Reproduced with permission.<sup>[209]</sup> Copyright 2017, American Physical Society. f) Reproduced with permission.<sup>[210]</sup> Copyright 2014, American Chemical Society.

the plasmonic oscillation, resulting in the generation of a chiral electromagnetic field. Including the generation of a chiral electromagnetic field with the plasmonic properties of strong field enhancement and far-field coupling, chiral plasmonic nanostructures can be a powerful tool for the enhancement of the chiroptical response. Some recent designs and nanofabricated plasmonic metasurface geometries include: nanoantenna arrays of resonators with gammadion shapes<sup>[103,206,232]</sup> (Figure 5b), Archimedes spirals<sup>[207,233]</sup> (Figure 5c),  $\eta$ -shapes<sup>[234]</sup> U-shapes<sup>[208,235]</sup> (Figure 5d), and L-shapes<sup>[209]</sup> (Figure 5e), deposited metallic oligomers<sup>[210]</sup> (Figure 5f), fish-scale patterns,<sup>[236]</sup> and chiral arranged rectangular bars.<sup>[237–239]</sup> These structures demonstrate the wide array of possible metasurface designs which can be utilized for a chiroptical response. However, it must be remembered that for intrinsically achiral structures there is often a component of the CD response due to anisotropy in addition to the optical chirality. This effect must be differentiated from the CD spectra in order to determine the true effect of the structure upon the optical chirality.

### 3.2.1. Active Chiral Plasmonics

One promising area of current research is the integration of chiral plasmonics in systems in which the optical properties can be dynamically reconfigured. This is termed active chiral plasmonics. Typically chirality is an unchanging property of nanofabricated structures, which is fixed at the time of fabrication or synthesis. In the context of optical metasurfaces, systems with fixed optical properties impose hard limits on the operable ranges of devices. For example, the operating wavelength of chiroptical biosensors is generally determined by the engineered resonance of the constituent metasurface elements. Recently, researchers have demonstrated systems which can allow the user dynamic control over the plasmonic chiral response.<sup>[194,240,241]</sup> This tuning can allow the same metamaterial structure to fill a wide range of applications with different requirements. The post-fabrication tuning is generally controlled through the application of a reversible and easily modifiable external stimuli, such as a modification of the chemical environment or the application of an electric potential. This approach has the potential, by dynamically altering the chiroptical response during device operation, to enable advanced applications such as highly integrated polarization based engineering, and dynamic sensitivity and a broader useful range in molecular chiral sensing.<sup>[242]</sup> Such applications can exceed the current capabilities of chiral plasmonic structures by extending device capabilities beyond those imposed by the static limit.<sup>[243]</sup>

Dynamic control over the chiroptical response in active chiral plasmonic systems is generally effected by a scheme which affects the plasmonic modes of the system, directly altering the magnitude or handedness of the chiroptical response. Several dynamic control methods have been previously employed in optical metasurface systems, including: electrically doped graphene,<sup>[248]</sup> semiconductor nanosprings,<sup>[249]</sup> liquid crystal dispersions,<sup>[250]</sup> and mechano-tunability.<sup>[251]</sup> Some examples of metasurfaces designs which feature active control over the chiroptical response are shown in **Figure 6**.

Yin et al., demonstrated a metasurface system capable of a reconfigurable chiroptical response based on a two orthogonal corner-stacked nanorod system with the phase change material GST-326 as an active switching medium (see Figure 6a).<sup>[244]</sup> This material undergoes a large phase transition with a corresponding shift in refractive index ( $\Delta n = 2$ ) when thermally modulated between crystalline and amorphous states. The shift in refractive index greatly alters the local dielectric environment of the plasmon mode. A large mid-IR spectral shift in the CD response was demonstrated through thermal modulation of this system, with a tunable range of 4.15–4.90  $\mu\text{m}$ . Furthermore, this system was subsequently combined with an electronic bias layer to demonstrate a sign inversion of the CD spectral response.

A similar system was demonstrated by Zhang et al., operating a terahertz metamaterial with a photoinduced alteration in the chiroptical handedness.<sup>[252]</sup> This system consisted of a 3D metamolecule with two individual chiral sections. Silicon pads in the structure were used to modulate the optical response by affecting their conductivity through strong optical illumination with photon energy above the silicon bandgap. This switchability in the silicon conductivity allowed the researchers to dynamically modulate the electromagnetic chirality of the structure, producing a substantial modification in the CD and ORD spectral responses.

These approaches to active chiral plasmonics rely on the inclusion of an active medium directly in the metamaterial structure to alter the electromagnetic properties of the plasmonic system. However, the intricate fabrication required for such systems can often be difficult, requiring precise 3D nanolithography, and hindering the large scale implementation for real-world applications. These issues have led to the design active chiral plasmonic systems utilizing large scale integrated active elements. These systems generally require less intensive fabrication procedures and are better suited for real world applications.

One approach to active control is to modulate the chiral system through manipulation of a flexible substrate. This is accomplished by applying a chiral nanoshell array to a hydrogel substrate.<sup>[253]</sup> Alternatively, flexoelectric methods can alter the global geometric dimensions of the entire metasurface structure through an applied external electric voltage. By altering the physical dimensions of a chiral nanostructure, the plasmonic chiroptical response can be directly affected and controlled. Such a structure was demonstrated by Gilroy, et al. utilizing a polymer-based nanoelectromechanical material to manipulate the dimensions of a nanostructure based on chiral “shuriken”-shaped indentations in a polycarbonate substrate (see Figure 6b).<sup>[224,245]</sup> A clear modification of the device geometry was observed by SEM with voltage applied to the electromechanical material (a near 30% decrease in the total arm area of the indentation). This modification led to a notable change in the measured ORD spectra.

Another approach is modification of the chiroptical response through the introduction of external chemical reagents. In particular, this approach is especially well suited for chemical sensing. A chemical based active chiral plasmonic system was demonstrated by Wu et al., based on a near field coupling between two Au nanohole arrays which were separated

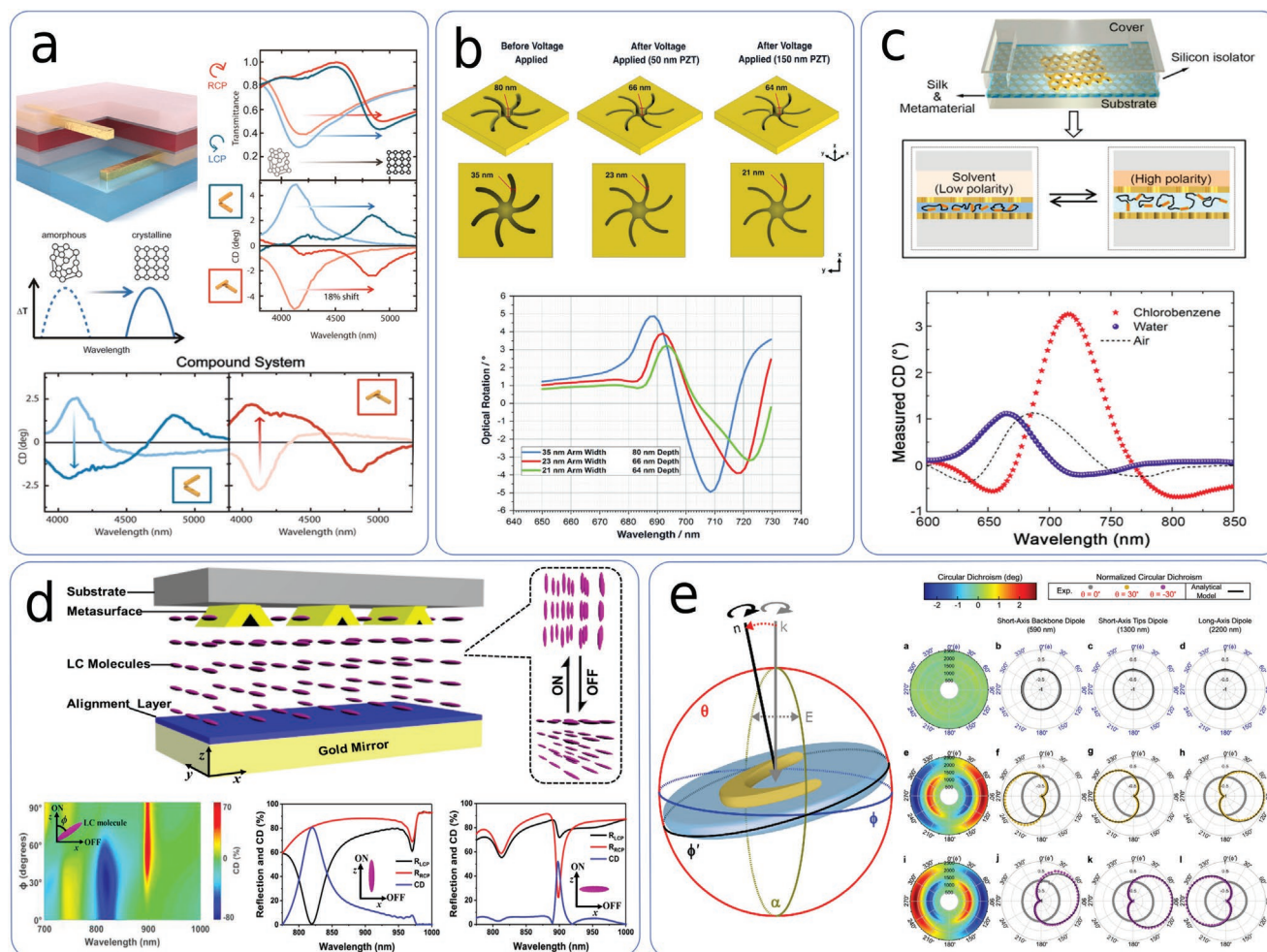


**Figure 6.** Some recent techniques to obtain active chiral plasmonics. a) Two electromagnetically coupled Au nanorods mediated by GST-326 phase-change material. Inducing the phase change produces a shift in the relative orientation of the two nanorods, altering the chiroptical response. Reproduced with permission.<sup>[244]</sup> Copyright 2015, American Chemical Society. b) Chiral shuriken-shaped indentations in an Au film controlled via a flexoelectric substrate. The form factor is visibly altered in response to an applied potential on different thicknesses of the flexoelectric layer (PZT), leading to a change in the chiroptical properties. Reproduced under the terms of the CC-BY Creative Commons Attribution 4.0 International license (<https://creativecommons.org/licenses/by/4.0/>).<sup>[245]</sup> Copyright 2021, The Authors, published by Wiley-VCH. c) A metal–dielectric–metal (MDM) structure consisting of two stacked identical nanohole arrays separated by a variable thickness silk fibroin layer. The nanohole arrays are slightly offset to produce a moiré pattern. The silk fibroin undergoes a controlled swelling in response to solvent uptake, creating a highly sensitive chemical sensor. Reproduced with permission.<sup>[246]</sup> Copyright 2018, American Chemical Society. d) A metasurface consisting of two angles and offset Au bars a liquid crystal cell. The liquid crystal molecules tilt in response to an applied voltage, leading to a calculated shift in the CD response. Reproduced with permission.<sup>[100]</sup> Copyright 2019, Elsevier. e) A crescent shaped Au nanostructure with an orientation dependent chiral plasmonic response. The extrinsic chiroptical response is created by altering the angle between the structure and the incident light. Reproduced with permission.<sup>[247]</sup> Copyright 2020, American Chemical Society.

by a thin dielectric spacer and arranged in a moiré pattern (see Figure 6c).<sup>[246,254]</sup> Since the response is governed by a coupled Fano-type resonance, the dielectric spacer thickness is critical to tuning the resonance. A dielectric spacer was prepared from silk fibroin extracted from the *Bombyx mori* cocoon. This material has been observed to swell up to 60% in volume in the presence of high-polarity solvents, with a high degree of reversibility depending on the solvent polarity. A large, reversible, shift in the CD spectral response (see  $>3^\circ$ ) was observed by successively exposing the system to cycles of isopropyl alcohol and water. A further benefit of this system is its ultra-thin size, making it ideal for integrated applications.

Liquid crystals, long rod-like molecules displaying a highly birefringent refractive index, can be easily reoriented in an electric field, making them prime candidates for reconfigurable optical control. These materials have been commonly utilized for decades in optical applications such as LCD displays and switchable polarization filters. More recently, liquid crystals have been combined with optical metasurface technology to enable active control over complex optical phenomena in both chiral<sup>[100,255,256]</sup> and non-chiral applications.<sup>[257–261]</sup> Yin et al., integrated a chiral Au bar metasurface structure as one side of a liquid crystal cell.<sup>[100]</sup> This structure was controlled by applying a voltage across the cell to reorient the liquid crystal molecules with respect to the metasurface structure (see Figure 6d).

A major shift in the CD spectral reflectance of  $\approx 75$  nm was demonstrated upon the liquid crystal reorientation.

Perhaps the most benign method of active control over the chiral response is the manipulation of extrinsically chiral passive metasurface designs post-fabrication.<sup>[104]</sup> Stevenson et al., recently showed how passive chiral metasurface systems can be manipulated by controlling the substrate orientation to generate an active chiral response (see Figure 6e).<sup>[247]</sup> This technique exploits the light–matter orientation dependence for plasmonic nanocrescent systems to dynamically control the extrinsic electromagnetic chirality. A huge modification of the normalized CD intensity ( $\Delta g = \pm 0.55$ ) was shown for modifications of the substrate orientation of  $\theta = \pm 30^\circ$ .

### 3.3. Optical Chirality Using Dielectric Structures

Along with plasmonic chiral metamaterials, another area of current interest in chiroptical metasurfaces is the creation of highly enhanced chiral fields utilizing all dielectric nanostructures. The chiral plasmonic metamaterials described above are generally based on metallic structures exhibiting a large plasmonic response, and we have outlined several important properties of optical plasmon modes which make them useful in this context. However, one major drawback of plasmonic enhancement is that plasmon modes enhance only the electric part of the local electromagnetic field, neglecting magnetic field enhancement. In many optical metasurface applications it is acceptable to neglect the magnetic part of the total field since the magnetic component is typically much weaker than the electric:  $\chi|\mathbf{B}|^2 \ll \alpha|\mathbf{E}|^2$ . However, this assumption can break down in certain situations, especially at or near nodes of electric field energy such as those responsible for superchiral fields, or generally in regions with low electric field strength.<sup>[52]</sup> Extreme plasmonic enhancement of the local field chirality is often correlated with such regions of low field strength, leading to suboptimal chiral field generation and opposing a mechanism of enhancing chiral preferential absorption.<sup>[54]</sup> To obtain optimal helicity of the local electromagnetic field, as seen in Equation (20), materials and structures must be considered which support both electric and magnetic multipole resonances.<sup>[55,106,108]</sup> This challenge is being met through the design and fabrication of all dielectric metamaterials,<sup>[262–264]</sup> where two important classes have emerged: dielectric nanoparticles and nanoantenna arrays.

Although dielectric nanoparticles (canonically nanospheres) are typically geometrically achiral structures, they are known to possess both electric and magnetic Mie resonances.<sup>[265]</sup> Furthermore, these resonances typically involve both near and far field interactions and can be altered by modifying the geometric dimensions, providing a convenient platform for tuning the system. Recently, Hanifeh and Capolino have simulated silicon nanospheres to determine the conditions necessary to achieve an “optimally chiral” nearfield for an array of nanoparticles, relating the desired condition to a relationship between the effective magnetic and electric polarizabilities.<sup>[266]</sup> Such an array would offer a significant improvement over current systems by both greatly enhancing the chiral asymmetry only locally near the metasurface, and not contributing to the fairfield CD response, eliminating the typical need to separate chiral responses from the sample and metasurface. Similarly,

Ho et al., have proposed an optical separation technique based on enhancing the chiral dissymmetry factor using silicon spherical nanoparticles.<sup>[54]</sup> By simulating both the electric and magnetic higher order multipole modes, they were able to produce a maximum sevenfold increase in the dissymmetry factor, which corresponds to a 170-fold increase in the CD signal. Critically, this was achieved by increasing the chirality in the local electric field without decreasing the electric field strength, leading to not only an increased chiral response, but also an enhancement in preferential chiral absorption beyond that observed for unaltered CPL.

Similar to nanosphere arrays, the optical antenna properties of dielectric metasurfaces can be harnessed to produce a chiral enhancement. Some geometries that have been explored include nanodisk dimers,<sup>[267]</sup> Z-shaped resonators,<sup>[268]</sup> cylinders,<sup>[269–271]</sup> and spherical trimers.<sup>[272]</sup> Nanodisk assemblies provide an interesting geometry to produce chiral enhancement since the electric and magnetic dipole resonances can be tuned nearly independently via the aspect ratio.<sup>[273]</sup> Also, these structures are interesting in the sense that a strong chiral response can be generated from achiral geometric arrays, highlighting the role of anisotropy versus geometric chirality in the generation of chiroptical activity. In a recent study, Solomon et al. simulated strong chiroptical activity in a periodic metasurface of Si nanodisks.<sup>[271]</sup> This geometry was shown to provide a large area enantiopure enhancements for both the chirality density and dissymmetry factor, leading to a potential for both chiral sensing and enantiomeric separation. By varying the disk radius, volumetric enhancements of 30-fold and 4.2-fold were observed for *C* and *g*, respectively. Critically, the handedness of the chiral enhancement was also found to be global to the metasurface, which is important for large scale implementations. Nanodisk geometries were also recently explored by Zhao and Reinhard, both theoretically and experimentally, for chiral field generation in dimers of silicon nanodisks.<sup>[267]</sup> A strong near-field chirality enhancement was found in the gap between the nanodisks when the structure was illuminated with linear polarized light and the handedness of the chiral field could be altered by changing the state of linear polarization. In another study, Ma et al., proposed an all dielectric metasurface based on an array of germanium z-shaped nanoresonators.<sup>[268]</sup> In this geometry there is a significant cross polarization generation based on breaking the in-plane mirror symmetry, and the transmitted light (of only a single circularly polarized component) can be endowed with a designed geometric phase factor based solely on manipulating the angle of the metasurface element. This suite of properties holds promise for future optical applications since the metasurface can effectively mimic the phase transmission of a wide range of optical components, including 2D hologram generation. By harnessing a wide range of chiroptical properties, dielectric metamaterials are poised to produce important advances in the functionality of chiral as well as general optical metasurfaces.

## 4. Applications

The study of chiral light–matter interactions has driven important developments in a variety of diverse scientific fields, including biophysics, biophotonics,<sup>[274–276]</sup> astrobiology,<sup>[277,278]</sup>

and quantum optics.<sup>[279–281]</sup> In particular, the usefulness of chiroptical techniques in the life sciences has long been recognized: the first experimental application of chiroptical techniques, dating back to the 1960s, was using circular dichroism to study alpha-helices in proteins,<sup>[282,283]</sup> which emerged from earlier theoretical interest in the ORD of helical polymers.<sup>[30,284]</sup> The biological applications of chiroptics mainly fall into two broad categories: i) investigations of how chiral structures influence basic biological functions; ii) identifying enantiomers of chiral biomolecules as markers for disease detection and prognosis. Beyond these applications, the revolutionary discovery of exoplanets in the last 3 decades has revitalized interest in using chiral biosignatures to search for extraterrestrial life. In the following sections, we highlight a number of studies illustrating each of these different facets of chirality in biology, and the role of optics in their past and future exploration. The first sections look at the way chirality impacts biological function at different scales of organization, from individual molecules, to cells and to entire organs. We then summarize recent progress in discovering predictive chiral biomarkers for disease. One frontier in the quest to obtain highly sensitive and specific biosensors for medical applications is the development of enhanced optical techniques for detecting low concentrations of specific enantiomers, surpassing traditional approaches like CD spectroscopy. The final two sections consider more speculative applications which have been of growing interest in the last few years: chiral

biomarkers for extraterrestrial life, and chirality in biological processes involving coherent quantum phenomena.

## 4.1. The Role of Chiral Molecules in Biological Function

### 4.1.1. Chiral Regulation of DNA Function

All forms of DNA found in nature are intrinsically chiral, with the most common configuration (known as B-DNA) forming a double-stranded right-handed helix. This chirality has significant implications for the functional interactions of DNA with proteins and drug molecules, various aspects of which can be probed by optical methods. To motivate the discussion, we begin with a summary of the relevant DNA biophysics. At the most basic level chirality introduces an asymmetry when the DNA is under torsional stress (see **Figure 7a**): negative torques, acting opposite to the helical orientation (undertwist), tend to decrease the helicity and lower the energetic barrier to separating the two strands; in contrast, positive torques (overtwist) tend to make the DNA more stable against strand separation.<sup>[285]</sup> Since fundamental biological processes such as DNA replication and transcription require transiently opening up the two strands, most organisms facilitate these functions by keeping their DNA on average under a small negative torsional stress through a variety of DNA-binding enzymes.<sup>[285,286]</sup> Hyperthermophiles, organisms which optimally grow at temperatures

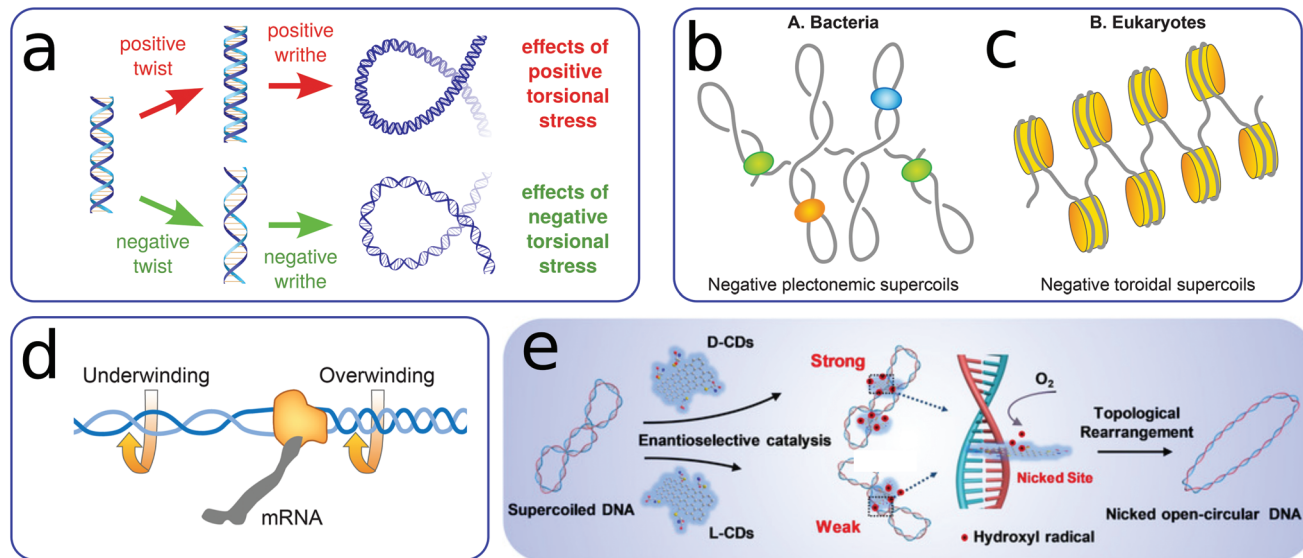


**Figure 7.** The role of chirality in DNA function. a) DNA responds asymmetrically to negative and positive torsional stress, which affects helical structure (twist) and can lead to chains crossing over themselves (writhe) in supercoils. DNA-binding enzymes like Type I and II topoisomerases (Topo I/II) can relieve the torsional stress accumulated during regular cellular function. b,c) Supercoiling takes a variety of forms in different classes of organisms, influenced by DNA-binding proteins: in bacteria, supercoils form figure-eight-like plectonemes, either free or anchored by proteins (colored ovals) (b); in eukaryotes toroidal supercoils are formed when DNA is looped around histone proteins (orange) for packaging in chromatin (c). d) Torsional stress is an inevitable byproduct of gene expression. An RNA polymerase moving along DNA toward the right, transcribing it into messenger RNA, produces positive stress (overwinding) ahead of itself, and negative stress (underwinding) behind it. b–d) Reproduced under terms of the CC0 public domain dedication.<sup>[288]</sup> Published by PLOS, 2019. e) A synthetic enzyme based on a chiral carbon dot that interacts with DNA enantioselectively. The D-form binds strongly, intercalating itself into the DNA and catalyzing the cleavage of one strand by generating reactive oxygen species. This relieves torsional stress in the DNA, partially mimicking the behavior of natural topoisomerase enzymes. Reproduced with permission.<sup>[289]</sup> Copyright 2020, Wiley-VCH.

above 85 ° C, are interesting exceptions. As double-stranded DNA is more unstable under such conditions, these organisms compensate in the opposite direction, using a reverse gyrase enzyme that induces positive torsion.<sup>[287]</sup>

Since torsional stress would quickly relax if the ends of the DNA chain were free to twist, some kind of constraint must be present to prevent this relaxation: either the whole chain forms a loop (like circular plasmid DNA in bacteria), or different points on the chain are clamped together by proteins, forming topological domains in which torsional stress can be maintained.<sup>[288]</sup> These induced stresses affect not only the local properties of the DNA chain, but also its larger-scale structure and the way genetic material is packaged inside cells. Negative or positive twist can be converted into writhe, where the entire DNA chain crosses over itself in so-called supercoiled structures (i.e., figure-eights). As seen in Figure 7a, negative torsional stress leads to negative writhe, defined by the following sign convention: if you project the chain contour onto a plane and move along it in one direction, the writhe is negative if every time a crossing is encountered the lower chain passes from the left side to the right side of the upper chain; it is positive if the chain passes from right-to-left. In bacterial DNA the negative writhe is accommodated in intertwining figure-eight-like structures known as plectonemic supercoils (Figure 7b), while in eukaryotes—like humans—it manifests as left-handed loops in the DNA chain around histone proteins, forming toroidal supercoils (Figure 7c).<sup>[288]</sup> The latter allows long DNA chains to be compactly packaged as chromatin within cell nuclei.

The situation is made more complicated by the fact that torsional stress in DNA is not static: the cellular machinery that transiently opens up DNA strands in order to replicate the chain or to transcribe genes into messenger RNA also induces significant torque on the DNA. For example, as RNA polymerase II (Pol II) moves along the chain carrying out transcription, it creates positive torsional stress ahead of itself, and negative stress in its wake<sup>[288,290,291]</sup> (see Figure 7d). Without any mechanism of relief, this stress would accumulate to dangerous levels that could catastrophically destabilize the DNA and lead to cell death. Hence the importance of specialized enzymes known as topoisomerases, which bind ahead and behind the transcription machinery to relieve torsional stress. Type I topoisomerases (Topo I) alter twist by cleaving and then reattaching one of the DNA strands, while Type II enzymes (Topo II) alter the writhe by doing the same with both strands simultaneously.<sup>[286]</sup> However, allowing some amount of extra torsional stress is actually essential for transcription: the positive stress ahead of Pol II makes histone unbinding more favorable (since it counteracts the left-handed looping), and helps to clear the path for the passing transcription machinery. Conversely, the negative stress behind Pol II favors the rebinding of histones and reassembly of the chromatin structure.<sup>[292]</sup>

Many features of DNA torsional biophysics are amenable to interrogation through non-invasive chiroptical techniques. Indeed, one of the most surprising discoveries in DNA structure was made through circular dichroism in the early 1970s. Observations of unusual reversed CD spectra for DNA fragments were inferred to correspond to a left-handed helix structure.<sup>[293,294]</sup> This configuration, later confirmed through X-ray crystallography<sup>[295]</sup> and called Z-DNA, can occur in living

organisms as alternative, higher-energy pathway to accommodate negative torsional stress, in addition to supercoiling.<sup>[296]</sup> Transient conversion of B-DNA to Z-DNA can occur naturally in the negative torsional wake of Pol II transcription. However, misregulation of Z-DNA is also implicated in disease:<sup>[297]</sup> CD studies have shown elevated Z-DNA levels in the hippocampus of severely affected Alzheimer's patients,<sup>[298]</sup> and the autoimmune disorder systemic lupus erythematosus produces antibodies specific to Z-DNA.<sup>[299]</sup>

CD studies can also shed light on drug therapies that affect topoisomerase function. Because these enzymes are crucial for normal DNA replication and transcription, they are important clinical targets for antibiotics and cancer drugs.<sup>[300]</sup> Fluoroquinolones, one of the most commonly used families of antibiotics, inhibit bacterial Topo II from reattaching DNA after cleavage, leading to a proliferation of damaged DNA that causes the bacterial cell to die.<sup>[301]</sup> Anthracycline drugs like doxorubicin act similarly against eukaryotic Topo II, and hence are used as cancer chemotherapy agents to attack rapidly proliferating tumor cells.<sup>[302]</sup> All these Topo II inhibitors drugs intercalate DNA, inserting themselves between neighboring base pairs and interacting with the enzyme to block DNA reattachment. This intercalation perturbs the local chiral structure of the DNA in a way that is detectable by CD.<sup>[303]</sup>

Finally, there is recent interest in designing synthetic chiral nanoparticles that mimic some of the functions of natural DNA-binding enzymes. Notable examples include chiral quantum dots that can cleave proteins or DNA. One DNA cleavage system used a tetrahedral CdTe nanoparticle, with an attached  $\iota$  enantiomer of cysteine. This could be excited by circularly polarized light to fully cleave DNA at a specific location via the generation of reactive oxygen species. Another synthetic enzyme, a chiral carbon dot (Figure 7e), is able to intercalate DNA and mimic the cleavage behavior of Topo I by cutting just one strand of the DNA (again using reactive oxygen species).<sup>[289]</sup> The carbon dot interacts with DNA enantioselectively, with the  $\nu$ -form of the dot more effective than the  $\iota$ -form. Despite missing Topo I's ability to reattach the DNA strand after cleavage, the carbon dot was able to regulate supercoiling in plasmid DNA in way reminiscent of Topo I, enhancing gene expression from the plasmid.

#### 4.1.2. Multiscale Chirality: Intrinsic Molecular Chirality Influences Larger-Scale Functionality

Interestingly, chirality exists in biology not only at the molecular level, but also at a macroscopic scale. Living organisms exhibit multilevel asymmetries from the molecular to the cellular level, which can in turn affect the tissue, organismal, and behavioral levels. At the organismal level, morphological asymmetries can represent key features in animal bodies, from snail shell coiling to the distribution of human body organs.<sup>[304]</sup> The occurrence of left-right (L/R) asymmetry in the early stages of embryonic development is critical for the proper location and morphogenesis of visceral organs (heart, lungs, stomach, intestine, and kidneys).<sup>[305]</sup> For example, the human heart is shifted slightly to the left, and consequently the lung on the corresponding side is slightly smaller than the other. Incorrect

development of L/R asymmetry underlies many pathological conditions, such as congenital heart disease, and is also a major cause of miscarriage.<sup>[306]</sup>

It is a widely debated question whether the macroscopic asymmetries of living organisms are linked to or, even more strongly, dictated by biomolecular chirality. The fruit fly (*Drosophila melanogaster*) presents an interesting case study.<sup>[306]</sup> The L/R asymmetry of the fruit fly involves not only asymmetric positioning of organs, but also chiral looping for tubular organs like the spermiduct, which twists around the hindgut in a right-handed loop. Remarkably, this large scale right-handed chiral organization is controlled by a single protein, myosin 1D (Myo1D). Myosins are a class of motor proteins that perform numerous functions within cells, contributing to cell motility, the transport of internal organelles, and the contraction of muscle fibers. They do so by binding and exerting forces on actin—a chiral protein that forms long double-stranded helices—in the cell cytoskeleton. The mechanical forces on the actin cytoskeleton influence cell shape, which in turn dictates tissue organization. By this mechanism, the structure of entire organs can be controlled. In the case of Myo1D, a recent study established the basic molecular mechanism that initiates this hierarchy of larger-scale consequences.<sup>[307]</sup> An in vitro assay in which actin filaments were allowed to glide over a surface coated with Myo1D showed that the filaments were driven in circular, counterclockwise paths. This is in contrast to another fruit fly myosin protein, Myo1C, which exhibited much straighter paths. The latter is typical for most myosin proteins, which exert forces roughly parallel to the actin axis. The inherent chirality of the Myo1D–actin interaction—the ability of Myo1D to exert a chiral rotational force on actin—plays itself out at all higher levels. In fact, by forcing the expression Myo1D in typically symmetrical fruit fly organs (where it is normally not expressed) such as the trachea, an unnatural right-handed twist can be induced on the organ (see Figure 8). Similarly, the forced expression of Myo1D in the fruit fly larval epidermis provokes a right-handed twist of the entire body. The altered body morphology interfered with the normal crawling ability of the larvae, and forced it to move via rolling instead. The same experiments done with Myo1C instead of Myo1D lead to analogous consequences, but with left-handed instead

of right-handed twists. The exact mechanism for these opposite results with Myo1c is not fully understood, since Myo1c did not induce actin rotation in the gliding assays. But apparently over-expressing it alters the force balance between different motor types in the organism sufficiently to generate a large-scale twist.

The significance of Myo1D is not only confined to a single organism: it has also been shown to be essential in the development of L/R asymmetry in zebrafish.<sup>[308]</sup> Thus, a simple chiral molecular mechanism is capable of triggering chiral organization from the nano- to the macroscale in both an invertebrate and a vertebrate. As is often the case in biology, insights into fundamental processes can also give inspiration to engineered designs. Actin is an attractive building block for functional nanomaterials due to its biocompatibility, low cost, and controllable, scalable self-assembly.<sup>[309]</sup> Mechanisms like the Myo1D–actin interaction might point a way toward creating self-assembled materials exhibiting chirality at multiple scales. This could potentially provide another avenue for fabricating optically interesting chiral materials, similar to the self-assembled DNA origami approach discussed earlier. Moreover, such materials would be inherently reconfigurable, dependent on external influences such as the concentration of the fuel molecule ATP or competing motors like Myo1C. Changing these concentrations affects motor functionality, allowing tunability of the chiral structure and consequently the chiroptical response.

#### 4.2. Predictive Chiral Biomarkers

The close relationship between biomolecular chirality and functionality, highlighted in the above discussion, also suggests potential medical applications: measured levels of specific chiral molecules can serve as biomarkers for disease diagnosis and prognosis. These biomarkers are ideal targets for highly sensitive chiroptical techniques that discriminate among enantiomers (as described in the next section). Several classes of chiral molecules have been investigated for their potential as predictive biomarker potential. Among these are:

1. Metabolites: The small molecules produced by cellular metabolic pathways have gained increased attention in cancer

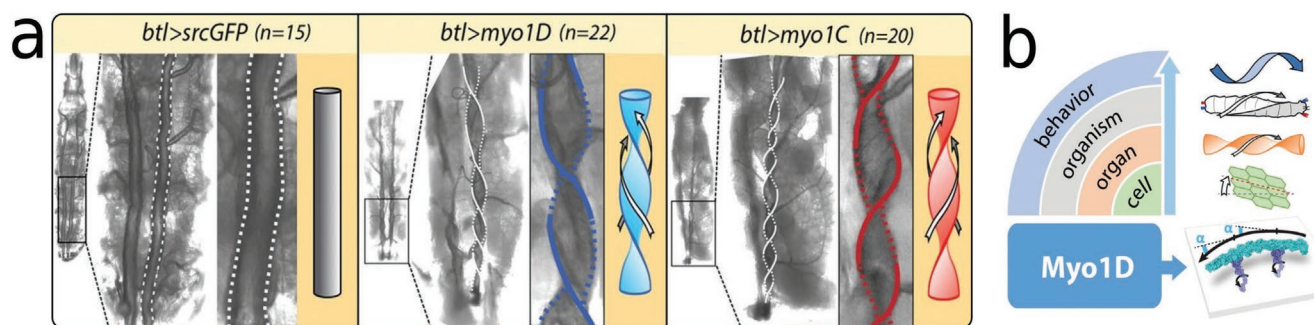


**Figure 8.** Multilevel asymmetry induced in the fruit fly *Drosophila melanogaster* by the myosin protein (Myo1D/1C). a) Left: The trachea in a control fruit fly larvae, showing a linear morphology; Center: right-handed twisting of the trachea after induced expression of Myo1D; Right: left-handed twisting of the trachea after the induced expression of Myo1C. Myo1C acts as an antagonist for the dextral activity of Myo1D. b) Myo1D chiral action occurs throughout increasing biological functional levels. The bottom sketch shows an actin strand (light blue) interacting with Myo1D (violet). Myo1D forces the actin to turn through an angle  $\alpha$ . The chiral interaction between Myo1D and actin leads to asymmetry at the cell, organ, and whole-body levels. a,b) Reproduced with permission.<sup>[307]</sup> Copyright 2018, The Authors, published by American Association for the Advancement of Science (AAAS).

research.<sup>[310]</sup> It has been shown that mutations in enzymes could lead to the production of new chiral metabolites that promote cancer development and progression.<sup>[311]</sup> As an example, mutations in isocitrate dehydrogenase 1 (IDH1) and 2 (IDH2) genes characterize both low-grade and high-grade glioma patients.<sup>[312]</sup> The activity of the mutated IDH1/2 enzymes results in the elevated production of the D-enantiomer of the metabolite 2-hydroxyglutarate both locally in the brain tissue and systemically.<sup>[313]</sup>

2. Byproducts of oxidative stress: Several disorders including cancer, atherosclerosis, and neurodegenerative diseases are associated with molecular oxidation caused by free radicals. However, quantifying and isolating free radicals is not an easy task. Hence the detection of their reaction products is often investigated to yield biomarkers for oxidative stress-related diseases. Among those products there are isoprostanes, arising from the oxidative degradation of fatty acids catalyzed by free radicals. Isoprostane regioisomers (like the cis-configured F<sub>2</sub>-isoprostane) in biological fluids such as blood, urine, and cerebrospinal fluid are candidate biomarkers to evaluate the pathological progression of diseases like Alzheimer's.<sup>[314]</sup>
3. Amino acids: D-Amino acids (D-AAAs) are present in microorganisms, animals, plants and humans, with a relatively low concentration compared to their L-enantiomers (L-AAAs). Researchers are increasingly devoting efforts to detecting specific D-AAAs in the human body as biomarkers for age-related disorders such as cataracts and atherosclerosis, and neurological diseases such as schizophrenia and amyotrophic lateral sclerosis (ALS).<sup>[315]</sup> For example, in a mammal's brain, it is suggested that D-serine (D-Ser) is correlated with the sugar metabolism of astrocytes in the early stages of cognitive decline.<sup>[316]</sup> Furthermore, a sudden increase in levels of serine racemase, the enzyme that converts L-Ser to D-Ser, is linked with neuroinflammation and aging, clear signs of an ongoing neurodegenerative disease.<sup>[317]</sup> Therefore, Kimura et al.,<sup>[318]</sup> proposed the enantiomeric proportion of D-AAAs as promising chiral candidate biomarkers for dementia diagnosis. By means of chiral metabolomics, a recognition technique for detecting small differences in chiral AA amounts, a link was established between the proportion of D-AAAs and early cognitive decline. This proposed method for diagnosing the risk of cognitive decline showed both high accuracy (sub-femtomole levels) and high throughput. Relationships between D-AAAs and other diseases, including ALS and renal failure, have also been reported. The amounts of D-Ser in the spinal cord of ALS model mice significantly increased compared to those in the control mice, and the alteration can be associated with the progression of the disease.<sup>[319]</sup> In the serum and urine of acute kidney injury model mice, drastic changes in the D-Ser amounts are observed.<sup>[320]</sup> In the case of human chronic kidney disease patients, the levels of several D-AAAs including serine, proline, and alanine significantly increased as the disease progressed.<sup>[321]</sup> These results indicate the potential of D-AAAs as new biomarkers of renal failure. Further clinical evaluations are expected. Du et al.,<sup>[322]</sup> experimentally investigated the potential functional role of D-AA accumulation in tumor cell proliferation, showing that human MCF-7 breast cancer cells contain up to 22 times more specific

D-AA than non-cancerous epithelial cells. Furthermore, it was demonstrated that the metabolism of cancer cells can be influenced by the D-AA concentration in the extracellular environment, indicating a potentially critical role in tumor cell proliferation.<sup>[323]</sup> Finally, D-AAAs may prove useful as molecular fingerprints to distinguish bacterial types: for example, *Vibrio cholerae*, the gram-negative bacterium that causes cholera, is known to produce specifically D-methionine and D-leucine.<sup>[324]</sup>

#### 4.2.1. Enantioselective Sensing Techniques

Given the potential importance of chiral biomolecules as disease biomarkers,<sup>[325]</sup> research into the design, construction, and application of point-of-care devices with enantioselective sensing properties has been rapidly expanding. Since chiral enantiomers possess almost indistinguishable physical/chemical characteristics except for the interaction with other enantiomeric compounds and chiral light, there is an ongoing effort to identify highly sensitive and effective methods to quantify and discriminate the chiral enantiomers present in a mixture. Furthermore, the chiral discrimination of one specific enantiomer is fundamental for pharmaceuticals existing as stereoisomers, with each enantiomer having different biological, pharmacodynamic, and pharmacokinetic properties. The body's metabolism of such chiral medicines, as well as their interaction with the external environment, can alter the compound inducing an interconversion of enantiomers.<sup>[326,327]</sup> This chiral switching effect can lead to unpredicted toxicity inside the organism, underlining the necessity to implement efficient enantioselective detection methods.

High-performance liquid chromatography methods, gas chromatography, and capillary electrophoresis, are among the conventional separation-based techniques for chiral discrimination of enantiomers. However such separation-based methods can be time-consuming, expensive, and are difficult to adapt for point-of-care devices.<sup>[328]</sup> Established chiroptical techniques such as CD spectroscopy and chiral polarimetry provide alternative approaches, but these methods also suffer from limitations, including a lack of sensitivity to biomolecules with a small molecular mass. This lack of sensitivity is due to weak light-matter interaction. In order to push the efficiency of the enantiomeric discrimination at low molar sensitivity, plasmonic chiral metamaterials have been proposed, with promising results in terms of chiroptical signal enhancement and integration with lab-on-chip biomedical devices.<sup>[146,147]</sup> Exploiting superchiral surface waves as a means to intensify the enantioselective forces has the potential to push this methodology even further, allowing for all-optical separation of enantiomeric compounds.<sup>[329]</sup> However, the phenomenon of *false* chirality should also be taken into account for enantiomeric discrimination. This effect describes systems where the two chiral states are interconverted via time reversal and space inversion. This is in contrast to *true* chirality where the two states are interconverted via spatial inversion and not by time reversal symmetry combined with spatial rotation.<sup>[330,331]</sup> For instance, collinear electric and magnetic fields form a falsely chiral influence. This distinction is important since only truly chiral states induce the separation of enantiomers in all cases.<sup>[332]</sup>

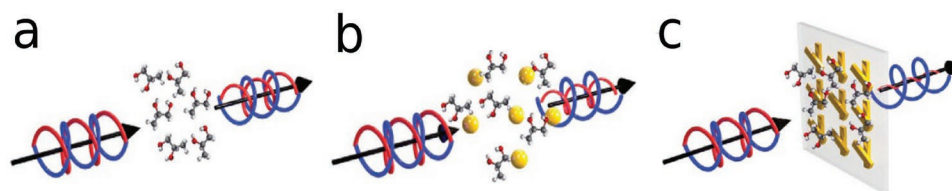


**Figure 9.** Scheme of CD signal enhancement and plasmonic chiral metasurface detection. a) The interaction between circularly polarized light and chiral molecules produces a relatively weak chiroptical response. b) The synergy between chiral molecules and achiral plasmonic nanostructures amplifies the chiroptical response through surface plasmon resonance. c) Advanced chiral detection with chiral plasmonic metamaterials. These systems can significantly increase the molecular chiroptical response. a–c) Reproduced under the terms of the CC-BY Creative Commons Attribution 4.0 International license (<https://creativecommons.org/licenses/by/4.0>).<sup>[333]</sup> Copyright 2017, The Authors, published by Springer Nature.

The first chiral biosensing technology using a metasurface was reported by Hendry et al., in 2010,<sup>[51]</sup> in which a monolayer gammadion structure was exploited as a sensing platform for a variety of proteins. The method was especially sensitive to proteins with high  $\beta$ -sheet content, giving it the potential to detect molecules such as  $\beta$ -structured amyloid plaques, which have a decisive role in diseases such as Parkinson's disease, Alzheimer's disease, and transmissible spongiform encephalopathies. The optical phenomenon utilized in this work was a spectral shift in the far-field spectrum, which is caused by the near-field interactions between the chiral molecules and the metasurface. Subsequent papers have achieved similar results by exploiting the enhanced sensitivity of superchiral evanescent fields to the chiral structure of different biomolecules.<sup>[334–337]</sup> By utilizing the locally intense chiral light–matter interaction at a twisted metamaterial platform surface, Zhao et al., have reached picogram precision for the enantioselective discrimination of biomolecules over a large interval of molecular weights.<sup>[333]</sup> Furthermore this plasmonic “twisted” metamaterial provides a clear detection of molecular handedness, resolving the ambiguity that arises from analyzing only the spectral shift due to alterations in the refractive index. By combining an intertwined pair of metamaterial structures with opposite rotations, the researchers were able to suppress the background CD response from the metamaterial, thereby isolating the chiroptical response of the target biomolecule and enabling a clearer identification of its chiroptical properties. Despite the high sensitivity achieved by these chiral spectroscopic techniques (reaching  $\approx 44$  molecules per unit cell of the metamaterial, corresponding to a sensitivity of  $\approx 55$  zeptomoles of molecules), the concentration of sample necessary for accurate detection must not be below a certain threshold ( $\approx 1$  mM), due to the nanometer-scale working distance between the analyte and the sensing surface. One solution recently proposed by Liu et al., is to exploit Marangoni convection generated from microbubbles to accumulate the sample on the surface, allowing chiral sensing of metabolites in diabetes at concentrations down to 100 pM.<sup>[338]</sup>

Such a metamaterial platform can be incorporated in a micro-/nanofluidic device, flowing the chiral molecules between the twisted layers instead of working from the top, further increasing the enantioselective precision. Indeed, microfluidic chips in general offer a promising route to more efficient sensing devices. For example, electrochemical detection in microfluidic devices exhibits high sensitivity, inherent ease of miniaturization, and high compatibility with micro- and nanotechnologies.<sup>[341]</sup> Microfluidic platforms are also ideal

for multiplex detection, since independent channels allow for parallel, real-time detection at different sensing sites.<sup>[342]</sup>

Another avenue for enhancement would be using plasmonic metamaterials, which allow not only high sensitivity but also widening and shifting the CD band of the molecules. This advantage is not to be overlooked, since CD spectra in the UV range often contain important structural information about biomolecules (such as the secondary and tertiary structure of proteins). Shifting the phenomenon into the visible allows one to minimize degradation of the biomolecules, which would occur during prolonged UV exposure.

Recently the idea of synergistically combining inorganic nanomaterials and chiral biomolecules (see **Figure 9**) in order to obtain a hybrid object with an amplified and shifted chiral response, in the visible and near-infrared ranges, is increasingly gaining ground.<sup>[6,343–345]</sup> Biomolecule-mediated chiral nanostructures<sup>[346]</sup> have potential applications in chiroptical biosensing, enantiomer discrimination, and clinical theranostics. Metallic nanoparticles amplify the chirality through the localized surface plasmon resonance effect (see **Figure 9b**) and intensify the absorption CD peak. At the same time, chiral biomolecules can be exploited to control the position of the achiral building block at the nanoscale.<sup>[347]</sup> Li et al., were the first to develop a hybrid chiral technology capable of detecting microRNAs (i.e., miR-21, a cancer biomarker) in the cellular environment in real time via DNA-driven nanoassembly.<sup>[339]</sup> The hybrid sensing pyramid-like architecture is made of gold nanoparticles (AuNPs) assembled with upconversion nanoparticles (UCNPs) via a nucleic acid skeleton (DNA frame) (see **Figure 10a**). Thanks to the presence of recognition sequences of microRNA, the hybrid system works as a chiroplasmonic sensing structure, with attomolar sensitivity. The physical detection mechanism relies on double functionality. When the pyramid, through the complementary DNA sequences, detects the microRNA in the intracellular environment, it disassembles and its chiral properties disappear and the luminescent signal emerges. The CD signals show a linear correlation with the intracellular miRNA concentration (see **Figure 10b**). In addition to microRNA detection, these technologies can also be adapted for chiral sensing of small peptides and proteins, using an antigen–antibody pair to bond plasmonic nanoparticles.<sup>[340]</sup> In this case, the proposed system has a simpler structure, consisting of two NPs, AuNP and AgNP, linked to form a heterodimer with chiral properties via an antigen–antibody bridge (see **Figure 10c**). This system allows the detection, through CD signal analysis, of both small molecules such as MCLR (an environmental toxin) and larger molecules such as PSA,

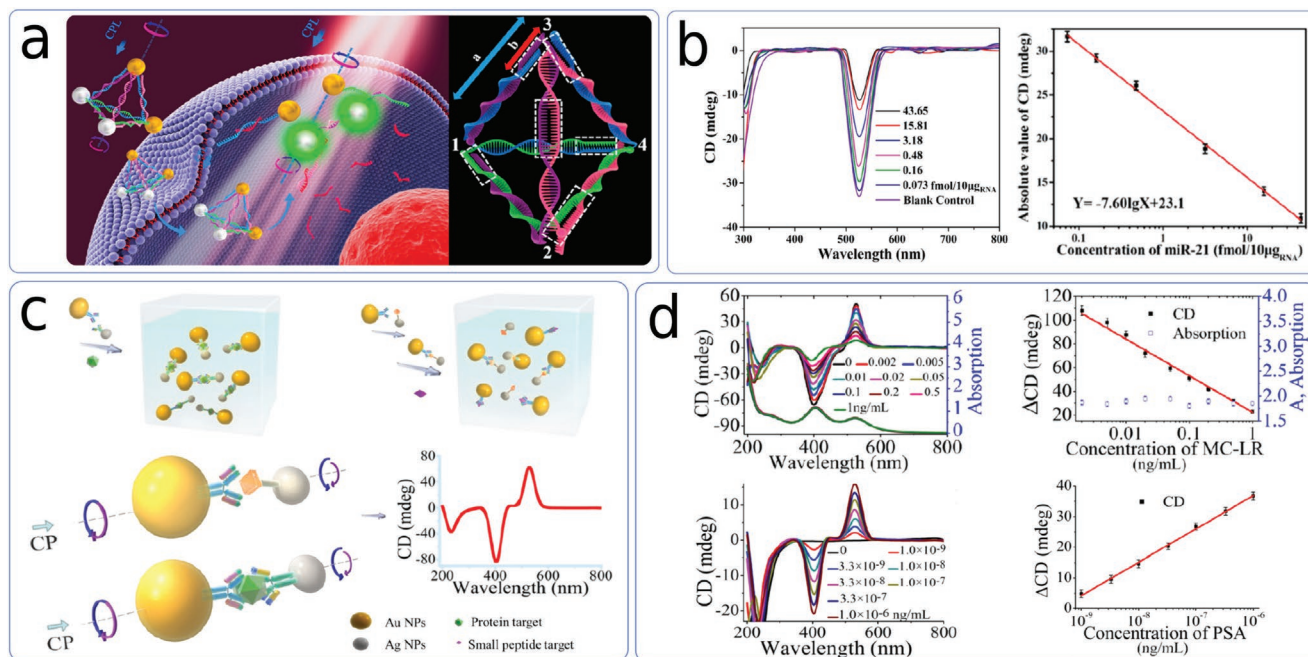


**Figure 10.** Detection of biomolecules with advanced optical materials. a) DNA-driven self-assembled pyramids with gold nanoparticles (AuNPs) and upconversion nanoparticles (UCNPs). Dual-signal mode intracellular microRNA detection is based on: i) the luminescence signal from UCNPs; and ii) the CD signal from prolate AuNPs in UV region. MicroRNA recognition sequences are shown in blue, while non-complementary part is shown in red. When microRNA is present, the DNA frame dissociates. b) CD spectra (left) and CD plot (right) at 521 nm wavelength with different concentrations of intracellular microRNA. The CD intensity decreases linearly as the concentration of microRNA increases. a,b) Reproduced with permission.<sup>[339]</sup> Copyright 2015, American Chemical Society. c) Plasmonic heterodimers: AgNP + AuNP connected by antigen-antibody bridges, useful for small peptide and large protein detection thanks to a strong CD signal. d) Top: CD and UV absorption spectra with increasing concentration of MCLR solution along with the linear correlation. Bottom: CD spectra with increasing concentration of PSA solution along with the linear correlation. c,d) Reproduced with permission.<sup>[340]</sup> Copyright 2013, American Chemical Society.

a cancer biomarker in serum (see Figure 10d). The sensitivity achieved is very high:  $10^{-13}$  M for the detection of MCLR, and  $10^{-20}$  M for the detection of PSA.

#### 4.3. Using Chirality as a Biomarker for Extraterrestrial Life

As mentioned above, L-enantiomer amino acids (L-AAs) are observed to predominate in living systems. Similarly, DNA and RNA are seen to preferentially incorporate right-handed sugars (D-deoxyribose and D-ribose, respectively). This homochirality is a striking chemical signature of all life on Earth.<sup>[348,349]</sup> Though its origin and significance are not completely understood, homochirality may be a prerequisite for any kind of amino-acid-based life: although artificial proteins involving a mixture of L-AAs and D-AAs can fold into structures resembling ordinary homochiral proteins, these structures have fewer internal hydrogen bonds and consequently are less thermodynamically stable.<sup>[350]</sup> Thus, natural selection for the more stable L-AA dominated proteins could have eventually led to the homochirality seen in all modern organisms. However, as discussed below, the observed L-AA homochirality—as opposed to D-AA—in terrestrial life could simply be a result of the inherent randomness of evolution, perhaps biased by a pre-existing excess of L-AAs in our solar system arising from non-biological processes. If life on other planets relies on a biochemistry similar to that employed on Earth, analogous selective processes might be

expected. In that case, excessive ratios of AA enantiomers (favoring either L or D -AAs) in extraterrestrial samples could be an indicator of extraterrestrial life.

Our main source of extraterrestrial samples to date has been from debris such as meteorites or interplanetary dust particles reaching the Earth's surface. This accumulated material totals about  $10^7$  kg each year.<sup>[351]</sup> One particular class of meteorites, carbonaceous chondrites, contains carbon up to several percent by weight, mainly in the form of organic compounds including AAs. The Murchison meteorite of 1969, belonging to this class, inaugurated the study of extraterrestrial AAs when analysis revealed the presence of a variety of AAs, including glycine, alanine, and valine.<sup>[352]</sup> This surprising result paved the way for subsequent analysis of AAs in other meteoritic samples, including the measurement of L and D-enantiomeric excess. From these studies a complex picture has emerged: certain AAs show up with a large enantiomeric excess, while others are approximately racemic (equal mixtures of L and D). This was the case with the Tagish Lake meteorite, where  $\approx 60\%$  more L than D-aspartic acid was found, relative to the total amount of both, while other AAs in the same meteorite such as alanine were approximately racemic.<sup>[351]</sup> Interpretation of these results is made more complicated by the fact that AAs undergo a slow process of stochastic conversion from one enantiomer to the other over geological time scales. Thus all meteorite AAs will eventually become racemic, but the process occurs at different rates for different AAs under various external conditions. This

implies that the measured enantiomeric excesses are not necessarily the same as those at time of the meteorite formation. Despite this caveat, an interesting pattern has emerged: where AA enantiomer asymmetries exist in meteorites, the L form is almost exclusively dominant, just as in life on Earth. However, based on other indicators (such as isotope composition and the distribution of AA types), the general consensus is that this does not reflect a biological origin for meteorite AAs.<sup>[351]</sup>

Nonetheless, non-biological chiral AA formation could still have played a significant role in the origins of life. Extrapolating backward to the early Earth, the observed L-AA bias could have been seeded during heavy bombardment by space debris around 4 billion years ago. This timeline coincides with the emergence of life on Earth. However, this explanation leads to the question of how the L-bias first arose in meteorites, since non-biological chemical pathways for AA formation generally lead to racemic mixtures.<sup>[351]</sup> One well-studied proposed resolution to this question involves the exposure of an initially racemic mixture of AAs to circularly polarized UV light.<sup>[353,354]</sup> AA enantiomers are known to absorb CPL differently depending on their handedness relative to the incident light, leading to different rates of photodegradation. Experiments have shown that this process can create enantiomer excesses on the order of several percent. While UV CPL would not be sufficient in itself to explain the AA enantiomer compositions seen in meteorites, it could act in conjunction with chemical mechanisms to amplify an existing enantiomeric excess.<sup>[351]</sup> A plausible candidate for sources of CPL in the early solar system is clouds of interstellar dust in regions where massive stars are forming. Light reflected from such clouds (i.e., in the Orion complex) is known to exhibit circular polarization.<sup>[354]</sup> In addition to UV CPL, alternative explanations have also been proposed, for example magnetically polarized cosmic rays.<sup>[355]</sup>

Understanding these chiroptical mechanisms for biomolecular symmetry breaking is relevant not just for life on Earth, but also in the search for extraterrestrial life. Creating a reliable rubric for identifying the signatures of extraterrestrial life requires precisely quantifying all non-biological processes (like UV CPL) which could potentially create enantiomer excesses. While significant experimental progress has been made in quantifying the CPL interaction with AAs, more work still needs to be done to demonstrate whether CPL can induce an analogous symmetry breaking in sugars.<sup>[354]</sup> This is relevant to the search for extraterrestrial life, since sugar acids in meteorites have been found to exhibit D-enantiomer excesses. Research in these directions is becoming more urgent as our access to extraterrestrial samples is rapidly increasing. For example, the Mars Organic Molecule Analyzer (MOMA) instrument, part of the 2022 ExoMars rover mission, will enable detailed analysis of chiral biomolecules from Martian samples. Future technological advances may also enable the use of chiroptical methods to directly measure the optical signature of enantiomer ratios in distant extraterrestrial environments, such as plumes from ice volcanoes on Europa or Titan.<sup>[356]</sup>

#### 4.4. Chirality in Quantum Biology

Chirality has also found implications in apparently distant and disconnected fields, such as quantum mechanics and life

sciences. In this regard, several efforts have been made to provide a physical interpretation of the quantum coherent phenomena in biology in recent years.<sup>[357]</sup> For example, quantum mechanics is required to describe photoactivated mechanisms mediated by light-sensing proteins. Such biological photoreceptors, thanks to the presence of chromophores, absorb photons and then undergo a change in their excited states.<sup>[358]</sup> Naturally occurring mechanisms, like the rhodopsin photoisomerization activated by light absorption—rhodopsin is the retinal molecule mediated primary event in vision—are strictly dependent on quantum-mechanical processes of the electronic states such as the position of the potential energy surfaces and the symmetries of electronic states.<sup>[359]</sup> In addition, other biological functions may depend on electron tunneling, like in respiration and photosynthesis. One interesting example is related to our sense of smell and the chiral interaction between left- and right-handed forms of enantiomers with different receptors. Recent experimental data suggests the reason for our enhanced olfactory sensitivity is a mechanism of phonon-assisted inelastic tunneling of an electron from a donor to an acceptor mediated by the odorant molecule.<sup>[360]</sup> In this regard, Franco et al.<sup>[361]</sup> reported that fruit flies can distinguish between the heavier (deuterated compounds) and lighter versions of the same molecule. These findings are inconsistent with a simple “lock-and-key” model for odor discrimination, and instead, support the existence of a molecular vibration-sensing mechanism to olfactory reception. This result helps to conclude that odorants with corresponding spectra should smell similarly and, to the contrary, molecules with equivalent shape but distinct vibrational spectra should elicit similar olfactory responses. From a theoretical point of view, the enantiomers are expressed by the quantum Hamiltonian of the system as non-distinct objects. However, enantiomers possess a doubly degenerate ground state while an achiral molecule always has a non-degenerate ground state. The nuclear potential for chiral molecules can be approximated to a double well potential, and from the theory it is well known that if this potential is finite, tunneling is expected. The stability of the molecule depends on the magnitude of the potential, since the probabilities of tunneling and oscillations of natural optical activity are lower at higher magnitude. In other words, molecular stability requires a high nuclear potential, and in the limit of infinite potential, tunneling disappears.<sup>[362]</sup> Recently, Michaeli and Naaman demonstrated that chiral biomolecules with a helical-like structure—such as double-stranded DNA and oligopeptide—produce a robust coherent electron transfer. This study focuses on the spin-selectivity of the transmission process, concluding that electron spin entanglement with the direction of electron motion is essential for understanding the tunneling effect in biological systems. This process—chiral-induced spin selectivity (CISS)—can be defined as enantio-selective since electrons with a particular spin can cross the molecule more readily in one specific direction corresponding with the molecule handedness. Furthermore, the process takes place with minimal energy loss since in the biological context an increase in temperature can cause denaturation and other temperature-related mechanisms.<sup>[363]</sup> In this context, an intriguing application was proposed by Yuan et al.,<sup>[364]</sup> regarding chiral light-matter interactions subject to stimulated emission (see **Figure 11**).

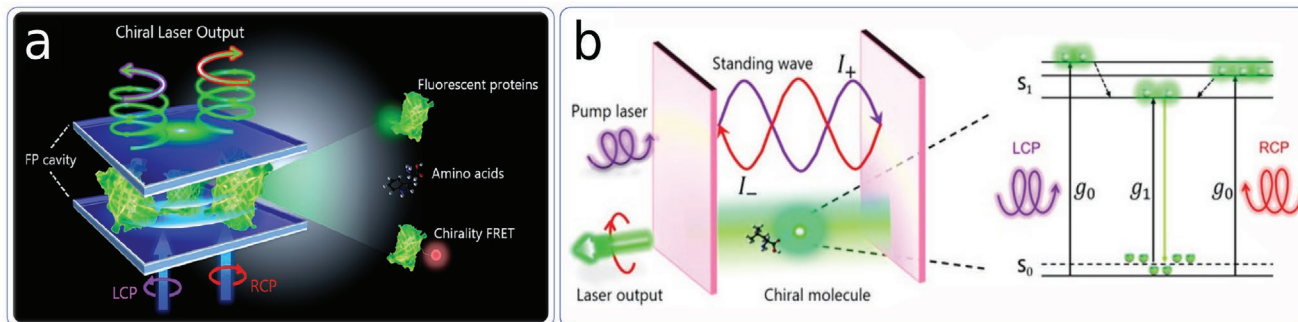


**Figure 11.** Applications of chirality for quantum optics. a) Schematic of a chiral biological microlaser, utilizing chiral biomolecules as the laser gain media. b) Chiral light–matter interactions in a Fabry–Pérot laser cavity. Left: The laser cavity supports standing wave modes, and includes a chiroptically active gain medium. Right: Jablonski diagram of a fluorescein molecule linked to a chiral biomolecule. Under CPL irradiation, the chiral molecule is excited from the ground level  $S_0$  to a higher energy level  $S_1$ . Stimulated emission can take place after a sufficient population inversion is achieved, achieving laser emission. a,b) Reproduced with permission.<sup>[364]</sup> Copyright 2021, American Chemical Society.

In this study, a chiral green fluorescent protein (GFP) was placed in a Fabry–Pérot cavity and used to enhance the chirality of the local electromagnetic field. As illustrated in Figure 11 the GFP and a chiral biomolecule, acting as the laser gain medium, are alternately excited by LCP and RCP pump lasers. The lasing dissymmetry factor, taking into account the relative laser output between LCP and RCP pumping, is used to characterize the chirality. A significant lasing dissymmetry factor can be obtained, illustrating the role of biological chirality in the lasing operation. Furthermore, this apparatus was envisaged as a future mechanism to analyze spin-orbit interactions.<sup>[365]</sup>

## 5. The Role of Machine Learning in Chiral Metasurface Design

In the majority of chiral metasurface applications shown above, the enhancement of the incident or natural chiral response of a material is the main target of all engineered designs. This is especially true for applications such as bio-molecular sensing, where the primary purpose of including a chiral metasurface in the apparatus design is the local enhancement of chiroptical effects near the metasurface.<sup>[152,242,366]</sup> Since the degree of chiral asymmetry in a plasmonic metasurface is due to nanoscale manipulation of the metasurface geometry, the resonant tuning and chiral enhancement can be designed and optimized by modifying this geometry, leading to enhanced performance.<sup>[140,192]</sup> However, this procedure is difficult in practice. One issue is the extreme complexity in the space of possible metasurface designs. This is a result of the large number and range of parameters that can potentially be tuned and the complicated relationships between the physical geometry and the resultant chiroptical response. Another issue is the large amount of computational resources necessary for evaluating the chiroptical response of a potential design since many such evaluations are typically completed in the optimization of a single metasurface. Given these issues, the performance limit for possible metasurface designs in terms of both the resonance tuning and local chiral enhancement is primarily a function of the skill and patience of the engineer. This can lead to un- or under-optimized metasurfaces for applications and low design productivity.

In response to this complexity, algorithmic optimization approaches have been implemented to aid in the design process. Some approaches to optimization in general metasurface design include genetic algorithms,<sup>[367–369]</sup> adjoint methods,<sup>[370,371]</sup> and topology optimization,<sup>[372–375]</sup> among others.<sup>[376]</sup> Furthermore, such methods can be easily improved by techniques that utilize integrated theoretical analysis and recent advances in computational power to decrease the simulation time, consequently improving the optimization speed.<sup>[377,378]</sup> These optimization methods have seen success in a wide range of general and application targeted metasurface design tasks, including optimization of the chiroptical response.

A major issue with traditional gradient-based optimization strategies is that the methods necessary to obtain an optical simulation from a known metasurface geometry are generally extremely computationally expensive. This means that computation of the required number of geometric configurations for typical design procedures is generally very time intensive. A recent approach to overcome this difficulty is the application of machine-learning techniques to the design of metasurfaces.<sup>[383–386]</sup> Machine learning is fundamentally different from traditional numerical optimization approaches in that a representation of the space is learned through the successive optimization of a large number of internal weight parameters, whereas traditional optimization is performed on a case-by-case basis.<sup>[387]</sup> This training step typically requires an extensive data set in order to ensure that the network is converging to a correct representation and to avoid overtraining errors such as overfitting of the available data which can reduce the effective performance.<sup>[388]</sup> After training, the machine-learning model can be used to predict results from a wide range of input parameters, at relatively low computational cost.<sup>[389]</sup> This approach has already been implemented to great effect in the larger field of inverse designed optical metasurfaces,<sup>[390–395]</sup> and in particular plasmonic metasurfaces.<sup>[396,397]</sup>

Several machine-learning-based approaches to the design of chiral metasurfaces have been recently implemented. Li et al., have implemented a deep-learning framework combining Bayesian optimization—which is a derivative-free optimization method—with a convolutional neural network (CNN) (see Figure 12a).<sup>[379]</sup> The CNN model is first trained to map the

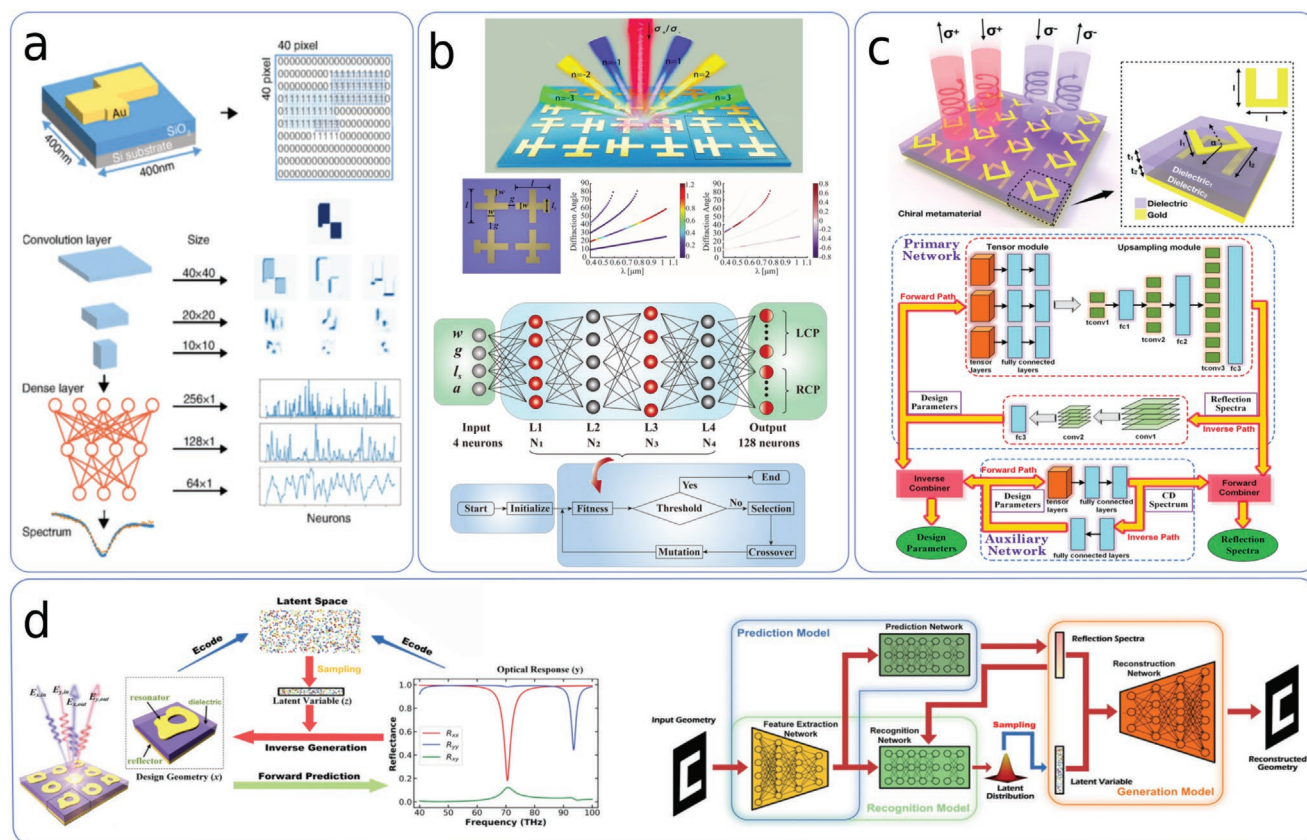


**Figure 12.** Machine-learning-based techniques for the design and inverse design of chiral plasmonic metasurface structures. a) Deep convolutional neural network model of the CD response, combined with Bayesian methods to optimize the CD response. This “Bo-Net” model was applied to optimize 2D Au nanoantennas for a large CD response. Reproduced with permission.<sup>[379]</sup> Copyright 2019, American Physical Society. b) Similar to (a), the metasurface response can be estimated by a fully connected deep neural network, and combined with a genetic algorithm to optimize the metasurface structure. The utilization of a machine-learning model greatly improves the computational efficiency of the optimization, and is applied to a T-shaped metasurface structure. Reproduced under the terms of the CC-BY Creative Commons Attribution 4.0 International license (<https://creativecommons.org/licenses/by/4.0>).<sup>[380]</sup> Copyright 2020, The Authors, published by DeGruyter. c, d) Other machine-learning approaches include: c) A dual bidirectional machine-learning optimization algorithm for optimizing a chiral plasmonic metasurface, assembled via a forward and inverse combiner. Note that the reflectance and CD spectra, and material parameters are common throughout the model (yellow arrows). This method was applied to a meta-atom consisting of two stacked U-shaped plasmonic nanostructures embedded in a dielectric medium; and d) a generative auto-encoder scheme utilizing a latent space approach to metasurface optimization. The 2D metallic resonator is projected into a latent space, which is encoded via the neural network. This model can be used to perform on-demand inverse design given a target chiroptical spectral response. c) Reproduced with permission.<sup>[381]</sup> Copyright 2018, American Chemical Society. d) Reproduced with permission.<sup>[382]</sup> Copyright 2019, Wiley-VCH.

geometrical properties of the metasurface to the chiroptical properties, while the Bayesian optimization serves to recommend optimized inputs to the CNN model. The model is then queried to produce structures with an optimized spectral response. It was found that this combined network structure was able to optimize the metasurface structure over the global parameter space, providing a maximum CD response of 82%. Similarly, Tao et al., have utilized deep learning to predict the CD spectral response based on the geometrical parameters in diffractive chiral metasurfaces.<sup>[398]</sup> The metasurface properties were then optimized by utilizing a genetic algorithm (see Figure 12b).<sup>[380]</sup> It was shown that the deep-learning method performs much faster and more accurately in predicting the CD spectral response than several methods to which it is compared. In particular, deep learning was able to predict the corresponding CD spectra roughly seven orders of magnitude faster (1ms vs 5.5 h) than an RCWA method, which was the method used to produce the data on which the network was trained.

Ma et al., implemented a system consisting of two bidirectional deep neural networks—a primary and an auxiliary network—combined in a partial stacking strategy to design and optimize the chiroptical response of plasmonic metasurfaces (see Figure 12c).<sup>[381]</sup> The metasurface geometry considered in this study consisted of two stacked gold split-ring resonators with a prescribed twist and separation, operating in the terahertz region. This model was utilized for both the forward (structure to CD spectra) and inverse (CD spectra to structure) design of chiral photonic metasurfaces and their related circularly polarized transmission spectra, characterizing the chiroptical response with the CD spectra. The trained model showed exceptional performance for both the forward and inverse design tasks in this design scheme, demonstrating the ability to predict both the chiroptical response of known geometries throughout the parameter range, and to predict metamaterial structures best corresponding to an input CD spectral response.

A similar system was implemented by Ashalley et al., designing a multitask joint-learning model for both the forward and inverse design of a yin-yang-shaped Au nanostructured metasurface and the corresponding CD spectral response.<sup>[399]</sup> The chiroptical response was modified by the manipulation of several geometric parameters defining the metasurface element. This model was shown to predict CD spectral responses virtually identical to simulated spectra from the same geometry, as well as to accurately predict the geometric parameters corresponding to an input CD spectra. This operation for both forward and inverse design tasks makes the network especially useful for the engineering of metasurface elements since both operations are utilized in the design process. The speed at which these methods are shown to operate (several orders of magnitude faster than traditional FDTD/FEM simulations) makes this approach useful for the engineering of optimized chiral nanostructures, enabling extreme advances in speeding the design process.

Given the exponentially large parameter space associated with free-form 2D metasurface design, these methods have, by necessity, generally limited the parameter space of possible designs by only considering the optimization of a few geometric parameters at a time. New machine-learning methods have been applied to the design of chiral plasmonic metasurfaces in an attempt to overcome this difficulty. Ma et al., have recently approached this problem by applying a probabilistic graphic model. This model operates by first clustering similar metasurface design geometries into groups, then varying the design and resulting chiroptical response within that group through the use of a variational auto-encoder (VAE) structure (see Figure 12d).<sup>[382]</sup> The VAE structure serves to project the distribution of chiral systems into a latent space—a representation which learns the general properties of the group, but is not normally recognizable—which is then sampled to probe new geometries within the distribution. This model was applied to a dataset consisting of a two level split-ring resonator design operating in the terahertz regime, and the chiroptical response was characterized by the CD spectra. This model was observed to produce structures exhibiting highly optimized spectral responses, illustrating the ability to learn the highly nonlinear and non-intuitive relationship between metasurface structure and the observed optical response. Many of the structures retrieved were shown to produce the required spectral response at high fidelity, however with a structural configurations that were extremely unusual by typical design standards.

## 6. Conclusion/Prospective

Since the 1840s, when the concept of chirality in optics was first introduced by Lord Kelvin, significant progress has been made in investigating the crucial role of chirality in the interaction between light and matter. This progress has superintended important scientific and technological advances in a diverse range of fields, some of which have been shown above. The chiroptical interaction has been historically employed to elucidate the properties of natural chiral materials, leading to techniques such as CD spectroscopy focused on investigating both intrinsic and extrinsic chiral materials based on their optical

response. However, in the last 2 decades, nanoscale engineered materials have enabled a revolution in precise manipulations of the wavefront of light, allowing the chiral properties of light to be molded in accordance with engineered designs. In particular, metamaterials have demonstrated the ability to concentrate light in deeply subwavelength volumes, producing a huge enhancement in local chiral fields strength. By combining chiral structured light, exhibiting both spin and orbital angular momentum, with chiroptically tailored metamaterials, the strength of the light–matter interaction can be controlled. This approach has enabled advanced applications such as ultra-specific sensing and the resolution of important chiral-mediated biological interactions.

Herein, we report on the role of chirality in light–matter interactions. We cite a few of the many current applications, spanning a wide array of research fields, from optics and biology, to astrobiology, medicine, and quantum physics. While the systems mentioned in this review have achieved significant progress in enhancing the chiroptical response of both natural and synthetic materials, several important challenges and opportunities still remain.

First, since optical metamaterials are engineered structures, the road to increased performance is necessarily paved by the development of new, innovative design techniques. However, designing these materials is generally an extremely difficult task given the large parameter space and complex functional relationships associated with engineering nanoscale geometries. Applying new design methodologies, such as machine learning and other advanced algorithmic approaches, has the potential to unlock new designs and increase device functionality. In particular, physics-assisted artificial intelligence has shown great promise in designing advanced optical materials. However, a current drawback in these methods is the dependence on large and computationally costly data sets. This problem could be addressed by a focus on machine-learning techniques specifically designed for small data sets. Progress in this direction has the potential to extend these powerful methods to more inaccessible applications and more complex geometries.

Second, the functional abilities of the enhanced chiroptical sensor devices shown above are generally limited by two aspects: the operable range of the utilized metamaterial structure, and the availability of sensitive and specific biomarkers for disease. The operable range of many metamaterial structures could be extended by utilizing active chiral plasmonic metamaterials to mediate the sensing interaction, employing tunability in the sensor design. This synthesis could be aided by the introduction of new active control techniques such as optically modulated materials, which can allow for local as well as global tunability in the metamaterial structure. Local active control has the potential to enable more complete control over the wavefront of incident light—where most current studies are focused on averaged bulk properties (e.g., CD spectroscopy)—thus increasing the functionality and sensitivity of current devices over a much broader range. The search for new predictive biomarkers could be accelerated by combining the enantioselective detection of nucleic acids and proteins, and utilizing the highly enhanced structures reported above. Furthermore, the study of mutations in cellular chirality has the potential to drive progress in understanding the clinically relevant mechanisms of disease.

These approaches may lead to an effective screening of new physiologically active molecules and biomarkers. Addressing these points are vital for advancing point-of-care biosensors and lab-on-a-chip devices, and could represent a significant step toward the next-generation of healthcare solutions for various unmet clinical needs. Finally, materials and applications summarized in the present review represent only a fraction of the several studies performed in this broad research area. This review was aimed to trace a road map for future scientific questions and technological applications based on chiral light-chiral matter interactions.

## Acknowledgements

A.L. and G.P. contributed equally to this work. The authors acknowledge support from the Ohio Third Frontier Project "Research Cluster on Surfaces in Advanced Materials" (RC-SAM) at Case Western Reserve University. A.L., M.H., and G.S. acknowledge financial support from the NSF grant no. 1904592, "Instrument Development: Multiplex Sensory Interfaces Between Photonic Nanostructures and Thin Film Ionic Liquids" for supporting research into the sensor applications of metasurfaces and the use of machine learning in optical metasurface design. G.P. acknowledges financial support from the "AIM: Attraction and International Mobility" – PON R&I 2014-2020 Calabria. G.N. acknowledges financial support from the "Dottorati innovativi a caratterizzazione industriale" - PON R&I FSE-FESR 2014-2020. A.G. acknowledges financial support from the "NLHT- Nanoscience Laboratory for Human Technologies" - (POR Calabria FESR-FSE 14/20).

## Conflict of Interest

The authors declare no conflict of interest.

## Keywords

biophysics, chiral plasmonics, machine learning, photonics, plasmonics

Received: September 14, 2021

Revised: April 7, 2022

Published online:

- [1] V. Tverdislov, E. Malyshko, S. Il'chenko, O. Zhulyabina, L. Yakovenko, *Biophysics* **2017**, 62, 331.
- [2] J. Wang, X. Chen, M. L. Clarke, Z. Chen, *Proc. Natl. Acad. Sci. USA* **2005**, 102, 4978.
- [3] R. M. Weis, H. M. McConnell, *Nature* **1984**, 310, 47.
- [4] H. D. Flack, *Helv. Chim. Acta* **2003**, 86, 905.
- [5] W. Ma, L. Xu, A. F. de Moura, X. Wu, H. Kuang, C. Xu, N. A. Kotov, *Chem. Rev.* **2017**, 117, 8041.
- [6] Y. Wen, M.-Q. He, Y.-L. Yu, J.-H. Wang, *Adv. Colloid Interface Sci.* **2021**, 102376.
- [7] V. Saranathan, C. O. Osuji, S. G. Mochrie, H. Noh, S. Narayanan, A. Sandy, E. R. Dufresne, R. O. Prum, *Proc. Natl. Acad. Sci. USA* **2010**, 107, 11676.
- [8] M. Ren, E. Plum, J. Xu, N. I. Zheludev, *Nat. Commun.* **2012**, 3, 833.
- [9] J. Gal, *Nat. Chem.* **2017**, 9, 604.
- [10] H. Flack, *Acta Crystallogr., Sect. A: Found. Crystallogr.* **2009**, 65, 371.
- [11] W. T. B. Kelvin, *Baltimore Lectures on Molecular Dynamics and the Wave Theory of Light*, C J Clay and Sons, London, UK **1904**.
- [12] L. D. Barron, in *Strategies of Life Detection* (Eds: O. Botta, J. L. Bada, J. Gomez-Elvira, E. Javaux, F. Selsis, R. Summons), Vol. 25, Space Sciences Series of ISSI, Springer, Boston, MA, USA **2008**, p. 187.
- [13] G. V. Levin, P. A. Straat, *Astrobiology* **2016**, 16, 798.
- [14] a) L. Kang, Q. Ren, D. Werner, *ACS Photonics* **2017**, 4, 1298; b) Y. Tang, A. E. Cohen, *Science* **2011**, 332, 333.
- [15] M. Hanifeh, M. Albooyeh, F. Capolino, *ACS Photonics* **2020**, 7, 2682.
- [16] J. D. Jackson, *Classical Electrodynamics*, John Wiley & Sons, New York **1999**.
- [17] H. Jerrard, *Opt. Laser Technol.* **1982**, 14, 309.
- [18] R. C. Jones, *JOSA* **1948**, 38, 671.
- [19] R. Azzam, N. Bashara, *J. Opt. Soc. Am.* **1972**, 62, 1252.
- [20] A. Gerrard, J. M. Burch, *Introduction to Matrix Methods in Optics*, Courier Corporation, North Chelmsford, MA, USA **1994**.
- [21] I. Lindell, A. Sihvola, S. Tretyakov, A. J. Viitanen, *Electromagnetic Waves in Chiral and Bi-Isotropic Media*, Artech House, London, UK **1994**.
- [22] J. A. Kong, *Proc. IEEE* **1972**, 60, 1036.
- [23] M. Kamandi, M. Albooyeh, C. Guclu, M. Veysi, J. Zeng, K. Wickramasinghe, F. Capolino, *Phys. Rev. Appl.* **2017**, 8, 064010.
- [24] A. Serdyukov, I. Semchenko, S. Tretyakov, A. Sihvola, *Electromagnetics of Bi-Anisotropic Materials: Theory and Applications*, Gordon and Breach Science Publishers, London, UK **2001**, p. 337.
- [25] C. Caloz, A. Alu, S. Tretyakov, D. Sounas, K. Achouri, Z.-L. Deck-Léger, *Phys. Rev. Appl.* **2018**, 10, 047001.
- [26] T. G. Mackay, A. Lakhtakia, *Electromagnetic Anisotropy and Bianisotropy: A Field Guide*, World Scientific, Singapore **2010**.
- [27] S. Bassiri, N. Engheta, C. Papas, *Alta Freq* **1986**, 55, 83.
- [28] N. Engheta, D. L. Jaggard, *IEEE Trans. Antennas Propag.* **1988**, 30, 6.
- [29] M. Schäferling, *Chiral Nanophotonics: Chiral Optical Properties of Plasmonic Systems*, Springer, Berlin, Germany **2018**.
- [30] W. Moffitt, *J. Chem. Phys.* **1956**, 25, 467.
- [31] Y.-H. Chen, J. T. Yang, H. M. Martinez, *Biochemistry* **1972**, 11, 4120.
- [32] J. D. Roberts, M. C. Caserio, *Basic Principles of Organic Chemistry*, WA Benjamin, Inc., San Francisco, CA, USA **1977**.
- [33] J. Petersen, J. Volz, A. Rauschenbeutel, *Science* **2014**, 346, 67.
- [34] W. A. Bonner, *Origins Life Evol. Biosphere* **1991**, 21, 59.
- [35] L. Barron, E. Blanch, L. Hecht, *Adv. Protein Chem.* **2002**, 62, 51.
- [36] J. Pendry, *Science* **2004**, 306, 1353.
- [37] J. B. Pendry, *Contemp. Phys.* **2004**, 45, 191.
- [38] J. B. Pendry, *Phys. Rev. Lett.* **2000**, 85, 3966.
- [39] N. Berova, K. Nakanishi, R. W. Woody, *Circular Dichroism: Principles and Applications*, John Wiley & Sons, Hoboken, NJ, USA **2000**.
- [40] R. W. Woody, *Methods Enzymol.* **1995**, 246, 34.
- [41] S. S. Oh, O. Hess, *Nano Convergence* **2015**, 2, 24.
- [42] M. Oksanen, A. Hujanen, in *1992 22nd European Microwave Conf.*, Vol. 1, IEEE, Piscataway, NJ, USA **1992**, pp. 195–199.
- [43] Y. Tang, A. E. Cohen, *Phys. Rev. Lett.* **2010**, 104, 163901.
- [44] K. Y. Bliokh, F. Nori, *Phys. Rev. A* **2011**, 83, 021803.
- [45] D. M. Lipkin, *J. Math. Phys.* **1964**, 5, 696.
- [46] T. Kibble, *J. Math. Phys.* **1965**, 6, 1022.
- [47] R. P. Cameron, S. M. Barnett, A. M. Yao, *New J. Phys.* **2012**, 14, 053050.
- [48] J. L. Trueba, A. F. Ranada, *Eur. J. Phys.* **1996**, 17, 141.
- [49] A. Ranada, *Eur. J. Phys.* **1992**, 13, 70.
- [50] M. Schäferling, *Chiral Nanophotonics: Chiral Optical Properties of Plasmonic Systems*, Springer Series Optical Sciences, Vol. 205, Springer, Berlin, Germany **2017**.
- [51] E. Hendry, T. Carpy, J. Johnston, M. Popland, R. Mikhaylovskiy, A. Laphorn, S. Kelly, L. Barron, N. Gadegaard, M. Kadodwala, *Nat. Nanotechnol.* **2010**, 5, 783.
- [52] J. S. Choi, M. Cho, *Phys. Rev. A* **2012**, 86, 063834.
- [53] W. Kuhn, *Trans. Faraday Soc.* **1930**, 26, 293.

- [54] C.-S. Ho, A. Garcia-Etxarri, Y. Zhao, J. Dionne, *ACS Photonics* **2017**, 4, 197.
- [55] M. Hanifeh, M. Albooyeh, F. Capolino, *Phys. Rev. B* **2020**, 102, 165419.
- [56] O. V. Angelsky, A. Y. Bekshaev, S. G. Hanson, C. Y. Zenkova, I. I. Mokhun, Z. Jun, *Front. Phys.* **2020**, 8, 114.
- [57] A. Bekshaev, K. Y. Bliokh, M. Soskin, *J. Opt.* **2011**, 13, 053001.
- [58] M. Berry, N. Zheludev, Y. Aharonov, F. Colombo, I. Sabadini, D. C. Struppa, J. Tollaksen, E. T. Rogers, F. Qin, M. Hong, *J. Opt.* **2019**, 21, 053002.
- [59] S. Van Enk, G. Nienhuis, *Europhys. Lett.* **1994**, 25, 497.
- [60] L. D. Romero, D. Andrews, M. Babiker, *J. Opt. B: Quantum Semiclassical Opt.* **2002**, 4, S66.
- [61] J. W. Simmons, M. J. Guttman, *States*, Addison-Wesley, Reading, MA **1970**.
- [62] L. Allen, M. W. Beijersbergen, R. Spreeuw, J. Woerdman, *Phys. Rev. A* **1992**, 45, 8185.
- [63] L. Mandel, E. Wolf, *Optical Coherence and Quantum Optics*, Cambridge University Press, Cambridge, UK **1995**.
- [64] Q. Zhan, *Adv. Opt. Photonics* **2009**, 1, 1.
- [65] K. E. Ballantine, J. F. Donegan, P. R. Eastham, *Sci. Adv.* **2016**, 2, e1501748.
- [66] Y. Shen, X. Wang, Z. Xie, C. Min, X. Fu, Q. Liu, M. Gong, X. Yuan, *Light Sci. Appl.* **2019**, 8, 90.
- [67] D. McGloin, K. Dholakia, *Contemp. Phys.* **2005**, 46, 15.
- [68] M. A. Bandres, J. C. Gutiérrez-Vega, *Opt. Lett.* **2004**, 29, 144.
- [69] V. Garcés-Chávez, D. McGloin, M. Padgett, W. Dultz, H. Schmitzer, K. Dholakia, *Phys. Rev. Lett.* **2003**, 91, 093602.
- [70] W. N. Plick, M. Krenn, *Phys. Rev. A* **2015**, 92, 063841.
- [71] J. Vaughan, D. Willetts, *Opt. Commun.* **1979**, 30, 263.
- [72] M. Babiker, C. Bennett, D. Andrews, L. D. Romero, *Phys. Rev. Lett.* **2002**, 89, 143601.
- [73] F. Araoka, T. Verbiest, K. Clays, A. Persoons, *Phys. Rev. A* **2005**, 71, 055401.
- [74] I. V. Reddy, A. Baev, E. P. Furlani, P. N. Prasad, J. W. Haus, *ACS Photonics* **2018**, 5, 734.
- [75] R. A. Beth, *Phys. Rev.* **1936**, 50, 115.
- [76] A. Ashkin, J. M. Dziedzic, J. E. Bjorkholm, S. Chu, *Opt. Lett.* **1986**, 11, 288.
- [77] O. M. Maragò, P. H. Jones, P. G. Gucciardi, G. Volpe, A. C. Ferrari, *Nat. Nanotechnol.* **2013**, 8, 807.
- [78] S. Franke-Arnold, *Philos. Trans. R. Soc., A* **2017**, 375, 20150435.
- [79] N. Simpson, K. Dholakia, L. Allen, M. Padgett, *Opt. Lett.* **1997**, 22, 52.
- [80] H. He, M. Friese, N. Heckenberg, H. Rubinsztein-Dunlop, *Phys. Rev. Lett.* **1995**, 75, 826.
- [81] M. Donato, J. Hernandez, A. Mazzulla, C. Provenzano, R. Saija, R. Sayed, S. Vasi, A. Magazzù, P. Pagliusi, R. Bartolino, P. G. Gucciardi, O. M. Maragò, G. Ciparrone, *Nat. Commun.* **2014**, 5, 3656.
- [82] Z. Yan, N. F. Scherer, *J. Phys. Chem. Lett.* **2013**, 4, 2937.
- [83] M. Donato, A. Mazzulla, P. Pagliusi, A. Magazzù, R. Hernandez, C. Provenzano, P. Gucciardi, O. Maragò, G. Ciparrone, *Sci. Rep.* **2016**, 6, 31977.
- [84] G. Tkachenko, E. Brasselet, *Nat. Commun.* **2014**, 5, 3577.
- [85] K. Y. Bliokh, A. Y. Bekshaev, F. Nori, *Nat. Commun.* **2014**, 5, 3300.
- [86] S. Wang, C. Chan, *Nat. Commun.* **2014**, 5, 3307.
- [87] A. Hayat, J. B. Mueller, F. Capasso, *Proc. Natl. Acad. Sci. USA* **2015**, 112, 13190.
- [88] M. Kamandi, M. Albooyeh, M. Veysi, M. Rajaei, J. Zeng, H. K. Wickramasinghe, F. Capolino, *ACS Photonics* **2018**, 5, 4360.
- [89] H. Xin, Y. Li, Y.-C. Liu, Y. Zhang, Y.-F. Xiao, B. Li, *Adv. Mater.* **2020**, 32, 2001994.
- [90] D. L. Jaggard, N. Engheta, M. W. Kowarz, P. Pelet, J. C. Liu, Y. Kim, *IEEE Trans. Antennas Propag.* **1989**, 37, 1447.
- [91] V. Fedotov, A. Schwanecke, N. Zheludev, V. Khardikov, S. Prosvirnin, *Nano Lett.* **2007**, 7, 1996.
- [92] X. Duan, S. Yue, N. Liu, *Nanoscale* **2015**, 7, 17237.
- [93] M. Qiu, L. Zhang, Z. Tang, W. Jin, C.-W. Qiu, D. Y. Lei, *Adv. Funct. Mater.* **2018**, 28, 1803147.
- [94] M. V. Mukhina, V. G. Maslov, A. V. Baranov, A. V. Fedorov, A. O. Orlova, F. Purcell-Milton, J. Govan, Y. K. Gun'ko, *Nano Lett.* **2015**, 15, 2844.
- [95] C. Wang, Z. Li, R. Pan, W. Liu, H. Cheng, J. Li, W. Zhou, J. Tian, S. Chen, *ACS Photonics* **2020**, 7, 3415.
- [96] Y. Luo, C. Chi, M. Jiang, R. Li, S. Zu, Y. Li, Z. Fang, *Adv. Opt. Mater.* **2017**, 5, 1700040.
- [97] Z. Tang, *Chiral Nanomaterials: Preparation, Properties and Applications*, John Wiley & Sons, Hoboken, NJ, USA **2018**.
- [98] M. Hwang, B. Yeom, *Chem. Mater.* **2020**, 33, 807.
- [99] J. Kim, A. S. Rana, Y. Kim, I. Kim, T. Badloe, M. Zubair, M. Q. Mehmood, J. Rho, *Sensors* **2021**, 21, 4381.
- [100] S. Yin, W. Ji, D. Xiao, Y. Li, K. Li, Z. Yin, S. Jiang, L. Shao, D. Luo, Y. J. Liu, *Opt. Commun.* **2019**, 448, 10.
- [101] C. W. Bunn, *Chemical Crystallography*, Oxford University Press, Oxford, UK **1945**.
- [102] T. Cao, C.-w. Wei, Y. Li, *Opt. Mater. Express* **2016**, 6, 303.
- [103] A. Papakostas, A. Potts, D. M. Bagnall, S. L. Prosvirnin, H. J. Coles, N. I. Zheludev, *Phys. Rev. Lett.* **2003**, 90, 107404.
- [104] E. Plum, V. A. Fedotov, N. I. Zheludev, *J. Opt. A: Pure Appl. Opt.* **2009**, 11, 074009.
- [105] E. Plum, X.-X. Liu, V. Fedotov, Y. Chen, D. Tsai, N. Zheludev, *Phys. Rev. Lett.* **2009**, 102, 113902.
- [106] A. I. Kuznetsov, A. E. Miroshnichenko, Y. H. Fu, J. Zhang, B. Luk'Yanchuk, *Sci. Rep.* **2012**, 2, 492.
- [107] A. Y. Zhu, W. T. Chen, A. Zaidi, Y.-W. Huang, M. Khorasaninejad, V. Sanjeev, C.-W. Qiu, F. Capasso, *Light: Sci. Appl.* **2018**, 7, 17158.
- [108] L. Hu, Y. Huang, L. Pan, Y. Fang, *Sci. Rep.* **2017**, 7, 11151.
- [109] C. Rizza, A. Di Falco, M. Scalora, A. Ciattoni, *Phys. Rev. Lett.* **2015**, 115, 057401.
- [110] B. Wang, J. Zhou, T. Koschny, M. Kafesaki, C. M. Soukoulis, *J. Opt. A: Pure Appl. Opt.* **2009**, 11, 114003.
- [111] Y. Xia, Y. Zhou, Z. Tang, *Nanoscale* **2011**, 3, 1374.
- [112] C. Gautier, T. Bürgi, *ChemPhysChem* **2009**, 10, 483.
- [113] T. Duan, J. Ai, Y. Duan, L. Han, S. Che, *Chem. Mater.* **2021**, 33, 6227.
- [114] M. P. Moloney, Y. K. Gun'ko, J. M. Kelly, *Chem. Commun.* **2007**, 38, 3900.
- [115] N. Suzuki, Y. Wang, P. Elvati, Z.-B. Qu, K. Kim, S. Jiang, E. Baumeister, J. Lee, B. Yeom, J. H. Bahng, J. Lee, A. Violi, N. A. Kotov, *ACS Nano* **2016**, 10, 1744.
- [116] X. Huang, L. Zhao, Y. Long, P. Wang, D. Chen, Z. Yang, H. Liang, M. Xue, H. Weng, Z. Fang, X. Dai, G. Chen, *Phys. Rev. X* **2015**, 5, 031023.
- [117] X. Niu, X. Yang, H. Li, J. Liu, Z. Liu, K. Wang, *Microchim. Acta* **2020**, 187, 676.
- [118] A. Spadoni, *Ph.D. Thesis*, Georgia Institute of Technology, Atlanta, GA, USA **2008**.
- [119] Z. J. Wong, Y. Wang, K. O'Brien, J. Rho, X. Yin, S. Zhang, N. Fang, T.-J. Yen, X. Zhang, *J. Opt.* **2017**, 19, 084007.
- [120] *Compendium of Chemical Terminology. IUPAC Recommendations*, (Eds: A. D. McNaught, A. Wilkinson), Blackwell Science, Oxford, UK **1997**.
- [121] V. Mohanraj, Y. Chen, *Trop. J. Pharm. Res.* **2006**, 5, 561.
- [122] G. Schmid, *Nanoparticles: From Theory to Application*, John Wiley & Sons, Hoboken, NJ, USA **2011**.
- [123] H.-E. Lee, H.-Y. Ahn, J. Mun, Y. Y. Lee, M. Kim, N. H. Cho, K. Chang, W. S. Kim, J. Rho, K. T. Nam, *Nature* **2018**, 556, 360.
- [124] G. M. Whitesides, J. P. Mathias, C. T. Seto, *Science* **1991**, 254, 1312.
- [125] D. Jaggard, A. Mickelson, C. Papas, *Appl. Phys.* **1979**, 18, 211.

- [126] M. M. Green, N. C. Peterson, T. Sato, A. Teramoto, R. Cook, S. Lifson, *Science* **1995**, 268, 1860.
- [127] E. Yashima, K. Maeda, T. Nishimura, *Chem.–Eur. J.* **2004**, 10, 42.
- [128] S. Che, Z. Liu, T. Ohsuna, K. Sakamoto, O. Terasaki, T. Tatsumi, *Nature* **2004**, 429, 281.
- [129] B. M. Maoz, R. van der Weegen, Z. Fan, A. O. Govorov, G. Ellestad, N. Berova, E. Meijer, G. Markovich, *J. Am. Chem. Soc.* **2012**, 134, 17807.
- [130] L. Jacak, P. Hawrylak, A. Wojs, *Quantum dots*, Springer Science & Business Media, Berlin, Germany **2013**.
- [131] M. A. Reed, *Sci. Am.* **1993**, 268, 118.
- [132] D. Bera, L. Qian, T.-K. Tseng, P. H. Holloway, *Materials* **2010**, 3, 2260.
- [133] M. P. Moloney, J. Govan, A. Loudon, M. Mukhina, Y. K. Gun'ko, *Nat. Protoc.* **2015**, 10, 558.
- [134] Y. Jiang, E. A. Weiss, *J. Am. Chem. Soc.* **2020**, 142, 15219.
- [135] L. Torsi, G. M. Farinola, F. Marinelli, M. C. Tanese, O. H. Omar, L. Valli, F. Babudri, F. Palmisano, P. G. Zamboni, F. Naso, *Nat. Mater.* **2008**, 7, 412.
- [136] A. Bigdeli, F. Ghasemi, N. Fahimi-Kashani, S. Abbasi-Moayed, A. Orouji, Z. J.-N. Ivrih, F. Shahdost-Fard, M. R. Hormozi-Nezhad, *Analyst* **2020**, 145, 6416.
- [137] A. O. Govorov, Y. K. Gun'ko, J. M. Slocik, V. A. Gérard, Z. Fan, R. R. Naik, *J. Mater. Chem.* **2011**, 21, 16806.
- [138] T. G. Mackay, A. Lakhtakia, *SPIE Rev.* **2010**, 1, 018003.
- [139] Z. Wang, F. Cheng, T. Winsor, Y. Liu, *Nanotechnology* **2016**, 27, 412001.
- [140] J. T. Collins, C. Kuppe, D. C. Hooper, C. Sibilina, M. Centini, V. K. Valev, *Adv. Opt. Mater.* **2017**, 5, 1700182.
- [141] S. Tret'yakov, I. Nefedov, A. Sihvola, S. Maslovski, C. Simovski, *J. Electromagn. Waves Appl.* **2003**, 17, 695.
- [142] E. Plum, J. Zhou, J. Dong, V. Fedotov, T. Koschny, C. Soukoulis, N. Zheludev, *Phys. Rev. B* **2009**, 79, 035407.
- [143] R. Zhao, L. Zhang, J. Zhou, T. Koschny, C. Soukoulis, *Phys. Rev. B* **2011**, 83, 035105.
- [144] T. Cao, L. Zhang, R. E. Simpson, C. Wei, M. J. Cryan, *Opt. Express* **2013**, 21, 27841.
- [145] D.-H. Kwon, P. L. Werner, D. H. Werner, *Opt. Express* **2008**, 16, 11802.
- [146] G. Palermo, G. E. Lio, M. Esposito, L. Ricciardi, M. Manocchio, V. Tasco, A. Passaseo, A. De Luca, G. Strangi, *ACS Appl. Mater. Interfaces* **2020**, 12, 30181.
- [147] G. Palermo, K. V. Sreekanth, N. Maccaferri, G. E. Lio, G. Nicoletta, F. De Angelis, M. Hinczewski, G. Strangi, *Nanophotonics* **2021**, 10, 295.
- [148] K. Robbie, M. Brett, *J. Vac. Sci. Technol., A* **1997**, 15, 1460.
- [149] M. Thiel, M. Decker, M. Deubel, M. Wegener, S. Linden, G. von Freymann, *Adv. Mater.* **2007**, 19, 207.
- [150] A. Kuzyk, R. Jungmann, G. P. Acuna, N. Liu, *ACS Photonics* **2018**, 5, 1151.
- [151] J. M. Fernández-García, P. J. Evans, S. Filippone, M. Á. Herranz, N. Martín, *Acc. Chem. Res.* **2019**, 52, 1565.
- [152] J. Kumar, L. M. Liz-Marzán, *Bull. Chem. Soc. Jpn.* **2019**, 92, 30.
- [153] M. J. Urban, C. Shen, X.-T. Kong, C. Zhu, A. O. Govorov, Q. Wang, M. Hentschel, N. Liu, *Annu. Rev. Phys. Chem.* **2019**, 70, 275.
- [154] H.-L. Qian, C.-X. Yang, X.-P. Yan, *Nat. Commun.* **2016**, 7, 12104.
- [155] P. Han, K. Akagi, F. Federici Canova, H. Mutoh, S. Shiraki, K. Iwaya, P. S. Weiss, N. Asao, T. Hitosugi, *ACS Nano* **2014**, 8, 9181.
- [156] F. Komarov, A. Mironov, *Phys. Chem. Org. Solid State* **2004**, 5, 411.
- [157] T. B. L. Kist, M. Mandaji, *Electrophoresis* **2004**, 25, 3492.
- [158] M. A. Castriciano, D. Gentili, A. Romeo, M. Cavallini, L. M. Scolaro, *Sci. Rep.* **2017**, 7, 44094.
- [159] J. Seibel, L. Verstraete, B. E. Hirsch, A. M. Bragança, S. De Feyter, *J. Am. Chem. Soc.* **2018**, 140, 11565.
- [160] E. S. P. Leong, J. Deng, E. H. Khoo, S. Wu, W. K. Phua, Y. J. Liu, *RSC Adv.* **2015**, 5, 96366.
- [161] K. Arshak, M. Mihov, A. Arshak, D. McDonagh, D. Sutton, in *2004 24th Int. Conf. on Microelectronics (IEEE Cat. No. 04TH8716)*, Vol. 2, IEEE, Piscataway, NJ, USA **2004**, pp. 459–462.
- [162] I. Sakellari, X. Yin, M. L. Nesterov, K. Terzaki, A. Xomalis, M. Farsari, *Adv. Opt. Mater.* **2017**, 5, 1700200.
- [163] R. Rao, A. E. Islam, N. Pierce, P. Nikolaev, B. Maruyama, *Carbon* **2015**, 95, 287.
- [164] K. Ernst, M. Böhringer, C. McFadden, P. Hug, U. Müller, U. Ellerbeck, *Nanotechnology* **1999**, 10, 355.
- [165] E. S. P. Leong, J. Deng, S. Wu, E. H. Khoo, Y. J. Liu, *Proc. SPIE* **2014**, 9278, 927809.
- [166] M. A. Mateos-Timoneda, M. Crego-Calama, D. N. Reinhoudt, *Chem. Soc. Rev.* **2004**, 33, 363.
- [167] F. Yang, X. Wang, D. Zhang, J. Yang, D. Luo, Z. Xu, J. Wei, J.-Q. Wang, Z. Xu, F. Peng, X. Li, R. Li, Y. Li, M. Li, X. Bai, F. Ding, Y. Li, *Nature* **2014**, 510, 522.
- [168] D. Chen, J. E. MacLennan, R. Shao, D. K. Yoon, H. Wang, E. Korblova, D. M. Walba, M. A. Glaser, N. A. Clark, *J. Am. Chem. Soc.* **2011**, 133, 12656.
- [169] K. Robbie, M. Brett, A. Lakhtakia, *Nature* **1996**, 384, 616.
- [170] A. Selimis, V. Mironov, M. Farsari, *Microelectron. Eng.* **2015**, 132, 83.
- [171] T. Gissibl, S. Thiele, A. Herkommer, H. Giessen, *Nat. Commun.* **2016**, 7, 11763.
- [172] Y. Tajitsu, *IEEE Trans. Ultrason. Ferroelectr. Freq. Control* **2008**, 55, 1000.
- [173] D. W. Green, J.-M. Lee, E.-J. Kim, D.-J. Lee, H.-S. Jung, *Adv. Mater. Interfaces* **2016**, 3, 1500411.
- [174] S. Nagl, P. Schulze, S. Ohla, R. Beyreiss, L. Gitlin, D. Belder, *Anal. Chem.* **2011**, 83, 3232.
- [175] A. Boltasseva, V. M. Shalae, *Metamaterials* **2008**, 2, 1.
- [176] S. Dey, C. Fan, K. V. Gothelf, J. Li, C. Lin, L. Liu, N. Liu, M. A. Nijenhuis, B. Saccà, F. C. Simmel, H. Yan, P. Zhan, *Nat. Rev. Methods Primers* **2021**, 1, 13.
- [177] X. Shen, A. Asenjo-Garcia, Q. Liu, Q. Jiang, F. J. García de Abajo, N. Liu, B. Ding, *Nano Lett.* **2013**, 13, 2128.
- [178] M. Siavashpour, C. H. Wachauf, M. J. Zakhary, F. Praetorius, H. Dietz, Z. Dogic, *Nat. Mater.* **2017**, 16, 849.
- [179] Y. Huang, M.-K. Nguyen, A. K. Natarajan, V. H. Nguyen, A. Kuzyk, *ACS Appl. Mater. Interfaces* **2018**, 10, 44221.
- [180] A. Kuzyk, R. Schreiber, Z. Fan, G. Pardatscher, E.-M. Roller, A. Högele, F. C. Simmel, A. O. Govorov, T. Liedl, *Nature* **2012**, 483, 311.
- [181] A. Passaseo, M. Esposito, M. Cuscunà, V. Tasco, *Adv. Opt. Mater.* **2017**, 5, 1601079.
- [182] M. Esposito, V. Tasco, M. Cuscuna, F. Todisco, A. Benedetti, I. Tarantini, M. D. Giorgi, D. Sanvitto, A. Passaseo, *ACS Photonics* **2015**, 2, 105.
- [183] M. Manocchio, M. Esposito, V. Tasco, M. Cuscun, A. Passaseo, in *2019 Thirteenth Int. Congress on Artificial Materials for Novel Wave Phenomena (Metamaterials)*, IEEE, Piscataway, NJ, USA **2019**, pp. X-239–X-241.
- [184] K. Vernon-Parry, *III-Vs Rev.* **2000**, 13, 40.
- [185] P. J. Goodhew, J. Humphreys, *Electron Microscopy and Analysis*, CRC Press, Boca Raton, FL, USA **2000**.
- [186] T. Ohsuna, Z. Liu, S. Che, O. Terasaki, *Small* **2005**, 1, 233.
- [187] L. Zhang, L. Qin, X. Wang, H. Cao, M. Liu, *Adv. Mater.* **2014**, 26, 6959.
- [188] B. Yeom, H. Zhang, H. Zhang, J. I. Park, K. Kim, A. O. Govorov, N. A. Kotov, *Nano Lett.* **2013**, 13, 5277.
- [189] A. O. Govorov, Z. Fan, *ChemPhysChem* **2012**, 13, 2551.
- [190] A. O. Govorov, *J. Phys. Chem. C* **2011**, 115, 7914.
- [191] A. O. Govorov, Z. Fan, P. Hernandez, J. M. Slocik, R. R. Naik, *Nano Lett.* **2010**, 10, 1374.

- [192] V. K. Valev, J. J. Baumberg, C. Sibilia, T. Verbiest, *Adv. Mater.* **2013**, 25, 2517.
- [193] X. Wang, Z. Tang, *Small* **2017**, 13, 1601115.
- [194] M. Hentschel, M. Schäferling, X. Duan, H. Giessen, N. Liu, *Sci. Adv.* **2017**, 3, e1602735.
- [195] S. A. Maier, *Plasmonics: Fundamentals and Applications*, Springer Science & Business Media, Berlin, Germany **2007**.
- [196] M. L. Brongersma, P. G. Kik, *Surface Plasmon Nanophotonics*, Vol. 131, Springer, Berlin, Germany **2007**.
- [197] R. B. Schasfoort, *Handbook of Surface Plasmon Resonance*, Royal Society of Chemistry, London, UK **2017**.
- [198] L. M. Liz-Marzán, C. J. Murphy, J. Wang, *Chem. Soc. Rev.* **2014**, 43, 3820.
- [199] M. I. Stockman, *Opt. Express* **2011**, 19, 22029.
- [200] V. Giannini, A. I. Fernández-Domínguez, Y. Sonnefraud, T. Roschuk, R. Fernández-García, S. A. Maier, *Small* **2010**, 6, 2498.
- [201] J.-Y. Jing, Q. Wang, W.-M. Zhao, B.-T. Wang, *Opt. Lasers Eng.* **2019**, 112, 103.
- [202] F. Ding, Y. Yang, R. A. Deshpande, S. I. Bozhevolnyi, *Nanophotonics* **2018**, 7, 1129.
- [203] V. Amendola, R. Pilot, M. Frasconi, O. M. Maragò, M. A. Iati, *J. Phys.: Condens. Matter* **2017**, 29, 203002.
- [204] T. V. Shahbazyan, M. I. Stockman, *Plasmonics: Theory and Applications*, Springer, The Netherlands **2013**.
- [205] X. Lan, Z. Su, Y. Zhou, T. Meyer, Y. Ke, Q. Wang, W. Chiu, N. Liu, S. Zou, H. Yan, Y. Liu, *Angew. Chem., Int. Ed.* **2017**, 56, 14632.
- [206] C.-L. Yu, Y.-H. Hsiao, C.-Y. Chang, P.-J. Cheng, H.-T. Lin, M.-S. Lai, H.-C. Kuo, S.-W. Chang, M.-H. Shih, *Sci. Rep.* **2020**, 10, 7880.
- [207] M. L. Tseng, Z.-H. Lin, H. Y. Kuo, T.-T. Huang, Y.-T. Huang, T. L. Chung, C. H. Chu, J.-S. Huang, D. P. Tsai, *Adv. Opt. Mater.* **2019**, 7, 1900617.
- [208] Z. Li, M. Gokkavas, E. Ozbay, *Adv. Opt. Mater.* **2013**, 1, 482.
- [209] W. Ye, X. Yuan, C. Guo, J. Zhang, B. Yang, S. Zhang, *Phys. Rev. Appl.* **2017**, 7, 054003.
- [210] R. Ogier, Y. Fang, M. Svedendahl, P. Johansson, M. Käll, *ACS Photonics* **2014**, 1, 1074.
- [211] X. Mu, L. Hu, Y. Cheng, Y. Fang, M. Sun, *Nanoscale* **2021**, 13, 581.
- [212] A. Ben-Moshe, B. M. Maoz, A. O. Govorov, G. Markovich, *Chem. Soc. Rev.* **2013**, 42, 7028.
- [213] Z. Wang, Y. Wang, G. Adamo, J. Teng, H. Sun, *Laser Photonics Rev.* **2019**, 13, 1800276.
- [214] Z. Fan, A. O. Govorov, *Nano Lett.* **2010**, 10, 2580.
- [215] L. Lin, S. Lepeshov, A. Krasnok, T. Jiang, X. Peng, B. A. Korgel, A. Alú, Y. Zheng, *Mater. Today* **2019**, 25, 10.
- [216] E. Severoni, S. Maniappan, L. M. Liz-Marzán, J. Kumar, F. J. García de Abajo, L. Galantini, *ACS Nano* **2020**, 14, 16712.
- [217] V. E. Ferry, J. M. Smith, A. P. Alivisatos, *ACS Photonics* **2014**, 1, 1189.
- [218] L. Hu, T. Liedl, K. Martens, Z. Wang, A. O. Govorov, *ACS Photonics* **2019**, 6, 749.
- [219] T. Stauber, T. Low, G. Gómez-Santos, *Nano Lett.* **2020**, 20, 8711.
- [220] Q. Jiang, B. Du, M. Jiang, D. Liu, Z. Liu, B. Li, Z. Liu, F. Lin, X. Zhu, Z. Fang, *Nanoscale* **2020**, 12, 5906.
- [221] S. Zhang, H. Wei, K. Bao, U. Håkanson, N. J. Halas, P. Nordlander, H. Xu, *Phys. Rev. Lett.* **2011**, 107, 096801.
- [222] J. C. W. Song, M. S. Rudner, *Proc. Natl. Acad. Sci. USA* **2016**, 113, 4658.
- [223] M. V. Gorkunov, A. A. Antonov, Y. S. Kivshar, *Phys. Rev. Lett.* **2020**, 125, 093903.
- [224] C. Kelly, L. Khosravi Khorashad, N. Gadegaard, L. D. Barron, A. O. Govorov, A. S. Karimullah, M. Kadodwala, *ACS Photonics* **2018**, 5, 535.
- [225] X. Lan, X. Zhou, L. A. McCarthy, A. O. Govorov, Y. Liu, S. Link, *J. Am. Chem. Soc.* **2019**, 141, 19336.
- [226] T. Man, W. Ji, X. Liu, C. Zhang, L. Li, H. Pei, C. Fan, *ACS Nano* **2019**, 13, 4826.
- [227] M. Wang, J. Dong, C. Zhou, H. Xie, W. Ni, S. Wang, H. Jin, Q. Wang, *ACS Nano* **2019**, 13, 13702.
- [228] C. Zhou, X. Duan, N. Liu, *Acc. Chem. Res.* **2017**, 50, 2906.
- [229] A. Kuzyk, M. J. Urban, A. Idili, F. Ricci, N. Liu, *Sci. Adv.* **2017**, 3, e1602803.
- [230] M.-K. Nguyen, A. Kuzyk, *ACS Nano* **2019**, 13, 13615.
- [231] A. Kuzyk, R. Schreiber, H. Zhang, A. O. Govorov, T. Liedl, N. Liu, *Nat. Mater.* **2014**, 13, 862.
- [232] M. Kuwata-Gonokami, N. Saito, Y. Ino, M. Kauranen, K. Jefimovs, T. Vallius, J. Turunen, Y. Svirko, *Phys. Rev. Lett.* **2005**, 95, 227401.
- [233] T. Ohno, S. Miyaniishi, *Opt. Express* **2006**, 14, 6285.
- [234] B. Tang, Z. Li, E. Palacios, Z. Liu, S. Butun, K. Aydin, *IEEE Photonics Technol. Lett.* **2017**, 29, 295.
- [235] L. Li, J. Wang, L. Kang, W. Liu, L. Yu, B. Zheng, M. L. Brongersma, D. H. Werner, S. Lan, Y. Shi, Y. Xu, X. Wang, *ACS Nano* **2020**, 14, 16634.
- [236] V. A. Fedotov, P. L. Mladyonov, S. L. Prosvirnin, A. V. Rogacheva, Y. Chen, N. I. Zheludev, *Phys. Rev. Lett.* **2006**, 97, 167401.
- [237] L. Ouyang, W. Wang, D. Rosenmann, D. A. Czaplewski, J. Gao, X. Yang, *Opt. Express* **2018**, 26, 31484.
- [238] Z. Wang, Y. Wang, G. Adamo, B. H. Teh, Q. Y. S. Wu, J. Teng, H. Sun, *Adv. Opt. Mater.* **2016**, 4, 883.
- [239] V. E. Ferry, M. Hentschel, A. P. Alivisatos, *Nano Lett.* **2015**, 15, 8336.
- [240] O. Tsilipakos, A. C. Tasolamprou, A. Pitilakis, F. Liu, X. Wang, M. S. Mirmoosa, D. C. Tzarouchis, S. Abadal, H. Taghvaei, C. Liaskos, A. Tsioliaridou, J. Georgiou, A. Cabellos-Aparicio, E. Alarcón, S. Ioannidis, A. Pitsillides, I. F. Akyildiz, N. V. Kantartzis, E. N. Economou, C. M. Soukoulis, M. Kafesaki, S. Tretyakov, *Adv. Opt. Mater.* **2020**, 8, 2000783.
- [241] Q. He, S. Sun, L. Zhou, *Research* **2019**, 2019, 1849272.
- [242] F. Neubrech, M. Hentschel, N. Liu, *Adv. Mater.* **2020**, 32, 1905640.
- [243] L. Kang, R. P. Jenkins, D. H. Werner, *Adv. Opt. Mater.* **2019**, 7, 1801813.
- [244] X. Yin, M. Schäferling, A.-K. U. Michel, A. Tittl, M. Wuttig, T. Taubner, H. Giessen, *Nano Lett.* **2015**, 15, 4255.
- [245] C. Gilroy, K. McKay, M. Devine, R. W. H. Webster, N. Gadegaard, A. S. Karimullah, D. A. Maclaren, M. Kadodwala, *Adv. Photonics Res.* **2021**, 2, 2000062.
- [246] Z. Wu, X. Chen, M. Wang, J. Dong, Y. Zheng, *ACS Nano* **2018**, 12, 5030.
- [247] P. R. Stevenson, M. Du, C. Cherqui, M. R. Bourgeois, K. Rodriguez, J. R. Neff, E. Abreu, I. M. Meiler, V. A. Tamma, V. A. Apkarian, G. C. Schatz, J. Yuen-Zhou, J. S. Shumaker-Parry, *ACS Nano* **2020**, 14, 11518.
- [248] J. Li, J. Li, Y. Yang, J. Li, Y. Zhang, L. Wu, Z. Zhang, M. Yang, C. Zheng, J. Li, J. Huang, F. Li, T. Tang, H. Dai, J. Yao, *Carbon* **2020**, 163, 34.
- [249] A. S. Baimuratov, T. P. Pereziabova, M. Y. Leonov, W. Zhu, A. V. Baranov, A. V. Fedorov, Y. K. Gun'ko, I. D. Rukhlenko, *ACS Nano* **2018**, 12, 6203.
- [250] G. Chu, X. Wang, T. Chen, J. Gao, F. Gai, Y. Wang, Y. Xu, *ACS Appl. Mater. Interfaces* **2015**, 7, 11863.
- [251] P. T. Probst, M. Mayer, V. Gupta, A. M. Steiner, Z. Zhou, G. K. Auernhammer, T. A. F. König, A. Fery, *Nat. Mater.* **2021**, 20, 1024.
- [252] S. Zhang, J. Zhou, Y.-S. Park, J. Rho, R. Singh, S. Nam, A. K. Azad, H.-T. Chen, X. Yin, A. J. Taylor, X. Zhang, *Nat. Commun.* **2012**, 3, 942.
- [253] Y. Guan, Z. Wang, B. Ai, C. Chen, W. Zhang, Y. Wang, G. Zhang, *ACS Appl. Mater. Interfaces* **2020**, 12, 50192.
- [254] Z. Wu, J. Li, X. Zhang, J. M. Redwing, Y. Zheng, *Adv. Mater.* **2019**, 31, 1904132.

- [255] D. Xiao, Y. J. Liu, S. Yin, J. Liu, W. Ji, B. Wang, D. Luo, G. Li, X. W. Sun, *Opt. Express* **2018**, *26*, 25305.
- [256] S. Yin, D. Xiao, J. Liu, K. Li, H. He, S. Jiang, D. Luo, X. W. Sun, W. Ji, Y. J. Liu, *IEEE Photonics J.* **2018**, *10*, 4600909.
- [257] A. Lininger, A. Y. Zhu, J.-S. Park, G. Palermo, S. Chatterjee, J. Boyd, F. Capasso, G. Strangi, *Proc. Natl. Acad. Sci. USA* **2020**, *117*, 20390.
- [258] M. Decker, C. Kremers, A. Minovich, I. Staude, A. E. Miroshnichenko, D. Chigrin, D. N. Neshev, C. Jagadish, Y. S. Kivshar, *Opt. Express* **2013**, *21*, 8879.
- [259] A. Komar, R. Paniagua-Domínguez, A. Miroshnichenko, Y. F. Yu, Y. S. Kivshar, A. I. Kuznetsov, D. Neshev, *ACS Photonics* **2018**, *5*, 1742.
- [260] O. Buchnev, N. Podoliak, M. Kaczmarek, N. I. Zheludev, V. A. Fedotov, *Adv. Opt. Mater.* **2015**, *3*, 674.
- [261] J. A. Dolan, H. Cai, L. Delalande, X. Li, A. B. F. Martinson, J. J. de Pablo, D. López, P. F. Nealey, *ACS Photonics* **2021**, *8*, 567.
- [262] M. Sanz-Paz, C. Ernandes, J. U. Esparza, G. W. Burr, N. F. van Hulst, A. Maitre, L. Aigouy, T. Gacoin, N. Bonod, M. F. Garcia-Parajo, S. Bidault, M. Mivelle, *Nano Lett.* **2018**, *18*, 3481.
- [263] S. M. Kamali, E. Arbabi, A. Arbabi, A. Faraon, *Nanophotonics* **2018**, *7*, 1041.
- [264] P. Genevet, F. Capasso, F. Aieta, M. Khorasaninejad, R. Devlin, *Optica* **2017**, *4*, 139.
- [265] A. García-Etxarri, R. Gómez-Medina, L. S. Froufe-Pérez, C. López, L. Chantada, F. Scheffold, J. Aizpurua, M. Nieto-Vesperinas, J. J. Sáenz, *Opt. Express* **2011**, *19*, 4815.
- [266] M. Hanifeh, F. Capolino, *J. Appl. Phys.* **2020**, *127*, 093104.
- [267] X. Zhao, B. M. Reinhard, *ACS Photonics* **2019**, *6*, 1981.
- [268] Z. Ma, Y. Li, Y. Li, Y. Gong, S. A. Maier, M. Hong, *Opt. Express* **2018**, *26*, 6067.
- [269] J. Garcia-Guirado, M. Svedendahl, J. Puigdollers, R. Quidant, *Nano Lett.* **2019**, *20*, 585.
- [270] D. Beutel, P. Scott, M. Wegener, C. Rockstuhl, I. Fernandez-Corbaton, *Appl. Phys. Lett.* **2021**, *118*, 221108.
- [271] M. L. Solomon, J. Hu, M. Lawrence, A. García-Etxarri, J. A. Dionne, *ACS Photonics* **2018**, *6*, 43.
- [272] K. Ullah, B. Garcia-Camara, M. Habib, X. Liu, A. Krasnok, S. Lepeshov, J. Hao, J. Liu, N. Yadav, *J. Quant. Spectrosc. Radiat. Transfer* **2018**, *208*, 71.
- [273] I. Staude, A. E. Miroshnichenko, M. Decker, N. T. Fofang, S. Liu, E. Gonzales, J. Dominguez, T. S. Luk, D. N. Neshev, I. Brener, Y. Kivshar, *ACS Nano* **2013**, *7*, 7824.
- [274] R. Cireasa, A. Boguslavskiy, B. Pons, M. Wong, D. Descamps, S. Petit, H. Ruf, N. Thiré, A. Ferré, J. Suarez, J. Higué, B. E. Schmidt, A. F. Alharbi, F. Légaré, V. Blanchet, B. Fabre, S. Patchkovskii, O. Smirnova, Y. Mairesse, V. R. Bhardwaj, *Nat. Phys.* **2015**, *11*, 654.
- [275] S. Beaulieu, A. Comby, D. Descamps, B. Fabre, G. Garcia, R. Géneaux, A. Harvey, F. Légaré, Z. Mašín, L. Nahon, A. F. Ordonez, S. Petit, B. Pons, Y. Mairesse, O. Smirnova, V. Blanchet, *Nat. Phys.* **2018**, *14*, 484.
- [276] E. Mohammadi, K. Tsakmakidis, A.-N. Askarpour, P. Dehkoda, A. Tavakoli, H. Altug, *ACS Photonics* **2018**, *5*, 2669.
- [277] B. Wang, W. B. Sparks, T. A. Germer, A. Leadbetter, *Proc. SPIE* **2009**, *7441*, 744108.
- [278] W. Sparks, J. H. Hough, T. A. Germer, F. Robb, L. Kolokolova, *Planet. Space Sci.* **2012**, *72*, 111.
- [279] P. Lodahl, S. Mahmoodian, S. Stobbe, A. Rauschenbeutel, P. Schneeweiss, J. Volz, H. Pichler, P. Zoller, *Nature* **2017**, *541*, 473.
- [280] Z. Yang, S. Aghaeimebodi, E. Waks, *Opt. Express* **2019**, *27*, 21367.
- [281] D. Ayuso, O. Neufeld, A. F. Ordonez, P. Declève, G. Lerner, O. Cohen, M. Ivanov, O. Smirnova, *Nat. Photonics* **2019**, *13*, 866.
- [282] G. Holzwarth, W. Gratzer, P. Doty, *J. Am. Chem. Soc.* **1962**, *84*, 3194.
- [283] G. Holzwarth, P. Doty, *J. Am. Chem. Soc.* **1965**, *87*, 218.
- [284] R. W. Woody, *Biomed. Spectrosc. Imaging* **2015**, *4*, 5.
- [285] G. Witz, A. Stasiak, *Nucleic Acids Res.* **2010**, *38*, 2119.
- [286] S. S. Teves, S. Henikoff, *Nucleus* **2014**, *5*, 211.
- [287] M. Heine, S. B. Chandra, *J. Microbiol.* **2009**, *47*, 229.
- [288] S. C. Verma, Z. Qian, S. L. Adhya, *PLoS Genet.* **2019**, *15*, e1008456.
- [289] F. Li, S. Li, X. Guo, Y. Dong, C. Yao, Y. Liu, Y. Song, X. Tan, L. Gao, D. Yang, *Angew. Chem.* **2020**, *59*, 11087.
- [290] L. F. Liu, J. C. Wang, *Proc. Natl. Acad. Sci. USA* **1987**, *84*, 7024.
- [291] J. Ma, M. D. Wang, *Biophys. Rev.* **2016**, *8*, 75.
- [292] S. S. Teves, S. Henikoff, *Nat. Struct. Mol. Biol.* **2014**, *21*, 88.
- [293] Y. Mitsui, R. Langridge, B. E. Shortle, C. R. Cantor, R. C. Grant, M. Kodama, R. D. Wells, *Nature* **1970**, *228*, 1166.
- [294] F. M. Pohl, T. M. Jovin, *J. Mol. Biol.* **1972**, *67*, 375.
- [295] A. H.-J. Wang, G. J. Quigley, F. J. Kolpak, J. L. Crawford, J. H. Van Boom, G. van der Marel, A. Rich, *Nature* **1979**, *282*, 680.
- [296] A. Rich, S. Zhang, *Nat. Rev. Genet.* **2003**, *4*, 566.
- [297] S. Ravichandran, V. K. Subramani, K. K. Kim, *Biophys. Rev.* **2019**, *11*, 383.
- [298] A. Suram, J. K. Rao, K. Latha, M. Viswamitra, *Neuromolecular Med.* **2002**, *2*, 289.
- [299] E. Lafer, R. Valle, A. Möller, A. Nordheim, P. Schur, A. Rich, B. Stollar, *J. Clin. Invest.* **1983**, *71*, 314.
- [300] M. K. Kathiravan, M. M. Khilare, K. Nikoomanesh, A. S. Chothe, K. S. Jain, *J. Enzyme Inhib. Med. Chem.* **2013**, *28*, 419.
- [301] D. C. Hooper, G. A. Jacoby, *Cold Spring Harb. Perspect. Med.* **2016**, *6*, a025320.
- [302] J. Marinello, M. Delcuratolo, G. Capranico, *Int. J. Mol. Sci.* **2018**, *19*, 3480.
- [303] M. Airoidi, G. Barone, G. Gennaro, A. M. Giuliani, M. Giustini, *Biochemistry* **2014**, *53*, 2197.
- [304] M. Blum, K. Feistel, T. Thumberger, A. Schweickert, *Development* **2014**, *141*, 1603.
- [305] T. Nakamura, H. Hamada, *Development* **2012**, *139*, 3257.
- [306] C. Géminard, N. González-Morales, J.-B. Coutelis, S. Noselli, *Genesis* **2014**, *52*, 471.
- [307] G. Lebreton, C. Géminard, F. Lapraz, S. Pyrpassopoulos, D. Cerezo, P. Spéder, E. Ostap, S. Noselli, *Science* **2018**, *362*, 949.
- [308] T. Juan, C. Géminard, J.-B. Coutelis, D. Cerezo, S. Polès, S. Noselli, M. Fürthauer, *Nat. Commun.* **2018**, *9*, 1942.
- [309] K. C.-W. Wu, C.-Y. Yang, C.-M. Cheng, *Chem. Commun.* **2014**, *50*, 4148.
- [310] M. Thamim, K. Thirumoorthy, *Eur. Biophys. J.* **2020**, *49*, 549.
- [311] L. Dang, D. W. White, S. Gross, B. D. Bennett, M. A. Bittinger, E. M. Driggers, V. R. Fantin, H. G. Jang, S. Jin, M. C. Keenan, K. M. Marks, R. M. Prins, P. S. Ward, K. E. Yen, L. M. Liau, J. D. Rabinowitz, L. C. Cantley, C. B. Thompson, M. G. Vander Heiden, S. M. Su, *Nature* **2009**, *462*, 739.
- [312] H. Yan, D. W. Parsons, G. Jin, R. McLendon, B. A. Rasheed, W. Yuan, I. Kos, I. Batinic-Haberle, S. Jones, G. J. Riggins, H. Friedman, A. Friedman, D. Reardon, J. Herndon, K. W. Kinzler, V. E. Velculescu, B. Vogelstein, D. D. Bigner, *N. Engl. J. Med.* **2009**, *360*, 765.
- [313] J. Kalinina, J. Ahn, N. S. Devi, L. Wang, Y. Li, J. J. Olson, M. Glantz, T. Smith, E. L. Kim, A. Giese, R. L. Jensen, C. C. Chen, B. S. Carter, H. Mao, M. He, E. G. Van Meir, *Clin. Cancer Res.* **2016**, *22*, 6256.
- [314] V. Goss, A. Cazenave-Gassiot, A. Pringle, A. Postle, *Curr. Anal. Chem.* **2014**, *10*, 121.
- [315] J. J. Bastings, H. M. van Eijk, S. W. Olde Damink, S. S. Rensen, *Nutrients* **2019**, *11*, 2205.
- [316] M. Suzuki, J. Sasabe, Y. Miyoshi, K. Kuwasako, Y. Muto, K. Hamase, M. Matsuoka, N. Imanishi, S. Aiso, *Proc. Natl. Acad. Sci. USA* **2015**, *112*, E2217.
- [317] C. Madeira, M. V. Lourenco, C. Vargas-Lopes, C. K. Suemoto, C. O. Brandão, T. Reis, R. E. Leite, J. Laks, W. Jacob-Filho, C. A. Pasqualucci, L. T. Grinberg, S. T. Ferreira, R. Panizzutti, *Transl. Psychiatry* **2015**, *5*, e561.

- [318] R. Kimura, H. Tsujimura, M. Tsuchiya, S. Soga, N. Ota, A. Tanaka, H. Kim, *Sci. Rep.* **2020**, *10*, 804.
- [319] J. Sasabe, Y. Miyoshi, M. Suzuki, M. Mita, R. Konno, M. Matsuoka, K. Hamase, S. Aiso, *Proc. Natl. Acad. Sci. USA* **2012**, *109*, 627.
- [320] J. Sasabe, M. Suzuki, Y. Miyoshi, Y. Tojo, C. Okamura, S. Ito, R. Konno, M. Mita, K. Hamase, S. Aiso, *PLoS One* **2014**, *9*, e86504.
- [321] T. Kimura, K. Hamase, Y. Miyoshi, R. Yamamoto, K. Yasuda, M. Mita, H. Rakugi, T. Hayashi, Y. Isaka, *Sci. Rep.* **2016**, *6*, 26137.
- [322] S. Du, Y. Wang, N. Alatrash, C. A. Weatherly, D. Roy, F. M. MacDonnell, D. W. Armstrong, *J. Pharm. Biomed. Anal.* **2019**, *164*, 421.
- [323] W. G. North, G. Gao, V. A. Memoli, R. H. Pang, L. Lynch, *Breast Cancer Res. Treat.* **2010**, *122*, 307.
- [324] F. Cava, H. Lam, M. A. De Pedro, M. K. Waldor, *Cell. Mol. Life Sci.* **2011**, *68*, 817.
- [325] I. E. Tothill, *in Semin. Cell Dev. Biol.* **2009**, *20*, 55.
- [326] W. H. Brooks, W. C. Guida, K. G. Daniel, *Curr. Top. Med. Chem.* **2011**, *11*, 760.
- [327] A. Somogyi, F. Bochner, D. Foster, *Aust. Prescriber* **2004**, *27*, 47.
- [328] E. Rosini, P. D'Antona, L. Pollegioni, *Int. J. Mol. Sci.* **2020**, *21*, 4574.
- [329] G. Pellegrini, M. Finazzi, M. Celebrano, L. Duó, M. A. Iati, O. M. Maragó, P. Biagioni, *J. Phys. Chem. C* **2019**, *123*, 28336.
- [330] L. D. Barron, *J. Am. Chem. Soc.* **1986**, *108*, 5539.
- [331] L. D. Barron, *Chem. Phys. Lett.* **1986**, *123*, 423.
- [332] L. D. Barron, *Rend. Lincei* **2013**, *24*, 179.
- [333] Y. Zhao, A. N. Askarpour, L. Sun, J. Shi, X. Li, A. Alù, *Nat. Commun.* **2017**, *8*, 14180.
- [334] R. Tullius, A. S. Karimullah, M. Rodier, B. Fitzpatrick, N. Gadegaard, L. D. Barron, V. M. Rotello, G. Cooke, A. Laphthorn, M. Kadodwala, *J. Am. Chem. Soc.* **2015**, *137*, 8380.
- [335] A. S. Karimullah, C. Jack, R. Tullius, V. M. Rotello, G. Cooke, N. Gadegaard, L. D. Barron, M. Kadodwala, *Adv. Mater.* **2015**, *27*, 5610.
- [336] E. Khoo, E. S. Leong, S. Wu, W. Phua, Y. Hor, Y. Liu, *Sci. Rep.* **2016**, *6*, 19658.
- [337] C. Jack, A. S. Karimullah, R. Leyman, R. Tullius, V. M. Rotello, G. Cooke, N. Gadegaard, L. D. Barron, M. Kadodwala, *Nano Lett.* **2016**, *16*, 5806.
- [338] Y. Liu, Z. Wu, P. S. Kollipara, R. Montellano, K. Sharma, Y. Zheng, *ACS Nano* **2021**, *15*, 6448.
- [339] S. Li, L. Xu, W. Ma, X. Wu, M. Sun, H. Kuang, L. Wang, N. A. Kotov, C. Xu, *J. Am. Chem. Soc.* **2016**, *138*, 306.
- [340] X. Wu, L. Xu, L. Liu, W. Ma, H. Yin, H. Kuang, L. Wang, C. Xu, N. A. Kotov, *J. Am. Chem. Soc.* **2013**, *135*, 18629.
- [341] P. Batalla, A. Martín, M. A. López, M. C. González, A. Escarpa, *Anal. Chem.* **2015**, *87*, 5074.
- [342] S. S. Acimovic, M. A. Ortega, V. Sanz, J. Berthelot, J. L. Garcia-Cordero, J. Renger, S. J. Maerkl, M. P. Kreuzer, R. Quidant, *Nano Lett.* **2014**, *14*, 2636.
- [343] A. Biswas, A. Vázquez-Guardado, D. Chanda, *Proc. SPIE* **2021**, *11696*, 116960E.
- [344] H. Zhang, W. Zhang, S. Hou, R. Wang, X. Zhang, *Chin. Phys. B* **2021**, *30*, 113303.
- [345] Y. Wang, Q. Wang, Q. Wang, Y. Wang, Z. Li, X. Lan, J. Dong, W. Gao, Q. Han, Z. Zhang, *Opt. Express* **2021**, *29*, 8087.
- [346] K. Ariga, T. Mori, T. Kitao, T. Uemura, *Adv. Mater.* **2020**, *32*, 1905657.
- [347] H.-E. Lee, H.-Y. Ahn, J. Lee, K. T. Nam, *ChemNanoMat* **2017**, *3*, 685.
- [348] K. Tamura, *J. Mol. Evol.* **2019**, *87*, 143.
- [349] A. Pohorille, J. Sokolowska, *Astrobiology* **2020**, *20*, 1236.
- [350] J. Skolnick, H. Zhou, M. Gao, *Proc. Natl. Acad. Sci. USA* **2019**, *116*, 26571.
- [351] D. P. Glavin, A. S. Burton, J. E. Elsil, J. C. Aponte, J. P. Dworkin, *Chem. Rev.* **2019**, *120*, 4660.
- [352] K. Kvenvolden, J. Lawless, K. Pering, E. Peterson, J. Flores, C. Ponnamperuma, I. R. Kaplan, C. Moore, *Nature* **1970**, *228*, 923.
- [353] J. Bocková, N. C. Jones, U. J. Meierhenrich, S. V. Hoffmann, C. Meinert, *Commun. Chem.* **2021**, *4*, 86.
- [354] A. D. Garcia, C. Meinert, H. Sugahara, N. C. Jones, S. V. Hoffmann, U. J. Meierhenrich, *Life* **2019**, *9*, 29.
- [355] N. Globus, R. D. Blandford, *Astrophys. J. Lett.* **2020**, *895*, L11.
- [356] D. Avnir, *New Astron. Rev.* **2020**, *92*, 101596.
- [357] N. Lambert, Y.-N. Chen, Y.-C. Cheng, C.-M. Li, G.-Y. Chen, F. Nori, *Nat. Phys.* **2013**, *9*, 10.
- [358] V. Sundström, *Annu. Rev. Phys. Chem.* **2008**, *59*, 53.
- [359] D. Polli, P. Altoe, O. Weingart, K. M. Spillane, C. Manzoni, D. Brida, G. Tomasello, G. Orlandi, P. Kukura, R. A. Mathies, M. Garavelli, G. Cerullo, *Nature* **2010**, *467*, 440.
- [360] J. C. Brookes, F. Hartoutsiou, A. Horsfield, A. Stoneham, *Phys. Rev. Lett.* **2007**, *98*, 038101.
- [361] M. I. Franco, L. Turin, A. Mershin, E. M. Skoulakis, *Proc. Natl. Acad. Sci. USA* **2011**, *108*, 3797.
- [362] J. M. Ribó, *Symmetry* **2020**, *12*, 1982.
- [363] K. Michaeli, R. Naaman, *J. Phys. Chem. C* **2019**, *123*, 17043.
- [364] Z. Yuan, Y. Zhou, Z. Qiao, C. Eng Aik, W.-C. Tu, X. Wu, Y.-C. Chen, *ACS Nano* **2021**, *15*, 8965.
- [365] K. Rechcińska, M. Król, R. Mazur, P. Morawiak, R. Mirek, K. Łempicka, W. Bardyszewski, M. Matuszewski, P. Kula, W. Piecek, P. G. Lagoudakis, B. Pietka, J. Szczytko, *Science* **2019**, *366*, 727.
- [366] N. Yu, F. Capasso, *Nat. Mater.* **2014**, *13*, 139.
- [367] Z. Li, D. Rosenmann, D. A. Czaplewski, X. Yang, J. Gao, *Opt. Express* **2019**, *27*, 28313.
- [368] S. Jafar-Zanjani, S. Inampudi, H. Mosallaei, *Sci. Rep.* **2018**, *8*, 11040.
- [369] H. Yang, X. Cao, F. Yang, J. Gao, S. Xu, M. Li, X. Chen, Y. Zhao, Y. Zheng, S. Li, *Sci. Rep.* **2016**, *6*, 35692.
- [370] D. Sell, J. Yang, S. Doshay, J. A. Fan, *Adv. Opt. Mater.* **2017**, *5*, 1700645.
- [371] T. Phan, D. Sell, E. W. Wang, S. Doshay, K. Edee, J. Yang, J. A. Fan, *Light: Sci. Appl.* **2019**, *8*, 48.
- [372] Q. Yuan, H. Ma, S. Sui, J. Wang, L. Zheng, Y. Meng, S. Qu, *J. Phys. D: Appl. Phys.* **2020**, *53*, 335001.
- [373] Z. Lin, V. Liu, R. Pestourie, S. G. Johnson, *Opt. Express* **2019**, *27*, 15765.
- [374] J. Yang, J. A. Fan, *Opt. Lett.* **2017**, *42*, 3161.
- [375] Y. Noguchi, T. Yamada, M. Otomori, K. Izui, S. Nishiwaki, *Appl. Phys. Lett.* **2015**, *107*, 221909.
- [376] B. Gallinet, J. Butet, O. J. F. Martin, *Laser Photonics Rev.* **2015**, *9*, 577.
- [377] C. Liu, Y. Bai, J. Zhou, Q. Zhao, Y. Yang, H. Chen, L. Qiao, *npj Comput. Mater.* **2019**, *5*, 93.
- [378] C. Warren, A. Giannopoulos, A. Gray, I. Giannakis, A. Patterson, L. Wetter, A. Hamrah, *Comput. Phys. Commun.* **2019**, *237*, 208.
- [379] Y. Li, Y. Xu, M. Jiang, B. Li, T. Han, C. Chi, F. Lin, B. Shen, X. Zhu, L. Lai, Z. Fang, *Phys. Rev. Lett.* **2019**, *123*, 213902.
- [380] Z. Tao, J. Zhang, J. You, H. Hao, H. Ouyang, Q. Yan, S. Du, Z. Zhao, Q. Yang, X. Zheng, T. Jiang, *Nanophotonics* **2020**, *9*, 2945.
- [381] W. Ma, F. Cheng, Y. Liu, *ACS Nano* **2018**, *12*, 6326.
- [382] W. Ma, F. Cheng, Y. Xu, Q. Wen, Y. Liu, *Adv. Mater.* **2019**, *31*, 1901111.
- [383] S. So, T. Badloe, J. Noh, J. Bravo-Abad, J. Rho, *Nanophotonics* **2020**, *9*, 1041.
- [384] J. Zhou, B. Huang, Z. Yan, J.-C. G. Bünzli, *Light: Sci. Appl.* **2018**, *8*, 84.
- [385] I. Malkiel, M. Mrejen, A. Nagler, U. Arieli, L. Wolf, H. Suchowski, *Light: Sci. Appl.* **2018**, *7*, 60.

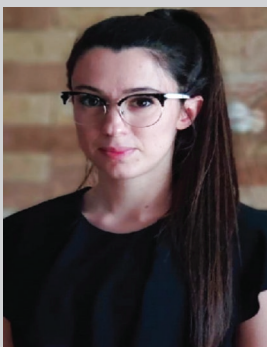
- [386] T. Christensen, C. Loh, S. Picek, D. Jakobović, L. Jing, S. Fisher, V. Ceperic, J. D. Joannopoulos, M. Soljačić, *Nanophotonics* **2020**, 9, 4183.
- [387] W. Ma, Z. Liu, Z. A. Kudyshev, A. Boltasseva, W. Cai, Y. Liu, *Nat. Photonics* **2020**, 15, 77.
- [388] W. Liu, Z. Wang, X. Liu, N. Zeng, Y. Liu, F. E. Alsaadi, *Neurocomputing* **2017**, 234, 11.
- [389] K. Yao, R. Unni, Y. Zheng, *Nanophotonics* **2019**, 8, 339.
- [390] J. Peurifoy, Y. Shen, L. Jing, Y. Yang, F. Cano-Renteria, B. G. DeLacy, J. D. Joannopoulos, M. Tegmark, M. Soljačić, *Sci. Adv.* **2018**, 4, eaar4206.
- [391] D. Liu, Y. Tan, E. Khoram, Z. Yu, *ACS Photonics* **2018**, 5, 1365.
- [392] S. Molesky, Z. Lin, A. Piggott, W. Jin, J. Vucković, A. Rodriguez, *Nat. Photonics* **2018**, 12, 659.
- [393] R. Lin, Y. Zhai, C. Xiong, X. Li, *Opt. Lett.* **2020**, 45, 1362.
- [394] D. C. Mocanu, E. Mocanu, P. Stone, P. H. Nguyen, M. Gibescu, A. Liotta, *Nat. Commun.* **2018**, 9, 2383.
- [395] C. C. Nadell, B. Huang, J. M. Malof, W. J. Padilla, *Opt. Express* **2019**, 27, 27523.
- [396] X. Li, J. Shu, W. Gu, L. Gao, *Opt. Mater. Express* **2019**, 9, 3857.
- [397] I. Sajedian, J. Kim, J. Rho, *Microsyst. Nanoeng.* **2019**, 5, 27.
- [398] Z. Tao, J. You, J. Zhang, X. Zheng, H. Liu, T. Jiang, *Opt. Lett.* **2020**, 45, 1403.
- [399] E. Ashalley, K. Acheampong, L. V. Besteiro, P. Yu, A. Neogi, A. O. Govorov, Z. M. Wang, *Photonics Res.* **2020**, 8, 1213.



**Andrew Lininger** is currently a Ph.D. candidate in physics at Case Western Reserve University. He received his B.S. in physics from the University of Akron. His research focuses on the design and fabrication of optical metasurfaces, including the application of machine-learning techniques to photonic design and the development of optical devices for advanced sensor applications.



**Giovanna Palermo** is currently an assistant professor (Rtd-A) at University of Calabria (Unical). She received a masters degree in electronic engineering and a Ph.D. in science and technology of mesophases and molecular materials, at Unical, in 2012 and 2015, respectively. The main research activity is focused in the design and characterization of metamaterials usable to realize high sensitivity biosensors.



**Alexa Guglielmelli** is currently a postdoctoral researcher in the NLHT-Lab. She received her B.S. in physics and M.S. in molecular biophysics from University of Calabria (Unical), Cosenza, Italy. She received a Ph.D. in physical, chemical, and materials sciences and technologies from the same university. Her research interests include plasmonic nanomaterials for applications in nanomedicine and biophotonics and thermotropic liquid crystals applications.



**Giuseppe Nicoletta** received his M.S. in applied physics at the University of Calabria (Unical) in 2018. He is currently pursuing his Ph.D. in physical, chemical and materials sciences and technologies at the same University. His research interests mainly focus on nanotechnologies, metasurfaces, and metalenses for optical applications.



**Madhav Goel** is currently a B.S. candidate in mathematics and physics at Case Western Reserve University. His research interests include design, fabrication, and optical applications of metasurfaces.



**Michael Hinczewski** is currently the Warren E. Rupp associate professor of Physics at Case Western Reserve University. He received his B.S. and Ph.D. degrees in physics from Yale University and MIT, respectively. His research focuses on applications of statistical physics to a variety of topics in biology, from fundamental processes (cell adhesion, signaling, evolution) to biomedical applications like plasmonic biosensors.



**Giuseppe Strangi** is currently professor of physics and Ohio research scholar in surfaces of advanced materials at Case Western Reserve University (CWRU), also holding secondary appointments at UNICAL and CNR (Italy). He is the President of the Scientific Committee of the Foundation “Con il Cuore”, and he is the General Chair of the International Conference – NANOPLASM “New Frontiers in Plasmonics and Nanophotonics”. His research interests include condensed matter physics, nanophotonics and plasmonics of electromagnetic materials, and cancer nanotechnology. He is a fellow of The Institute of Science of the Origins, of the Case Comprehensive Cancer Center (CWRU), and an OSA Fellow.